TECHNICAL TRANSACTIONS
CZASOPISMO TECHNICZNE

FUNDAMENTAL SCIENCES
NAUKI PODSTAWOWE

ISSUE 3-NP (17)
ZESZYT 3-NP (17)

YEAR 2014 (111)
ROK 2014 (111)

WYDAWNICTWO POLITECHNIKI KRAKOWSKIEJ

TECHNICAL TRANSACTIONS | CZASOPISMO TECHNICZNE

FUNDAMENTAL SCIENCES | NAUKI PODSTAWOWE

ISSUE 3-NP (17) | ZESZYT 3-NP (17)
YEAR 2014 (111) | ROK 2014 (111)

Pierwotną wersją każdego Czasopisma Technicznego jest wersja on-line
www.czasopismotechniczne.pl www.technicaltransactions.com

Fundamential Sciences Series
3-NP/2014

Editorial Board

MATHEMATICS

MATEMATYKA

TECHNICAL TRANSACTIONS | **CZASOPISMO TECHNICZNE**
FUNDAMENTAL SCIENCES | NAUKI PODSTAWOWE
3-NP/2014

MAGDALENA GRZECH*

A NEW APPROACH TO BOUNDED LINEAR OPERATORS ON $C(\omega^*)$

DOMKNIĘTE OPERATORY PRZESTRZENI $C(\omega^*)$ Z NOWEJ PERSPEKTYWY

A b s t r a c t

We discuss recent results on the connection between properties of a given bounded linear operator of $C(\omega^*)$ and topological properties of some subset of ω^* which the operator determines. A family of closed subsets of ω^*, which codes some properties of the operator is defined. An example of application of the method is presented.

Keywords: retraction, projection, ultrafilter, Cech-Stone compactification

S t r e s z c z e n i e

Artykuł przedstawia metodę badania własności ograniczonego operatora liniowego na $C(\omega^*)$ poprzez badanie własności pewnej rodziny domkniętych pozbiorów ω^* wyznaczonej przez ten operator. Przedstawiony został przykład zastosowania tej metody w przypadku projekcji.

Słowa kluczowe: retrakcja, projekcja, ultrafiltr, Cech-Stone compactification

The author is responsible for the language in all paper.

* Institute of Mathematics, Faculty of Physics, Mathematics and Computer Science, Cracow University of Technology, Poland; magdag@pk.edu.pl.

The Greek letter ω denotes the set of all natural numbers. We use the symbol ***fin*** for the ideal of finite subsets of ω. For $A, B \subseteq \omega$, the expression $A \subseteq {}^*B$ denotes the relation $B \setminus A \in \mathit{fin}$; similarly $A = {}^*B$ if and olny if $A \div B \in \mathit{fin}$. The space $\omega^* = \beta[\omega] \setminus \omega$ is the growth (Čech-Stone compactification) of the discrete topological space ω. If $A \in P(\omega)/\mathit{fin}$, A^* is the set $A^{\beta[\omega]} \setminus A$. The space ω* can be viewed as the space of all non-principal ultrafilters on ω. It is well known that $\boldsymbol{B}(\omega^*)$, the algebra of all clopen subsets of ω*, is isomorphic to $P(\omega)/\mathit{fin}$ (cf. [1]). Thus, for $A, B \in P(\omega)$, the condition $A = {}^*B$ is equivalent to $A^* = B^*$. ***An antichain*** in $\boldsymbol{B}(\omega^*)$ is a family of pairwise disjoint subsets of ω*. Recall that a set $A \subseteq \omega^*$ is said to have ***ccc (countable chain condition)*** if for every antichain $\{U_\alpha : \alpha \in \boldsymbol{I}\} \subseteq \boldsymbol{B}(\omega^*)$, there exists a finite or countable set $\boldsymbol{I}_0 \subseteq \boldsymbol{I}$ such that $A \cap U_\alpha = \varnothing$ for all $\alpha \in \boldsymbol{I} \setminus \boldsymbol{I}_0$.

The space $C(\omega^*)$ consists of all continuous real-valued. functions on ω* and it can be regarded as l_∞/c_0 i.e. the quotient space of l_∞ by the following equivalence relation:

$$\text{for } f_1, f_2 \in l_\infty,\ f_1 \approx^* f_2 \quad \text{iff } \lim_{n\to\infty}(f_1(n) - f_2(n)) = 0$$

Let f^* denote the equivalence class determined by f. Note that for $f_1, f_2 \in l_\infty$, we have $f_1 \approx^* f_2$ iff $f_1|\omega^* \approx^* f_2|\omega^*$, where f_i: $\beta[\omega] \to \mathbb{R}$ is a continuous extension of f_i $(i = 1, 2)$. Thus, $f^* = f|\omega^*$. An equivalent definition of the (classical) norm on l_∞/c_0 is following:

$$\|f^*\|_* = \sup \{\lim_p |f| : p \in \omega^*\}$$

where the symbol $\lim_p |f|$ denotes, for an ultrafilter p, the limit to which a sequence $\{|f(n)| : n \in \omega\}$ converges with respect to the ultrafilter p. Thus, $C(\omega^*)$, equipped with the supremum norm, is isometric to $(l_\infty/c_0, \| \cdot \|_*)$.

The domain of function f is denoted by dom f, the range by ran f; supp f is the closure of the set of all elements $p \in \operatorname{dom} f$, such that $f(p) \neq 0$.

The space C(ω*). It is appropriate to recap on some elemetary properties of functions in space $C(\omega^*)$. Let f: ω*®|R. (To simplify notation, the sign * will be omitted):

- For every $r \in \mathbb{R}$, the preimage $f^{-1}(r)$ is a closed G_δ set,
- If $f^{-1}(r) \neq \varnothing$, then $\operatorname{int} f^{-1}(r) \neq \varnothing$,
- For arbitrary $\varepsilon > 0$, there exist clopen sets $U_1, U_2, \ldots, U_n \in \boldsymbol{B}(\omega^*)$ and reals $r_1, r_2, \ldots, r_n$ such that;

$$\|f - \Sigma_{i \in \{1, \ldots, n\}}\, r_i\, \chi\, U_i\| < \varepsilon,$$

where $\chi\, U_i$ denotes the characteristic function of U_i.

Bounded linear operators on C(ω*). Assume that T: $C(\omega^*) \to C(\omega^*)$ is linear and bounded, and its norm is equal to M.

Fix an ultrafilter $q \in \omega^*$ and define:

$$\mathcal{N}_q = \{U \in \boldsymbol{B}(\omega^*) : V \forall \in \boldsymbol{B}(\omega^*)\ V \subseteq U \Rightarrow T(\chi_V)(q) = 0\},\ \mathcal{S}_q = \omega^* \setminus \mathcal{N}_q.$$

$\mathcal{N}_q$ is an open set. Consider $\mathcal{S}_q$. It is closed (by definition) and nowhere dense. To show this suppose that $\operatorname{int}(\mathcal{S}_q) \neq \varnothing$ and argue to a contradiction.

Let $U \in \boldsymbol{B}(\omega^*)$ and $U \subseteq \operatorname{int}(\mathcal{S}_q)$. Consider a family of pairwise disjoint sets $V_\alpha \subseteq U$, $\alpha < \omega_1$. By definition of $\mathcal{S}_q$, for every $\alpha < \omega_1$ there exists $W_\alpha \subseteq V_\alpha$, $W_\alpha \in \boldsymbol{B}(\omega^*)$ such that $T(\chi_{W\alpha})(q) \neq 0$. Thus, for some $\varepsilon > 0$ there exists an uncountable set $\Gamma \subseteq \omega_1$ with:

$$\forall \alpha \in \Gamma\ |T(\chi_{W\alpha})(q)| > 0.$$

Moreover, we may assume that all the $T(\chi_{W\alpha})(q)$ are positive (or negative). Fix $k \in \omega$ such that $k > (M/\varepsilon) + 1$ and a finite set $\Gamma_0 \subseteq \Gamma$ which contains at least k elements. Since T is linear, it follows that:

$$|T(\Sigma_{\alpha\in\Gamma 0}\, \chi_{W\alpha}\})(q)| = |\Sigma_{\alpha\in\Gamma 0}\, T(\chi_{W\alpha})(q)| \geq k\varepsilon > \varepsilon\, [(M/\varepsilon) + 1] > M,$$

this contradicts the assumption that M is the norm of T.

In a similar way we show that S_q has the c.c.c.

Lemma 1 *Suppose that* $f \in \mathbf{C}(\omega^*)$ *and* $\operatorname{supp} f \cap S_q = \varnothing$. *Then* $T(f)(q) = 0$.

Proof. Suppose that this is not true. Then, since T is continuous, there exist clopen sets U_1, U_2, ..., $U_n \subseteq \operatorname{supp} f$ and reals r_1, r_2, ..., r_n such that:

$$\|f - \Sigma_{i\in\{1,\ldots,n\}}\, r_i\, \chi_{Ui}\| < \varepsilon,$$

for $\varepsilon < |T(f)|(q)/(2M)$. It follows that;

$$|T\,(f - \Sigma_{\,i\in\{1,\ldots,n\}}\, r_i\, \chi_{Ui})| < |T(f)|(q)/2$$

thus $|T(\Sigma_{i\in\{1,\ldots,n\}}\, r_i\, \chi_{Ui})| > |T(f)|(q)/2$. So, there exists $i \leq n$ such that $|T(\chi_{Ui})\, q)| > 0$. Therefore $U_i \setminus \mathcal{N}_q \neq \varnothing$. But it implies that $\varnothing \neq S_q \cap U_i \subseteq S_q \cap \operatorname{supp} f = \varnothing$, a contradiction.

Note that the condition $T(f)(q) = 0$ does not imply that $S_q \cap \operatorname{supp} f = \varnothing$. Now an example of application of the notion S_q is presented.

Projections of $C(\omega^*)$ and retractions of ω^*. Assume that r: $\omega^* \circledR F \subseteq \omega^*$ is a retraction (i.e. r is continuous and $\mathbf{r} \circ \mathbf{r} = \mathbf{r}$). Recall how to define a projection P: $\mathbf{C}(\omega^*) \to V$ (i.e. a bounded linear operator such that $\mathbf{P} \circ \mathbf{P} = \mathbf{P}$) by using $\mathbf{r}$ (cf. [2]). For $f \in \mathbf{C}(\omega^*)$, $q \in \omega^*$ put:

$$\mathbf{P}(f)(q) = f(\mathrm{r}(q).$$

$\mathbf{P}$ is linear and for every $f \neq \mathbf{C}(\omega^*)$, $\|\mathbf{P}(f)\| \leq \leq \|f\|$, thus $\mathbf{P}$ is bounded. Moreover:

$$\mathbf{P}(\mathbf{P}(f))(q) = \mathbf{P}(f)(\mathrm{r}(q)) = f(\mathbf{r}(\mathbf{r}(q))) = f(\mathbf{r}(q)) = \mathbf{P}(f)(q).$$

A retraction of ω^* induces a projection of $\mathbf{C}(\omega^*)$. One can ask if a projection determines a retraction. In order to (partially) answer this question, an equivalence relation on ω^* can be defined:

$$p, q \in \omega^*,\ p \approx q \text{ iff for all } U \in \mathbf{B}(\omega^*),\ \mathbf{P}(\chi_U)(q) = \mathbf{P}(\chi_U)(p).$$

Note that:

- if $p \approx q$ then $S_p = S_q$,
- the equivalence class $[p] = \bigcup_{U\in \boldsymbol{B}(\omega^*)} (\mathbf{P}(\chi_U))^{-1}\, (\{P(\chi_U)(p)\})$ is a closed subset of ω^*.

Theorem 1 *Assume that* $\mathbf{P}$: $\mathbf{C}(\omega^*) \to V$ *is a projection and the following assertion is satisfied:*

$$\textit{for each } p \in \omega^* \textit{ there exists } q_p \in [p] \textit{ such that } S_p = \{q_p\}.$$

Then $\mathbf{r}$: $\omega^* \ni p \to q_p \in \bigcup_{p\in\omega^*} S_p$ *is a retraction.*

Proof. Since $q_p \approx p$, $S_q = S_p = \{q_p\}$ and $\mathrm{r}(q_p) = q_p$. Therefore $\mathbf{r} \circ \mathbf{r} = \mathbf{r}$.

We shall show that r is continuous. Let $\tilde{U}$ be an open subset of $\bigcup_{p\in\omega^*} S_p$. Fix $q_p \in \tilde{U}$. Thus, there exists a U open subset of ω^* and $V \in \mathbf{B}(\omega^*)$ such that $U \cap \bigcup_{p\in\omega^*} S_p$ and $q_p \in V \subseteq U$.

Since $\mathcal{S}_{qp} = \{q_p\}$, it follows that $\mathbf{P}(\chi_V)(q_p) = x_p \neq 0$. Assume that for some $s \in \omega$, $\mathrm{P}(\chi_V)(q_p) = x_p \neq 0$. Thus, $\{q_p\} \cap V = \mathcal{S}_{qp} \cap V$, which implies that $q_s \in V$.

We showed that $q_s \in V \Rightarrow P(\chi_V)(q_s) \neq 0$. Put $W = (P(f))^{-1}(|\mathsf{R}\backslash\{0\})$. W is open and $r(W) \subseteq V \cap \bigcup_{p\in\omega^*} \mathcal{S}_p$. This finishes the proof.

References

[1] Comfort W.W., Negrepontis S., *The theory of ultrfilters*, Springer Verlag, New York 1974.

[2] Drewnowski L., Roberts J.W., *On the primariness of the Banach space l_∞/c_0*, Proc. Amer. Math. Soc. 112, 1991.

[3] Negrepontis S., *The Stone space of the saturated Boolean algebras*, Trans. Amer. Math. Soc. 13, 1981.

[4] Pełczyński A., *Projections in certain Banach spaces*, Studia Math. 19, 1960.

[5] Todorcevic S., *Partition problems in topology*, Contemporary Mathematics 84, Amer. Math. Soc., Providence, 1989.

TECHNICAL TRANSACTIONS | **CZASOPISMO TECHNICZNE**
FUNDAMENTAL SCIENCES | NAUKI PODSTAWOWE
3-NP/2014

MAGDALENA GRZECH*

SOME REMARKS ON NON-SEPARABLE GAPS IN $P(\omega)/FIN$

KILKA UWAG O LUKACH HAUSDORFFA I AUTOMORFIZMACH $P(\omega)/FIN$

A b s t r a c t

The Hausdorff gap is the well known example of a non-separable, increasingly ordered gap in $P(\omega)/fin$. In this paper new construction of a non-separable gap in $P(\omega)/fin$ is presented.

Keywords: Boolean algebra, Cech-Stone compactification, gap

S t r e s z c z e n i e

W artykule została przedstawiona nowa konstrukcja nierozdzielalnej luki w $P(\omega)/fin$.

Słowa kluczowe: algebra Boole'a, uzwarcenie Cecha-Stone'a, luka

The author is responsible for the language in all paper.

* Institute of Mathematics, Faculty of Physics, Mathematics and Computer Science, Cracow University of Technology, Poland; magdag@pk.edu.pl.

Boolean algebra $P(\omega)/\mathit{fin}$ plays an important role in the foundations of mathematics. Many mathematical problems can be reduced to questions on properties of $P(\omega)/\mathit{fin}$. Notion, which is frequently used in investigation concerning $P(\omega)/\mathit{fin}$ is the notion of gap (cf. [1], [4]).

Let us begin by reviewing some basic facts and definitions. By ω the set of all natural numbers is denoted. The symbol fin stands for the ideal of all finite subsets of ω. The ideal determines the following equivalence relation:

$$\text{For } A, B \subseteq \omega,\ A =_* B \text{ if and only if } A \div B \in \mathit{fin}.$$

$P(\omega)/\mathit{fin}$ is its factor algebra. An order in $P(\omega)/\mathit{fin}$ is defined as usual, namely:

$$A \subseteq_* B \text{ iff } A \setminus B \in \mathit{fin}.$$

Let λ, κ be cardinals. A gap of type λ, κ) in the $P(\omega)/\mathit{fin}$ is a pair:

$$(\{A_\gamma\colon \gamma < \lambda\},\ \{B_\beta\colon \beta < \kappa\})$$

of subsets of $P(\omega)/\mathit{fin}$ such that $A_\gamma \cap B_\beta =_* \varnothing$. If for every $\gamma_1 < \gamma_2 < \lambda$, $\beta_1 < \beta_2 < \kappa$ $A_{\gamma 1} \subseteq_* A_{\gamma 2}$ and $B_{\beta 1} \subseteq_* B_{\beta 2}$, the gap is said to be increasingly ordered. An element $C \subseteq \omega$ **fills** (separates) the gap if $A_\gamma \subseteq_* C$ and $B_\beta \cap C =_* \varnothing$ for every $\gamma < \lambda$, $\beta < \kappa$. If there is no such an element, the gap is called non-separable. One can ask gaps of what type exist in $P(\omega)/\mathit{fin}$.

A research concerning gaps in $(\omega)/\mathit{fin}$ is an important and deep line of investigation. Let us recall basic facts. It is easily proved that there are no non-separable gaps of type (ω, ω). On the other hand Hausdorff constructed a non-separable gap of type (ω_1, ω_1) (cf. [2]). This gap, say $\mathcal{L} = (\{X_\alpha\colon \alpha < \omega_1\},\ \{Y_\beta\colon \beta < \omega_1\})$, is increasingly ordered and $\{\gamma < \beta\colon \max X_\gamma \cap Y_\beta < k\}$ is finite for every $\beta < \omega_1$ and $k \in \omega$.

Under CH (the Continuum Hypothesis), there exist only gaps of type (ω_1, ω_1). If $2^\omega > \omega_1$ and MA (the Martin Axiom) holds the each increasingly ordered gap f type λ, κ) with λ, $\kappa < 2^\omega$, $\lambda \neq \omega_1$ or $\kappa \neq \omega_1$ is separated ([5]).

The smallest cardinal number for which there exists a non-separable gap in $P(\omega)/\mathit{fin}$ is the bounding number $\mathbf{b}$ (cf. [6]). Remind that $\mathbf{b}$ is the size of the smallest unbounded family in ω^ω equipped with the following order: for $f, g \in \omega^\omega$, $f \leq_* g$ iff $\{n\colon f(n) > g(n)\} \in \mathit{fin}$.

We present another construction of an (unordered) gap of type $(2^\omega, 2^\omega)$.
The set F consist of all finite sequences $\underline{\varepsilon} = (\varepsilon_0, \varepsilon_1, \ldots, \varepsilon_n)$ such that:

$$\varepsilon_0 = 0,\ \varepsilon_{2n+1} = 2 \text{ and } \varepsilon_{2n+2} \in \{0, 1\},\ n \in \omega.$$

Let

$$F_n = \{\underline{\varepsilon} \in F\colon \ell(\underline{\varepsilon}) \leq 2n\}$$

and

$$F_e = \{\underline{\varepsilon} \in F\colon \ell(\underline{\varepsilon}) = 2n \text{ for some } n \in \omega\}.$$

Divide ω into two disjoint, infinite subsets X and Y and fix two functions f and g such that:

(*) $f\colon F \to X$ is a bijection and if $\underline{\varepsilon} \subseteq \underline{\rho}$ then $f(\underline{\varepsilon}) \leq f(\underline{\rho})$.

(**) $g\colon F_e \times F_e \to Y$ is an injection and if $\underline{\varepsilon}^1 \subseteq \underline{\rho}^1$, $\underline{\varepsilon}^2 \subseteq \underline{\rho}^2$ then

$$g(\underline{\varepsilon}^1,\underline{\varepsilon}^2) \le g(\underline{\rho}^1, \underline{\rho}^2).$$

We define two families of finite subsets $\{A(\underline{\varepsilon})\colon \underline{\varepsilon} \in F\}$, $\{B(\underline{\varepsilon})\colon \underline{\varepsilon} \in F\}$ by induction on the lenght of $\underline{\varepsilon}$.

For $\underline{\varepsilon}$ such that $\ell(\underline{\varepsilon}) = 1$ or $\ell(\underline{\varepsilon}) = 2$ put $A(\underline{\varepsilon}) = B(\underline{\varepsilon}) = \emptyset$.
Assume that $\ell(\underline{\varepsilon}) = 3,4$. Then:

$$A_{(0,2,0)} = \{f((0)), f((0,2)), f((0,2,0))\},\ A_{(0,2,1)} = \{f((0)), f((0,2)), f((0,2,1))\},$$

$$B_{(0,2,0)} = \{f((0,2,1))\},\ B_{(0,2,1)} = \{f((0,2,0))\},$$

$$A_{(0,2,0,2)} = A_{(0,2,0)} \cup \{f((0,2,0,2))\},\ A_{(0,2,1,2)} = A_{(0,2,1)} \cup \{f((0,2,1,2))\}$$

$$B_{(0,2,0,2)} = B_{(0,2,0)} \cup \{g((0,2,1,2), (0,2,0,2))\},\ B_{(0,2,1,2)} = B_{(0,2,1)} \cup \{g((0,2,1,2), (0,2,0,2))\}$$

Assume inductively that for $n \ge 2$, we have defined families $\{A(\underline{\varepsilon})\colon \underline{\varepsilon} \in F_n\}$ and $\{B(\underline{\varepsilon})\colon \underline{\varepsilon} \in F_n\}$ satisfying the following conditions:

1. $A(\underline{\varepsilon}) \cap B(\underline{\varepsilon}) = \emptyset$ for every $\underline{\varepsilon} \in F_n$.
2. If $\underline{\varepsilon}, \underline{\rho} \in F_n$ and $\underline{\varepsilon}(k) \ne \underline{\rho}(k)$, for some $k \le 2n$, then

$$A(\underline{\varepsilon}) \cap B(\underline{\rho}) \ne \emptyset \text{ and } B(\underline{\varepsilon}) \cap A(\underline{\rho}) \ne \emptyset.$$

3. If $\underline{\varepsilon}, \underline{\rho} \in F_n$ and $\underline{\varepsilon} \subseteq \underline{\rho}$, then $A(\underline{\varepsilon}) \subseteq A(\underline{\rho})$ and $B(\underline{\varepsilon}) \subseteq B(\underline{\rho})$.
4. If $\underline{\varepsilon}, \underline{\rho} \in F_n$ and $\underline{\varepsilon}(k) \ne \underline{\rho}(k)$, let $\ell = \min\{k\colon \underline{\varepsilon}(k) \ne \underline{\rho}(k)\}$. Then $\max A(\underline{\varepsilon}) \cap B(\underline{\rho}) = f(\underline{\varepsilon}|_\ell)$, $\max B(\underline{\varepsilon}) \cap B(\underline{\rho}) = f(\underline{\varepsilon}|_{\ell-1})$, $\max A(\underline{\varepsilon}) \cap A(\underline{\rho}) = f(\underline{\varepsilon}|_{\ell-1})$.

For $\underline{\varepsilon} \in F_n$ put:

$$A(\underline{\varepsilon} \wedge 0) = A(\underline{\varepsilon}) \cup \{f(\underline{\varepsilon} \wedge 0)\},\ A(\underline{\varepsilon} \wedge 1) = A(\underline{\varepsilon}) \cup \{f(\underline{\varepsilon} \wedge 1)\},$$

$$B(\underline{\varepsilon} \wedge 0) = B(\underline{\varepsilon}) \cup \{f(\underline{\varepsilon} \wedge 1)\},\ B(\underline{\varepsilon} \wedge 1) = B(\underline{\varepsilon}) \cup \{f(\underline{\varepsilon} \wedge 1)\},$$

$$A(\underline{\varepsilon} \wedge 02) = A(\underline{\varepsilon} \wedge 0) \cup \{f(\underline{\varepsilon} \wedge 02)\},\ A(\underline{\varepsilon} \wedge 12) = A(\underline{\varepsilon} \wedge 1) \cup \{f(\underline{\varepsilon} \wedge 12)\},$$

$$B(\underline{\varepsilon} \wedge 02) = B(\underline{\varepsilon} \wedge 0) \cup \{g(\underline{\varepsilon} \wedge 02, \underline{\varepsilon} \wedge 12)\},\ B(\underline{\varepsilon} \wedge 12) = B(\underline{\varepsilon} \wedge 1) \cup \{g(\underline{\varepsilon} \wedge 02, \underline{\varepsilon} \wedge 12)\}.$$

It is obvious that the family F_{n+1} satisfies conditions (1) and (3).

For (2), let $\underline{\rho}, \underline{\varepsilon} \in F_{n+1}$. If $\ell(\underline{\rho}) = \ell(\underline{\varepsilon})$ or $\ell(\underline{\rho}) = 2n + 1$, $\ell(\underline{\varepsilon}) = 2n + 2$, the condition follows from the definition. Suppose that $\ell(\underline{\rho}) = k < 2n + 1 \le \ell(\underline{\varepsilon})$. Let $l = \min\{k\colon \underline{\varepsilon}_k \ne \underline{\rho}_k\}$. Then $\underline{\sigma} = \underline{\varepsilon}|l = \underline{\rho}|l$ and $\emptyset \ne A(\underline{\sigma})^\wedge\underline{\rho}_l) \cap B(\underline{\sigma} \wedge \underline{\varepsilon}_l) = A(\underline{\rho}) \cap B(\underline{\varepsilon})$. (The remaining cases can be checked in the same way.)

To check the assumption (4), note that $A(\underline{\varepsilon} \wedge i) \cap B(\underline{\varepsilon} \wedge j) = A(\underline{\varepsilon} \wedge i2) \cap B(\underline{\varepsilon} \wedge j2)$, for $i, j \in \{0, 1\}$, $i \ne j$. Since f satisfies the condition (*), it follows that $\max A(\underline{\varepsilon} \wedge i) \cap B(\underline{\varepsilon} \wedge j) = f(\underline{\varepsilon} \wedge i)$. Moreover $A(\underline{\varepsilon} \wedge i) \cap A(\underline{\varepsilon} \wedge j) = A(\underline{\varepsilon} \wedge i2) \cap A(\underline{\varepsilon} \wedge j2) = A(\underline{\varepsilon})$, thus

$$\max A(\underline{\varepsilon} \wedge i) \cap A(\underline{\varepsilon} \wedge j) = f(\underline{\varepsilon}).$$

If $\ell(\underline{\rho}) = k < 2n + 1 \le \ell(\underline{\varepsilon})$ and $\underline{\sigma} = \underline{\varepsilon}|l = \underline{\rho}|l$, $\underline{\rho}_l \ne \underline{\varepsilon}_l$ then

$$\max A(\underline{\sigma} \hat{} \underline{\rho}_l) \cap B(\underline{\sigma} \hat{} \underline{\varepsilon}_l) = \max A(\underline{\rho}) \cap B(\underline{\varepsilon}) = f(\underline{\rho}|l).$$

(The remaining cases can be checked in the same way.) This finishes the inductive construction.

Let X be the family of all sequences x: $\omega \to \{0, 1, 2\}$ which satisfy the conditions:

$$x(0) = 0,\ x(2n + 1) = 2,\ x(2n + 2) \in \{0, 1\}.$$

Then

$$\underline{A}(x) = \bigcup_{n\in\omega} A(x|n),\ \underline{B}(x) = \bigcup_{n\in\omega} B(x|n)$$

are infinite subsets of ω.

It is easy to check that for $x, y \in X$, if $x \neq y$ then:

$$\underline{A}(x) \cap \underline{B}(x) = \emptyset,\ \underline{A}(x) \cap \underline{B}(y) \neq \emptyset,\ \underline{A}(x) \cap \underline{A}(y) \in \mathbf{fin} \text{ and } \underline{B}(x) \cap \underline{B}(y) \in \mathbf{fin}.$$

Theorem 1 *The gap* $\mathcal{L} = (\{\underline{A}(x): x \in X\}, \{\underline{B}(x): x \in X\})$ *satisfies the following condition: for every uncountable set* $Y \subseteq X$, $\mathcal{L}_Y = (\{\underline{A}(x): x \in Y\}, \{\underline{B}(x): x \in Y\})$ *is non-separable.*

Proof. Suppose that for $Y = \{x_\alpha : \alpha < \kappa\} \subseteq X$, $\omega < \kappa \leq 2^\omega$, there exists a C which separeates the gap $\mathcal{L}_Y$. Let $s_\alpha = \underline{A}(x_\alpha)\backslash C$, $t_\alpha = \underline{B}(x_\alpha) \cap C$.

Then s_α, t_α are finite subsets of ω and since $\underline{A}(x_\alpha) \cap \underline{B}(x_\alpha) = \emptyset$, it follows that $s_\alpha \cap t_\alpha = \emptyset$. Δ-lemma implies that there exist an uncountable set $\Gamma \subseteq \kappa$ $\Gamma \subset \kappa$ and finite sets s, t such that for all $\alpha \in \gamma$, $s_\alpha = s$ and $t_\alpha = t$.

If $\alpha, \beta \in \Gamma$ and $\alpha \neq \beta$ then $\emptyset = s_\alpha \cap t_\beta = s \cap t = s_\alpha \cap t_\alpha = \emptyset$, a contradiction. This finishes the proof.

References

[1] Comfort W.W., Negrepontis S., *The theory of ultrfilters*, Springer Verlag, New York 1974.

[2] Hausdorff Summen von Mengen F_1, Fund. Math. 26, 1936, 241-255.

[3] Hechler S., *On existence of certain cofinal subsets of*, Axiomatic Set Theory, T. Jech (ed.), Proc. Symp. Pure Math. vol. 13 II, 1974, 155-173.

[4] Jech T., *Set Theory*, Academic Press, New York et al., 1978.

[5] Kunen K., *Weak P-points in* N^*, Colloq. Math. soc. Jano's Bolyai 23, Topology, Budapest 1978, 741-749.

[6] Rothberger F., *Une remarque concernant l'hipotése du continu*, Fund. Math. 31, 1939, 224-226.

TECHNICAL TRANSACTIONS | **CZASOPISMO TECHNICZNE**
FUNDAMENTAL SCIENCES | NAUKI PODSTAWOWE
3-NP/2014

MAGDALENA GRZECH*

SOME REMARKS ON HAUSDORFF GAPS AND AUTOMORPHISMS OF $\boldsymbol{P}(\omega)/\boldsymbol{FIN}$

O NIEROZDZIELALNYCH LUKACH W ALGEBRZE $P(\omega)/FIN$

A b s t r a c t

We present, under the Continuum Hypothesis (CH), a construction of an automorphism of $P(\omega)/\boldsymbol{fin}$ which maps a Hausdorff gap onto increasingly ordered gap of type (ω_1, ω_1) which is not a Hausdorff gap.

Keywords: compactification, automorphism, Boolean algebra

S t r e s z c z e n i e

Artykuł przedstawia, przy założeniu Hipotezy Continuum, konstrukcję automorfizmu algebry $P(\omega)/\boldsymbol{fin}$, który przeprowadza lukę Hausdorffa na lukę niemającą własności Hausdorffa.

Słowa kluczowe: uzwarcenie, automorfizm, algebra Boole'a

The author is responsible for the language in all paper.

* Institute of Mathematics, Faculty of Physics, Mathematics and Computer Science, Cracow University of Technology, Poland; magdag@pk.edu.pl.

It is known that cardinality of the group of automorphisms of $P(\omega)/\mathit{fin}$ depends on some additional axioms of ZFC. Under CH (the Continuum Hypothesis) the cardinality of the group is the largest posssible – it is equal to 2^c, where c denotes the continuum (cf. [2]). On the other hand, there are models of ZFC in which the cardinality is equal to the continuum, for example, in the model constructed by Shelah in [3]. In [4] it was shown by Shelah and Steprans that the assertion PFA + $c = \omega_2$ implies that all automorphisms of $P(\omega)/\mathit{fin}$ are trivial (i.e. induced by a bijection between co-finite subsets of ω). Velickovic [7] proved that the same thesis follows from OCA+MA. One of the methods of elimination an automorphim of $P(\omega)/\mathit{fin}$ is adding a new real which fills a non-separable gap in such a way that the image of the gap under that automorphism remains unfilled. It is known that each forcing which adds an element separating a Hausdorff gap collapses the to the ω. One can ask if the image of a Hausdorff gap under a automorphism must be a Hausdorff gap .

Basic facts and definitions. Byω we denote the set of all natural numbers (and the first infinite ordinal) and by fin the ideal of all its finite subsets.$P(\omega)/\mathit{fin}$ is the factor Boolean algebra and for $A, B \in P(\omega)$ we shall use the following notation: $A =_* B$ if $A \div B \in \mathit{fin}$, $A \subseteq_* B$ if $A \setminus B \in \mathit{fin}$.

Let λ, κ be ordinals. ***A gap of the type*** (λ, κ) in a Boolean algebra $(\mathcal{A},+,\bullet,0,1)$ is a pair $(\{a_\gamma: \gamma < \lambda\}, \{b_\beta: \beta < \kappa\})$ of subsets of $\mathcal{A}$ such that $a_\gamma \bullet b_\beta = 0$. If for every $\gamma_1 < \gamma_2 < \lambda$, $\beta_1 < \beta_2 < \kappa$, $a_{\gamma 1} \bullet a_{\gamma 2} = a_{\gamma 1}$ and $b_{\beta 1} \bullet b_{\beta 2} = b_{\beta 1}$ the gap is said to be ***incresingly ordered***. Elementc $\in \mathcal{A}$ ***fills (separates)*** the gap if $a_\gamma \bullet c = a_\gamma$ and $b_\beta \bullet c = 0$ for every $\gamma < \lambda$, $\beta < \kappa$. If there is no such an element, the gap is called ***non-separable***. A (strictly) decreasing sequence $(a_\beta: \beta < \gamma)$ of elements of the $\mathcal{A}$ of the lengthγ is called **g*-limit*** if there is no non-zero element $a \in \mathcal{A}$ such that for every $\beta < \gamma$, $a \bullet a_\beta = a$.

Assume that $\mathcal{L}=(\{X_\alpha: \alpha<\omega_1\}, \{Y_\beta: \beta < \omega_1)$ is an increasingly ordered gap in $P(\omega)/\mathit{fin}$. $\mathcal{L}$ is a ***Hausdorff gap*** if $\{\gamma < \beta: \max X_\gamma \cap Y_\beta < k\} = {}^*\varnothing$ for every $\beta < \omega_1$ and $k \in \omega$.

It is known that

1. In the algebra $P(\omega)/\mathit{fin}$ every countable gap (i.e. card(λ) = card(κ) = ω is filled.
2. There is no ω-limits (i.e.γ-limits with card (γ) = ω in the $P(\omega)/\mathit{fin}$.
3. A Hausdorff gap is non-separable (thus there exist non-separable gaps of the type (ω_1, ω_1) in the $P(\omega)/\mathit{fin}$.

In the following construction we shall apply the Sikorski's theorem (to define a required automorphism).

Theorem 1 (Sikorski [5, 6]**)** Let $\mathcal{A}$, $\mathcal{B}$ be Boolean algebras, $\mathcal{A}_0$ a subalgebra of $\mathcal{A}$ and $a_0 \in \mathcal{A} \setminus \mathcal{A}_0$. Assume that $T: \mathcal{A}_0 \to \mathcal{B}$ is a homomorphism. If there exists an element $b \in \mathcal{B}$ which fills a gap:

$$\mathcal{L} = (\{T(x): x \in \mathcal{A}_0, x \le a_0\}, \{T(x): x \in \mathcal{A}_0, x \bullet a_0 = 0\}),$$

then T can be extended to a homomorphism $T^*: \mathcal{A}_1 \to \mathcal{B}$ (where $\mathcal{A}_1$ is a subalgebra generated by $\mathcal{A}_0 \cup \{a_0\}$ with $T^*(a_0) = b$.

Moreover if T is monomorphism then T^* is monomorphism if and only if the following condition holds:

$$(*) \text{ for all } x, y \in \mathcal{A}_0 [\, (x \le a_0 \Leftrightarrow T(x) \le b) \quad \text{and} \quad (y \ge a_0 \Leftrightarrow T(y) \ge b)].$$

Thus, in order to extend a monomorphism, we have to ensure that an image of a (separeted) gap under the monomorphism satisfies the condition (*). Let us remind a (well known)

method how to find the required (in the (*)) element in the range of the monomorphism. Although the method can be applied in the case of Boolean algebras in which there are no countable gaps nor countable limits, we present it in the particular case of $P(\omega)/\mathit{fin}$.

Claim 1 (cf. [6]**)** Let T: $\mathsf{A} \to \mathsf{B}$ be a monomorphism of countable subalgebras of $P(\omega)/\mathsf{fin}$ and let $G \in P(\omega)/\mathsf{fin}\backslash\mathsf{A}$. Then there is a gap in B such that any element which fills the gap satisfies the condition (*).

Proof: Let $J = \{Z_n: n \in \omega\}$ be an enumeration of all elements $Z \in \mathsf{A}$ with $Z \cap G \neq_* \varnothing$ and $Z \backslash G \neq_* \varnothing$. Fix $n \in \omega$. For a $Z_n \in J$ and $X, Y \in \mathsf{A}$ we have:

If $Y \cap G =_* \varnothing$ then $Z_n \cap Y \cap G =_* \varnothing$. Since $Z \cap G \neq_* \varnothing$, it follows that $Z_n \backslash Y \neq_* \varnothing$. T is a monomorphism thus we have $T(Z_n)\backslash T(Y) \neq_* \varnothing$. In a similar way we show that if $X \subseteq_* G$ then $T(Z_n)\backslash T(X) \neq_* \varnothing$.

Since A is countable, there exists an enumeration $\{Y_m \in \mathsf{A}: m \in \omega\}$ of all elements which are almost disjoint with G. Thus:

$$\{T(Z_n)\backslash(T(Y_1) \cup ... \cup T(Y_m)): m \in \omega\}$$

is a countable decreasing chain in $P(\omega)/\mathit{fin}$. Since there are no countable limits in $P(\omega)/\mathit{fin}$, we can choose an infinite subset $S(Z_n) = S_n$ which is almost contained in each

$$T(Z_n)\backslash(T(Y_1) \cup ... \cup T(Y_m)).$$

In a similar way we can choose $I(Z_n) = I_n \subseteq_* T(Z_n)\backslash(T(X_1) \cup ... \cup T(X_m))$ for $X_m \in \mathsf{A}$, $X_m \subseteq_* G$ Consider the gap $\mathcal{P} = (\mathcal{M}, \mathcal{O})$ where:

$$\mathcal{M} = \{T(X) \in \mathsf{A}: X \subseteq_* G\} \cup \{T(I_n): n \in \omega\},$$

$$\mathcal{O} = \{T(Y) \in \mathsf{A}: Y \cap G =_* \varnothing\} \cup \{T(S_n): \quad n \in \omega\}.$$

Since P is countable, there exists element H which fills the gap. It is easy to see that such an element H satisfies the condition.

Main theorem. We prove that:

Theorem 2 If CH holds then there exists an automorphism T of $P(\omega)/\mathsf{fin}$ and two increasingly ordered gaps of the type (ω_1, ω_1):

$$\mathcal{L}_H = (\{X_\alpha: \alpha < \omega_1\}, \{Y_\beta: \beta < \omega_1\}), \quad \mathcal{L} = (\{A_\alpha: \alpha < \omega_1\}, \{B_\beta: \beta < \omega_1\})$$

such that

1. for all $\beta < \omega_1$ and every $k \in \omega$, a set $\{\alpha < \beta: \max(X_\alpha \cap Y_\beta) < k\}$ is finite,
2. if $\beta = \lambda + \omega$ for some limit ordinal $\lambda < \omega_1$ then there exists $k \in \omega$ such that a set $\{\alpha < \beta: \max(A_\alpha \cap B_\beta) < k\}$ is infinite,
3. for every $\alpha, \beta < \omega_1$, $T(A_\alpha) = X_\alpha$, $T(B_\beta) = Y_\beta$.

Proof: We construct the required automorphism and gaps by using transfinite induction. Fix a set $\{G_\alpha: \alpha < \omega_1\}$ of generators of $P(\omega)/\mathsf{fin}$. At the step $\alpha = 0$ fix two pairs of disjoint infinite subsets of ω: A_0, B_0 and X_0, Y_0 such that both sets $\omega\backslash(A_0 \cup B_0)$ and $\omega\backslash(X_0 \cup Y_0)$ are infinite. Let:

$$T_0(A_0) = X_0, \quad \text{and} \quad T_0(B_0) = Y_0.$$

Denote by $\underline{\mathbf{D}}_0$ and $\underline{\mathbf{P}}_0$ the Boolean algebras generated by $\{A_0, B_0\}$ and $\{X_0, Y_0\}$ (respectively) and extend T_0 to the isomorphism from $\underline{\mathbf{D}}_0$ onto $\underline{\mathbf{P}}_0$. Consider the first generator G_0 and the algebra $\underline{\mathbf{D}}_0$. In the way described in the Claim find element H_r in the $\underline{\mathbf{P}}_0$ and put $T_0(G_0) = H_r$. Then apply the claim to the G_0, the algebra $\underline{\mathbf{P}}_0$ and the T_0^{-1}. Choose any element H_d which fills the obtained gap in $\underline{\mathbf{D}}_0$ and define $T_0^{-1}(G_0) = H_d$. Then, using Sikorski's theorem, extend the isomorphism T_0 to an isomorphism from $\mathbf{D}_0$ (the subalgebra generated by $\{A_0, B_0, G_0, T^{-1}(G_0)\}$) onto $\mathbf{P}_0$ (the subalgebra generated by $\{X_0, Y_0, G_0, T_0(G_0)\}$).

Assume inductively that for every $\beta < \alpha$ we have defined increasing sequences of subalgebras $\mathbf{D}_\beta$, $\mathbf{P}_\beta$ of $P(\omega)/\mathit{fin}$, isomorphisms T_β: $\mathbf{D}_\beta \to \mathbf{P}_\beta$ and gaps

$$\mathcal{L} = (\{A_\gamma : \gamma < \alpha\}, \{B_\gamma : \gamma < \alpha\}) \text{ and } \mathcal{L}_H = (\{X_\gamma : \gamma < \alpha\}, \{Y_\gamma : \gamma < \alpha\})$$

such that

1. For all $\beta < \alpha$, $A_\beta, B_\beta, G_\beta \in \mathbf{D}_\beta$ and $X_\beta, Y_\beta, G_\beta \in \mathbf{P}_\beta$,
2. $\mathcal{L}$, $\mathcal{L}_H$ are increasingly ordered gaps,
3. For all $\beta < \alpha$, $A_\beta \cap B_\beta = \emptyset$ and $X_\beta \cap Y_\beta = \emptyset$; both sets $\omega \setminus (A_\beta \cup B_\beta)$ and $\omega \setminus (X_\beta \cup Y_\beta)$ are infinite,
4. For all $\beta < \alpha$ and every $k \in \omega$, the set $\{\gamma < \beta : \max(Y_\beta \cap X_\gamma) < k\}$ is finite,
5. If $\beta < \alpha$ is equal to $\lambda + \omega$, for some limit ordinal λ, then there exists $k \in \omega$ such that $\{\gamma < \beta : \max(B_\beta \cap A_\gamma) < k\}$ is infinite,
6. If $\beta = \lambda + n$, for some limit ordinal λ and a natural number $n > 0$, then

$$(\bigcup_{k \le n} A_{\lambda + k}) \cap (\bigcup_{k \le n} B_{\lambda + k}) = \emptyset.$$

7. For $\gamma < \beta < \alpha$, $T_\beta | \mathbf{D}_\gamma = T_\gamma$ and $T(A_\beta) = X_\beta$, $T(B_\beta) = Y_\beta$.

Assume that α is a successor ordinal, $\alpha = \beta + 1$. Then there exist a limit ordinal λ and a natural number $n > 0$ such that $\alpha = \lambda + n$. Choose infinite and disjoint subsets A, B of ω such that:

$$(A_\beta \cup B_\beta) \cap (A \cup B) = \emptyset \text{ and } \omega \setminus (A_\beta \cup B_\beta \cup A \cup B) \text{ is infinite}$$

and both sets $B \cap \bigcup_{k \le n} A_{\lambda + k}$ and $A \cap (\bigcup_{k \le n} B_{\lambda + k})$ are empty. Put:

$$A_\alpha = A_\beta \cup A, \quad B_\alpha = B_\beta \cup B.$$

Let $\underline{\mathbf{D}}_\alpha$ be subalgebra generated by $\mathbf{D}_\beta$ and the elements A_α, B_α. Apply The Claim to choose candidates for images of A_α, B_α (and then Sikorski's theorem to extend T_β). Denote this extension by T^*_β. Note, that each of sets $T^*_\beta(A_\alpha)$ and $T^*_\beta(B_\alpha)$ separates $\mathcal{L}_H$ and we may assume that they are disjoint. Define

$$X_\alpha = T^*_\beta(A_\alpha), \quad Y_\alpha = T^*_\beta(B_\alpha).$$

Since $Y_\beta \subseteq^* Y_\alpha$ and for every natural number k, the set $\{\gamma < \beta : \max(Y_\beta \cap X_\gamma) < k\}$ is finite, it follows that the set $\{\gamma < \alpha : \max(Y_\alpha \cap X_\gamma) < k\}$ is finite as well. If $G_\alpha \in \underline{\mathbf{D}}_\alpha$ then we add, in the same way, an image $T^*_\beta(G_\alpha)$. Let $\underline{\mathbf{P}}_\alpha$ be the subalgebra generated by $\mathbf{P}_\beta$ and the elements X_α, Y_α and $T^*_\beta(G_\alpha)$. If $G_\alpha \in \underline{\mathbf{P}}_\alpha$, then a preimage $T^{*-1}_\beta(G_\alpha)$ of a generator G_α has to be added. We fix the preimage in the way described above. We conclude the successor step with definitions of $\mathbf{D}_\alpha$ and $\mathbf{P}_\alpha$. $\mathbf{D}_\alpha$ is a subalgebra generated by $\mathbf{D}_\beta$ and A_α, B_α, G_α, $T^{*-1}_\beta(G_\alpha)$

while $\mathbf{P}_\alpha$ is generated by $\mathbf{P}_\beta$ and X_α, Y_α, G_α, $T^*_\beta(G_\alpha)$. Moreover $T_\alpha = T^*_\beta : \mathbf{D}_\alpha \to \mathbf{P}_\alpha$. It is obvious that all inductive assumptions are satisfied.

Assume that α is a limit ordinal. Put:

$$\underline{\mathbf{D}}_\alpha = \bigcup_{\beta<\alpha} \mathbf{D}_\beta,\ \underline{\mathbf{P}}_\alpha = \bigcup_{\beta<\alpha} \mathbf{P}_\beta,\quad T = \bigcup_{\beta<\alpha} T_\beta.$$

In order to construct elements X_α and Y_α we modify slightly Hausdorff argument (presented in [1]). The sequence $(\omega\backslash(X_\beta \cup Y_\beta): \beta < \alpha)$ is countable and decreasing; it follows that there exists an infinite set $D \subseteq \omega$ with $D \subseteq_* \omega\backslash(X_\beta \cup Y_\beta)$ for all $\beta < \alpha$. Thus $X_\beta \cup Y_\beta \subseteq_* D^c = \omega\backslash D$. Since:

$$\mathcal{L}_H = (\{X_\gamma: \gamma < \alpha\},\ \{Y_\gamma: \gamma < \alpha\})$$

is countable, one can choose a set F which separates the gap i.e. for all $\beta < \alpha$, $Y_\beta \subseteq_* F$ and $X_\beta \cap F =_* \varnothing$. Moreover, we may assume that $F \subseteq D^c$ (replacing F with $F \cap D$, if necessary). Applying the claim and Sikorski's theorem we fix a $\$T^{-1}(F)$, which fills the gap $\mathcal{L}$. Note that for every $\beta < \alpha$ and $k \in$ the set $\{\gamma < \beta: \max(F \cap X_\gamma) < k\}$ is finite however it does not follow that for each $k \in \omega$ the set $\{\gamma < \alpha: \max(F \cap X_\gamma) < k\}$ is finite. In order to ensure that the assertion holds we have to enlarge the set F. For $k \cap \omega$ let

$$\mathcal{J}_k = \{\gamma < \alpha: \max(F \cap X_\gamma) < k\}.$$

We define (inductively) a (countable) increasing sequence $F = F_0 \subseteq F_1 \subseteq F_2 \subseteq \ldots$ such that for every n, $k \in \omega$ the set $\{\gamma \in \mathcal{J}_n: \max(F_{n+1} \cap X_\gamma) < k\}$ is finite and $F_n \cap X_\gamma =_* \varnothing$.

Assume that sets $F = F_0 \subseteq F_1 \subseteq F_2 \subseteq \ldots \subseteq F_n$ and their preimages under T have been defined. Denote by $\mathbf{P}_{\alpha, n+1}$ the subalgebra generated by $\mathbf{P}_{\alpha, n}$ and F_{n-1} and by $\mathbf{D}_{\alpha, n+1}$ the subalgebra generated by $\mathbf{D}_{\alpha, n}$ and $T^{-1}(F_{n-1})$, for $n > 0$.

If $\mathcal{J}_{n+1}$ is finite, then $F_{n+1} = F_n$. So suppose that $\mathcal{J}_{n+1}$ is infinite. Then $\mathcal{J}_{n+1}$ can be increasigly enumerated with natural numbers and $\sup \mathcal{J}_{n+1} = \alpha$. Indeed, this is implied by the fact, that for each $\beta < \alpha$ the set $\beta \cap \mathcal{J}_{n+1} = \{\gamma < \beta: \max(F \cap X_\gamma) < k\}$ is finite.

The subalgebra $\mathbf{P}_{\alpha, n}$ is countable thus we can fix an enumeration $\{K_i: i \in \omega\}$ of all elemets $K \in \mathbf{P}_{\alpha, n}$ such that $K \cap X_\gamma =_* \varnothing$ for $\gamma < \alpha$.

Thus let $\mathcal{J}_{n+1} = \{l: l \in \omega\}, \gamma_l < \gamma_{l+1}$. The sequence $\{X_\gamma: \gamma < \alpha\}$ is increasing, which implies that $X_{\gamma l}\backslash(X_{\gamma 0} \cup X_{\gamma 1} \cup \ldots \cup X_{\gamma l-1}) \neq *\varnothing$. Moreover, $X_{\gamma l} \subseteq_* D^c$, thus

$$D^c \cap [X_{\gamma l}\backslash(X_{\gamma 0} \cup X_{\gamma 1} \cup \ldots \cup X_{\gamma l-1})] \neq^* \varnothing.$$

It follows that for every $l \in \omega$ there exists a natural number

$$j_l \in D^c \cap [X_{\gamma l}\backslash(X_{\gamma 0} \cup X_{\gamma 1} \cup \ldots \cup X_{\gamma l-1})] \cap (\omega\backslash\bigcup_{i \le l} K\_i)$$

with $j_l > l$. Put

$$F_{n+1} = F_n \cup \{j_l: l \in \omega\}.$$

It is easy to note that $\{j_l: l \in \omega\} \cap X_{\gamma i}$ is finite for every $i \in \omega$. Since the sequence $\{X_\gamma: \gamma < \alpha\}$ is increasing it follows that $\{j_l: l \in \omega\} \cap X_\gamma =\_ *\varnothing$ and $F_{n+1} \cap X_\gamma =_* \varnothing$ for each $\gamma < \alpha$. Moreover for each $k \in \omega$ the set $\{\gamma \in \mathcal{J}_n: \max(F_{n+1} \cap X_\gamma) < k\}\$$ is finite. Extend the range of the isomorphism T in the following way: $\mathcal{D} = (\mathcal{M}, O)$

$$\mathcal{M} = \{T^{-1}(X) \in \mathbf{D}_{\alpha,n}: X \subseteq_* F_n\} \cup \{T^{-1}(I(Z)): Z \in J\},$$

$$O = \{T^{-1}(Y) \in \mathbf{D}_{\alpha,n}: Y \cap F_n =_* \varnothing\} \cup \{T^{-1}(S(Z)): Z \in J\},$$

where $J = \{Z \in \mathbf{P}_{\alpha, n+1}: Z \cap F_n \neq_* \varnothing, Z \setminus F_n \neq_* \varnothing\}$ and elements $S(Z)$, $I(Z)$ are defined for each $Z \in J$ in the way described in proof of the Claim.

Since $\mathcal{D}$ is countable, then there exist infinite sets C_n, H_n such that C_n separates the gap and H_n is almost disjoint with every element of the sets forming the gap. Note that since $F_n \cap X_\beta =_* \varnothing$ and $Y_\beta \subseteq_* F_n$ then, by the Claim, $C_n \cap A_\beta =_* \varnothing$ and $C_n \subseteq_* B_\beta$, for $\beta < \alpha$. If, for some limit ordinal λ, $\alpha = \lambda + \omega$ then, by inductive assumption, $(\bigcup_{k\in\omega} A_{\lambda+k}) \cap (\bigcup_{k\in\omega} B_{\lambda+k}) = \varnothing$. Moreover, since for every $L \in \mathbf{D}_{\alpha,n}$ with $L \cap A_\gamma =_* \varnothing$ there exists $i \in \omega$ such that $T(L) = K_i$, it follows that $C_n \cap L =_* \varnothing$. Thus we may assume that

$$C_n \cap \bigcup_{k\in\omega} A_{\lambda+k} = \varnothing.$$

Put $T^{\wedge}\{-1\}(F_n) = C_n$.
Since

$$\bigcup_{n\in\omega} C_n \cap \bigcup_{k\in\omega} A_{\lambda+k} = \varnothing$$

then in the case $\alpha = \lambda + \omega$, for some limit ordinal λ, we can choose B_α which fills the gap:

$$(\{B_\gamma: \gamma < \alpha\} \cup \{C_n: n \in \omega\}, \{A_\gamma: \gamma < \alpha\})$$

and $B_\alpha \cap A_{\lambda+k} = \varnothing$ for each $k \in \omega$. Apply the the Claim theorem to determine a Y_α and Sikorski's theorem to extend the T. Note, that the element separates the gap

$$\mathcal{P} = (\{F_n: n \in \omega\}, \{X_\gamma: \gamma < \alpha\}).$$

We may assume that $F \subseteq Y_\alpha \subseteq D^c$. We have to show that for each $k \in \omega$ the set $\{\gamma < \alpha: \max(Y_\alpha \cap X_\gamma) < k\}$ is finite. Assume to the contrary that for some $k \in \omega$ the set is infinite. Since $F \subseteq Y_\alpha$ then $\{\gamma < \alpha: \max(Y_\alpha \cap X_\gamma) < k\} \subseteq \mathcal{J}_k$. The latter assumtion implies that the set $\mathcal{I} = \{\gamma \in \mathcal{J}_k: \max(Y_\alpha \cap X_\gamma) < k\}$ is infinite as well. But since $F \subseteq Y_\alpha$, $\mathcal{I} \subseteq \{\gamma \in \mathcal{J}_n: \max F_{n+1} \cap X_\gamma < k\} =_* \varnothing$, a contradiction.

Put $X_\alpha = D^c \setminus Y_\alpha$. Now, apply the Claim to define A_α and using Sikorski's theorem extend the T.

Define $\mathbf{D}_\alpha$ ($\mathbf{P}_\alpha$) as the subalgebra generated by $\bigcup_{n\in\omega} \mathbf{D}_{\alpha,n}$, A_α and B_α ($\bigcup_{n\in\omega} \mathbf{P}_{\alpha,n}$ and X_α and Y_α). The automorphism T_α is equal to the (extended) T: $\mathbf{D}_\alpha \to \mathbf{P}_\alpha$.

This finishes the the limit step of the construction.

After ω_1 steps each of algebras $\mathbf{P} = \bigcup_{\alpha<\omega_1} \mathbf{P}_\alpha$ and $\mathbf{D} = \bigcup_{\alpha<\omega_1} \mathbf{D}_\alpha$ contains all of the generators G_α, thus $\mathbf{P} = \mathbf{D} = P(\omega)/\mathrm{fin}$. $T = \bigcup_{\alpha<\omega} 1\ T_\alpha$ is an isomorphism of $P(\omega)/\mathrm{fin}$. The gap

$$\mathcal{L}_H = (\{X_\gamma: \gamma < \omega_1\}, \{Y_\gamma: \gamma < \omega_1\})$$

is a Hausdorff gap, while the gap

$$\mathcal{L} = (\{A_\gamma: \gamma < \omega_1\}, \{B_\gamma: \gamma < \omega_1\})$$

does not satisfy the condition.

References

[1] F Hausdorff Summen von Mengen, F. Mengen, Fund. Math. 26, 1936, 241-255

[2] Rudin W., *Homogenity problems in the theory of Čech compactification*, Duke Math. Journal 23, 1956, 409-419.

[3] Shelah S., *Proper Forcing*, Lecture Notes in Mathematics 940, Springer Verlag, Berlin 1982.

[4] Steprans J., Shelah S., *PFA implies all automorphisms are trivial*, Proc. Amer. Math. Soc. vol. 104, no. 4, 1988, 1220-1225.

[5] Sikorski R., *On an analogy between measures and homomorphisms*, Ann. Soc. Pol. Math. 23, 1950, 1-20.

[6] Sikorski R., *Boolean Algebras*, Sprnger-Verlag, Berlin 1969.

[7] Velickovic B., *OCA and automorphisms of P(ω)/fin Topology and its Applications*, vol. 49, 1993, 1-13.

TECHNICAL TRANSACTIONS | **CZASOPISMO TECHNICZNE**
FUNDAMENTAL SCIENCES | NAUKI PODSTAWOWE
3-NP/2014

MONIKA HERZOG*

THE DEGREE OF APPROXIMATION OF FUNCTIONS FROM EXPONENTIAL WEIGHT SPACES

RZĄD APROKSYMACJI FUNKCJI Z WYKŁADNICZYCH PRZESTRZENI WAGOWYCH

A b s t r a c t

This paper presents a study of the approximation properties of modified Szász-Mirakyan operators for functions from exponential weight spaces. We present theorems giving the degree of approximation by these operators using a modulus of continuity.

Keywords: linear positive operators, Bessel function, modulus of continuity, degree of approximation

S t r e s z c z e n i e

W artykule badamy aproksymacyjne własności zmodyfikowanych operatorów typu Szásza-Mirakyana dla funkcji z wykładniczych przestrzeni wagowych. Przedstawiamy twierdzenia podające rząd aproksymacji funkcji przez operatory tego typu, wykorzystując moduł ciągłości.

Słowa kluczowe: dodatni operator liniowy, funkcja Bessela, moduł ciągłości, rząd aproksymacji

* Institute of Mathematics, Faculty of Physics, Mathematics and Computer Science, Cracow University of Technology; mherzog@pk.edu.pl.

1. Introduction

Let us denote the set of all real-valued functions continuous on $\mathbb{R}_0 = [0;\infty)$ by $C(\mathbb{R}_0)$. In paper [6] we investigated Szász-Mirakyan type operators defined as follows

$$L_n^{\nu}(f;x) = \begin{cases} \sum_{k=0}^{\infty} q_{n,k}^{\nu}(x) f\left(\frac{2k}{n+p}\right), & x > 0; \\ f(0), & x = 0 \end{cases} \tag{1}$$

and

$$q_{n,k}^{\nu}(x) = \frac{1}{I_{\nu}(nx)} \frac{(nx)^{2k+\nu}}{2^{2k+\nu}\Gamma(k+1)\Gamma(k+\nu+1)},$$

where Γ is the gamma function and I_{ν} the modified Bessel function defined by

$$I_{\nu}(z) = \sum_{k=0}^{\infty} \frac{z^{2k+\nu}}{2^{2k+\nu}\Gamma(k+1)\Gamma(k+\nu+1)}.$$

Approximation properties of these operators in exponential weight spaces were studied. Such spaces were denoted by

$$E_p = \{f \in C(\mathbb{R}_0): w_p f \text{ is uniformly continuous and bounded on } \mathbb{R}_0\},$$

where w_p is the exponential weight function defined as follows

$$w_p(x) = e^{-px}, \ p \in \mathbb{R}_0 \tag{2}$$

for $x \in \mathbb{R}_0$.
In the spaces we introduced the norm

$$\|f\|_p = \sup\{w_p(x)|f(x)|: x \in \mathbb{R}_0\} \tag{3}$$

and we established ([6], Theorem 2.1) that operators L_n^{ν} are linear, positive, bounded and transform the space E_p into E_p.

In the present paper, we shall prove theorems giving a degree of approximation of functions from E_p by these operators. We use the weighted modulus of continuity of the first and the second order defined as follows,

$$\omega\big(f, E_p; t\big) = \sup\big\{\|\Delta_h f\|_p:\ h \in [0,t]\big\} \tag{4}$$

and

$$\omega^2\big(f, E_p; t\big) = \sup\Big\{\big\|\Delta_h^2 f\big\|_p:\ h \in [0,t]\Big\} \tag{5}$$

respectively, where

$$\Delta_h f(x) = f(x+h) - f(x), \quad \Delta_h^2 f(x) = f(x+2h) - 2f(x+h) + f(x)$$

for $x, h \in \mathbb{R}_0$.

The note was inspired by the results of [8, 9] which investigate approximation problems for integral operators defined in weighted spaces. The considered method of proving the main theorems is also found in papers [1-4, 10].

2. Auxiliary results

The preliminary results, which we immediately obtained from papers [5-7] and definition (1), are recalled below.

Lemma 2.1 ([5], Lemma 8)
For all $v \in \mathbb{R}_0$ there exists a positive constant $M(v)$ such that for all $n \in \mathbb{N}$ and $x \in \mathbb{R}_0$, we have

$$\left|\frac{I_{v+1}(nx)}{I_v(nx)}\right| \le M(v), \ \ nx\left|\frac{I_{v+1}(nx)}{I_v(nx)} - 1\right| \le M(v).$$

Through elementary calculations we get

Lemma 2.2 ([6], Lemma 2.2)
For all $n \in \mathbb{N}$, $v, p \in \mathbb{R}_0$ and $x \in \mathbb{R}_0$

$$L_n^v(1,x) = 1, \ \ L_n^v(t,x) = \frac{nx}{n+p}\frac{I_{v+1}(nx)}{I_v(nx)},$$

$$L_n^v(t^2,x) = \left(\frac{nx}{n+p}\right)^2 \frac{I_{v+2}(nx)}{I_v(nx)} + \frac{2nx}{(n+p)^2}\frac{I_{v+1}(nx)}{I_v(nx)},$$

$$L_n^{\nu}(t-x,x) = x\left(\frac{n}{n+p}\frac{I_{\nu+1}(nx)}{I_{\nu}(nx)} - 1\right),$$

$$L_n^{\nu}((t-x)^2;x) = x^2\left(\left(\frac{n}{n+p}\right)^2\frac{I_{\nu+2}(nx)}{I_{\nu}(nx)} - \frac{2n}{n+p}\frac{I_{\nu+1}(nx)}{I_{\nu}(nx)} + 1\right) + \frac{2nx}{(n+p)^2}\frac{I_{\nu+1}(nx)}{I_{\nu}(nx)}.$$

Lemma 2.3 ([6], Lemma 2.5)
For all $\nu, p \in \mathbb{R}_0$ there exists a positive constant $M(\nu,p)$ such that for all $n \in \mathbb{N}$, we have

$$\left\|L_n^{\nu}\left(1/w_p\,;\cdot\right)\right\|_p \leq M(\nu,p).$$

An obvious consequence of the above lemma and definition (3) is
Theorem 2.4 ([6], Theorem 2.1)
For all $\nu, p \in \mathbb{R}_0$ there exists a positive constant $M(\nu,p)$ such that for all $n \in \mathbb{N}$ and $f \in E_p$, we have

$$\|L_n^{\nu}(f;\cdot)\|_p \leq M(\nu,p)\|f\|_p.$$

Applying Lemma 2.1 and Lemma 2.2, we obtain
Lemma 2.5
For all $\nu, p \in \mathbb{R}_0$ there exists a positive constant $M(\nu,p)$ such that for all $n \in \mathbb{N}$ and $x \in \mathbb{R}_0$, we have

$$|L_n^{\nu}((t-x)^2;x)| \leq M(\nu,p)\frac{x(x+1)}{n}.$$

Lemma 2.6 ([6], Lemma 2.6)
For all $\nu, p \in \mathbb{R}_0$ there exists a positive constant $M(\nu,p)$ such that for all $n \in \mathbb{N}$ and $x \in \mathbb{R}_0$, we have

$$w_p(x)\left|L_n^{\nu}\left(\frac{(t-x)^2}{w_p(t)};x\right)\right| \leq M(\nu,p)\frac{x(x+1)}{n}.$$

3. Approximation theorems

The following theorems estimate the weighted error of approximation for functions belonging to the spaces $E_p^k = \{f \in E_p : f',\ f'', \dots, f^{(k)} \in E_p\}$, where $f^{(i)}$ is denoted the *i*-th derivative of f.

Theorem 3.1

For all $\nu, p \in \mathbb{R}_0$ *there exists a positive constant* $M(\nu, p)$ *such that for all* $n \in \mathbb{N}$, $x \in \mathbb{R}_0$ *and* $g \in E_p^1$, *we have*

$$w_p(x)|L_n^{\nu}(g;x) - g(x)| \le M(\nu,p)\|g'\|_p \sqrt{\frac{x(x+1)}{n}}.$$

Theorem 3.2

For all $\nu, p \in \mathbb{R}_0$ *there exists a positive constant* $M(\nu, p)$ *such that for all* $n \in \mathbb{N}$, $x \in \mathbb{R}_0$ *and* $f \in E_p$, *we have*

$$w_p(x)|L_n^{\nu}(f;x) - f(x)| \le M(\nu,p)\omega\left(f, E_p; \sqrt{\frac{x(x+1)}{n}}\right).$$

The proof for the above theorems is analogous to the proof of Theorem 4 and Theorem 5 which are detailed in paper [5].

Theorem 3.2 implies the following corollary.

Corollary 3.3

If $\nu, p \in \mathbb{R}_0$ *and* $f \in E_p$, *then for all* $x \in \mathbb{R}_0$

$$\lim_{n\to\infty}\{L_n^{\nu}(f;x) - f(x)\} = 0.$$

Moreover, the above convergence is uniform on every set $[x_1, x_2]$ *with* $0 \le x_1 < x_2$.

Remark 3.4

The above result can be achieved in a different way; see [7] for more details.

Analogous with papers [8, 9], we define operators H_n^{ν} to estimate the error of approximation by the second moduli of continuity (5).

$$H_n^{\nu}(f;x) = L_n^{\nu}(f;x) - f(L_n^{\nu}(t;x)) + f(x) \tag{6}$$

for $\nu, p \in \mathbb{R}_0$, $f \in E_p$ and $x \in \mathbb{R}_0$. By using Lemma 2.2 we obtain

$$H_n^{\nu}(f;x) = L_n^{\nu}(f;x) - f\left(\frac{nx}{n+p}\frac{I_{\nu+1}(nx)}{I_{\nu}(nx)}\right) + f(x).$$

Observe that the operators are linear. Moreover, Lemma 2.2 allows us to write

$$H_n^{\nu}(1;x) = 1, \quad H_n^{\nu}(t-x;x) = 0. \tag{7}$$

Lemma 3.5
For all $\nu, p \in \mathbb{R}_0$ *there exists a positive constant* $M(\nu,p)$ *such that for all* $n \in N$, $x \in \mathbb{R}_0$ *and* $g \in E_p^2$, *we have*

$$w_p|H_n^{\nu}(g;x) - g(x)| \le M(\nu,p)\|g''\|_p \frac{x(x+1)}{n}.$$

Proof. Let $x \in \mathbb{R}_0$ and $g \in E_p^2$ be fixed. Through the use of the Taylor formula we can write

$$g(t) - g(x) = (t-x)g'(x) + \int_x^t (t-u)g''(u)\,du$$

for $t > 0$. By applying the linearity of H_n^{ν} and (7) we derive

$$|H_n^{\nu}(g;x) - g(x)| = |H_n^{\nu}(g(t) - g(x);x)| = \left|H_n^{\nu}\left(\int_x^t (t-u)g''(u)du\,;x\right)\right|. \tag{8}$$

Furthermore, the definition of H_n^{ν} implies

$$H_n^{\nu}\left(\int_x^t (t-u)g''(u)du\,;x\right) = L_n^{\nu}\left(\int_x^t (t-u)g''(u)du\,;x\right) - \int_x^{L_n^{\nu}(t;x)} (L_n^{\nu}(t;x)-u)g''(u)du$$

Estimating (8), we have

$$|H_n^{\nu}(g;x) - g(x)| \le L_n^{\nu}\left(\left|\int_x^t (t-u)g''(u)du\right|;x\right) + \left|\int_x^{L_n^{\nu}(t;x)} (L_n^{\nu}(t;x)-u)g''(u)du\right|.$$

Since

$$\left|\int_x^t (t-u)g''(u)du\right| \le \frac{1}{2}\|g''\|_p (t-x)^2 (e^{px}+e^{pt})$$

and

$$\begin{aligned}\left|\int_x^{L_n^\nu(t;x)} (L_n^\nu(t;x)-u)g''(u)du\right| &\le \frac{1}{2}\|g''\|_p (L_n^\nu(t;x)-x)^2\left(e^{px}+e^{pL_n^\nu(t;x)}\right)\\ &\le \frac{1}{2}\|g''\|_p \left(L_n^\nu(t-x;x)\right)^2 e^{px}\left(1+e^{pL_n^\nu(t-x;x)}\right)\\ &\le \frac{1}{2}M(\nu,p)\|g''\|_p \left(L_n^\nu(t-x;x)\right)^2 e^{px}\end{aligned}$$

we get

$$\begin{aligned}w_p(x)|H_n^\nu(g;x)-g(x)| &\\ &\le \frac{1}{2}\|g''\|_p L_n^\nu((t-x)^2;x)+\frac{1}{2}\|g''\|_p w_p(x) L_n^\nu\left(\frac{(t-x)^2}{w_p(t)};x\right)\\ &+\frac{1}{2}M(\nu,p)\|g''\|_p \left(L_n^\nu(t-x;x)\right)^2\end{aligned}$$

Applying Hölder's inequality to the term $L_n^\nu(t-x;x)$ and Lemmas 2.5, 2.6, we obtain the desired estimation.

Theorem 3.6
For all $\nu, p \in \mathbb{R}_0$ there exists a positive constant $M(\nu,p)$ such that for all $n \in \mathbb{N}$, $x \in \mathbb{R}_0$ and $f \in E_p$, we have

$$\begin{aligned}w_p|L_n^\nu(f;x)-f(x)| &\\ &\le M(\nu,p)\omega^2\left(f,E_p;\sqrt{\frac{x(x+1)}{n}}\right)+\omega\left(f,E_p;|L_n^\nu(t-x;x)|\right).\end{aligned}$$

Proof. Let $x \in \mathbb{R}_0$ and f_h be the second order Steklov mean of $f \in E_p$, i.e.

$$f_h(x)=\frac{4}{h^2}\int_0^{\frac{h}{2}}\int_0^{\frac{h}{2}}\left\{2f(x+s+t)-f\left(x+2(s+t)\right)\right\}dsdt\,, \qquad x \in \mathbb{R}_0, h>0.$$

Notice that

$$f(x) - f_h(x) = \frac{4}{h^2}\int_0^{\frac{h}{2}}\int_0^{\frac{h}{2}} \Delta_{s+t}^2 f(x)dsdt.$$

By definitions (3) and (5), we get the following estimations

$$\|f - f_h\|_p \le \omega^2\big(f, E_p; h\big)$$

and since

$$f_h''(x) = \frac{1}{h^2}\Big(8\Delta_{h/2}^2 f(x) - \Delta_h^2 f(x)\Big)$$

we can write

$$\|f_h''\|_p \le \frac{9}{h^2}\omega^2\big(f, E_p; h\big).$$

The above inequalities imply that the Steklov mean f_h and f_h'' belong to E_p. Moreover, by linearity of L_n^ν and connection (6), we have

$$\begin{aligned}|L_n^\nu(f;x) - f(x)| &\le H_n^\nu(|f - f_h|;x) + |f(x) - f_h(x)| + |H_n^\nu(f_h;x) - f_h(x)| \\ &+ \big|f\big(L_n^\nu(t;x)\big) - f(x)\big|.\end{aligned}$$

Applying the above estimation, Theorem 2.1 and Lemma 3.5, we conclude that

$$\begin{aligned}w_p(x)|L_n^\nu(f;x) - f(x)| &\le w_p(x)H_n^\nu(|f - f_h|;x) + w_p(x)|f(x) - f_h(x)| \\ &+ w_p(x)|H_n^\nu(f_h;x) - f_h(x)| + w_p(x)\big|f\big(L_n^\nu(t;x)\big) - f(x)\big| \\ &\le M(\nu,p)\|f - f_h\|_p + M(\nu,p)\|f_h''\|_p \frac{x(x+1)}{n} \\ &+ w_p(x)\big|f\big(L_n^\nu(t;x)\big) - f(x)\big| \\ &\le M(\nu,p)\omega^2\big(f, E_p; h\big)\left(1 + \frac{1}{h^2}\frac{x(x+1)}{n}\right) \\ &+ \omega\big(f, E_p; |L_n^\nu(t-x;x)|\big),\end{aligned}$$

where $L_n^\nu(t-x;x) = x\frac{I_{\nu+1}(nx)}{I_\nu(nx)} - x$. Substituting $h = \sqrt{\frac{x(x+1)}{n}}$, we get the assertion of our theorem.

The author would like to thank the referees for their helpful remarks which greatly improved the exposition of the paper.

References

[1] Becker M., *Global approximation theorems for Szász-Mirakjan and Baskakov operators in polynomial weight spaces*, Indiana Univ. Math. J. **27**, 1, 1978, 127-142.

[2] Becker M., Kucharski D., Nessel R.J., *Global approximation theorems for the Szász-Mirakjan operators in exponential weight spaces*, Linear Spaces and Approximation (Proc. Conf., Math. Res. Inst., Oberwolfach, 1977), ISNM, vol. 40, Birkhäuser, Besel 1978, 319-333.

[3] Durrmeyer J.L., *Une formule d'inversion de la transformée de Laplace: Applications à la théorie des moments*, Thèse de 3ème cycle. Faculté des Sciences Univ., Paris 1967.

[4] Heilmann M., *Direct and converse results for operators of Baskakov-Durrmeyer type*, Approx. Theory Appl. **5**, 1, 1989, 105-127.

[5] Herzog M., *Approximation of functions from exponential weight spaces by operators of Szász-Mirakyan type*, Comment. Math. **43**, 1, 2003, 77-94.

[6] Herzog M., *Approximation of functions of two variables from exponential weight spaces*, Czasopismo Techniczne, **1-NP**/2012, 3-10.

[7] Herzog M., *A note on the convergence of partial Szász-Mirakyan type operators*, Ann. Univ. Pedagog. Crac. Stud. Math. **13**, 2014, 45-50.

[8] Krech G., S*ome approximation results for operators of Szász-Mirakyan-Durrmeyer type*, Math. Slovaca (in print).

[9] Krech G., *On the rate of convergence for modified gamma operators*, Rev. Un. Mat. Argentina (in print).

[10] Rempulska L., Thiel A., *Approximation of functions by certain nonlinear integral operators*, Lith. Math. J. **48**, 4, 2008, 451-462.

TECHNICAL TRANSACTIONS | **CZASOPISMO TECHNICZNE**
FUNDAMENTAL SCIENCES | NAUKI PODSTAWOWE
3-NP/2014

GRAŻYNA KRECH*

AN INVESTIGATION OF THE APPROXIMATION OF FUNCTIONS OF TWO VARIABLES BY THE POISSON INTEGRAL FOR HERMITE EXPANSIONS

APROKSYMACJA FUNKCJI DWÓCH ZMIENNYCH CAŁKĄ POISSONA ZWIĄZANĄ Z WIELOMIANAMI HERMITE'A

A b s t r a c t

This paper presents a study of the approximation properties of the Poisson integral for Hermite expansions in the space L^p. The rate of convergence of functions of two variables by these integrals is established.

Keywords: rate of convergence; Poisson integral; Hermite expansions, positive linear operators

S t r e s z c z e n i e

Artykuł poświęcony jest własnościom aproksymacyjnym całek Poissona związanych z wielomianami Hermite'a. Udowodniono twierdzenie o rzędzie zbieżności funkcji dwóch zmiennych w przestrzeni L^p tymi operatorami.

Słowa kluczowe: promień zbieżności, całka Poissona, wielomiany Hermite'a, dodatnie operatory liniowe

* Institute of Mathematics, Pedagogical University of Cracow, Kraków, Poland; gkrech@up.krakow.pl.

1. Introduction

Let $1 \le p \le \infty$, we denote by $L^p(\mathbb{R}^2)$ the set of all the Lebesgue measurable functions f defined on $\mathbb{R}^2$ such that $\int_{-\infty}^{\infty}\int_{-\infty}^{\infty} |f(t_1,t_2)|^p \, dt_1 dt_2 < \infty$ if $1 \le p < \infty$, and if $p = \infty$ we require f to be bounded almost everywhere on $\mathbb{R}^2$.

In this paper, we present approximation properties of the Poisson integral $\overline{A}$ in the space $L^p(\mathbb{R}^2)$, $1 \le p \le \infty$ defined by:

$$\overline{A}(f;r,y_1,y_2) = \int_{-\infty}^{\infty}\int_{-\infty}^{\infty} r K(r,y_1,z_1)K(r,y_2,z_2) f(z_1,z_2)dz_1 dz_2, \quad 0 < r < 1,$$

where:

$$K(r,y,z) = \sum_{n=0}^{\infty} r^n h_n(y)h_n(z) = \frac{1}{\left(\pi(1-r^2)\right)^{\frac{1}{2}}} \exp\left(-\frac{1}{2}\cdot\frac{1+r^2}{1-r^2}\left(y^2+z^2\right)+\frac{2ryz}{1-r^2}\right),$$

$$h_n(x) = \left(2^n n!\sqrt{\pi}\right)^{-\frac{1}{2}} \exp\left(-\frac{x^2}{2}\right) H_n(x)$$

and H_n is the n th Hermite polynomial (see [11]). The norm in $L^p(\mathbb{R}^2)$ is given by:

$$\| f \|_p = \begin{cases} \left(\int_{-\infty}^{\infty}\int_{-\infty}^{\infty} |f(t_1,t_2)|^p \, dt_1 dt_2\right)^{\frac{1}{p}}, & 1 \le p < \infty, \\ \sup_{(t_1,t_2)\in\mathbb{R}^2} ess\, |f(t_1,t_2)|, & p = \infty. \end{cases}$$

Some convergence theorems, the Voronovskaya formula, and a boundary value problem for the integral $\overline{A}$ were presented in [5]. The following result was proved (see [5]):

Theorem 1 Let $\overline{y} = (\overline{y}_1, \overline{y}_2) \in \mathbb{R}^2$ and $f = f_1 + f_2$, where $f_1 \in L^1(\mathbb{R}^2)$, $f_2 \in L^\infty(\mathbb{R}^2)$. If f is continuous at $\overline{y}$, then:

$$\lim_{(r,y)\to(1^-,\overline{y})} \overline{A}(f;r,y) = f(\overline{y}), \quad y = (y_1,y_2).$$

In this paper we shall give an order of approximation of functions belonging to $L^p(\mathbb{R}^2)$ by the operator $\overline{A}$. It is worth mentioning that approximation properties of Poisson integrals for orthogonal expansions and their various modifications were also studied in [4, 12, 6–10], in one and two dimensions.

Some auxiliary results, which will be needed in the next part of this paper, are now presented. It is clear that $\overline{A}(f;r,y_1,y_2) = rA(f_1;r,y_1)A(f_2;r,y_2)$ for $f_1, f_2 \in L^p(\mathbb{R})$ and such that $f(z_1,z_2) = f_1(z_1)f_2(z_2)$, where $A(f)(r,y) = A(f;r,y) = \int_{-\infty}^{\infty} K(r,y,z)f(z)dz, \quad 0 < r < 1.$

The operator $\overline{A}$ is linear and positive. Basic facts on positive linear operators and its applications can be found in [2, 3].

In paper [7], we can find the following equalities:

$$A(1;r,y)=\left(\frac{2}{1+r^2}\right)^{1/2}\exp\left(-\frac{1}{2}\cdot\frac{1-r^2}{1+r^2}y^2\right),$$

$$A(\phi_{m,y};r,y)=\left(\frac{2}{1+r^2}\right)^{1/2}\exp\left(-\frac{1}{2}\cdot\frac{1-r^2}{1+r^2}y^2\right)$$

$$\times\sum_{p=0}^{\left[\frac{m}{2}\right]}\binom{m}{p}\frac{(m-p)!}{(m-2p)!2^p}\cdot\left(\frac{1-r^2}{1+r^2}\right)^p\left(-\frac{(1-r)^2}{1+r^2}y\right)^{m-2p}$$

for $0<r<1$, $y\in R$, where $[a]$ denotes the integral part of $a\in R$ and $\varphi_{m,y}(z)=(z-y)^m$.

From the above, we have the following result in the bivariate case.

Lemma 1 *Let* $\varphi_{n,y_i}(z_1,z_2)=(z_i-y_i)^n$, $y_i,z_i\in R$, $i=1,2$, $n\in N$. *It holds*

$$\overline{A}\left(\left|\varphi_{1,y_i}\right|;r,y_1,y_2\right)\le\frac{2r}{1+r^2}\cdot\left(\frac{1-r^2}{1+r^2}+\frac{(r-1)^4}{(1+r^2)^2}y_i^2\right)^{\frac{1}{2}}\exp\left(-\frac{1}{2}\cdot\frac{1-r^2}{1+r^2}\left(y_1^2+y_2^2\right)\right)\qquad(1)$$

for $0<r<1$.

Proof. Using Hölder's inequality, we get:

$$\overline{A}\left(\left|\phi_{1,y_1}\right|;r,y_1,y_2\right)\le\left(\int_{-\infty}^{\infty}\int_{-\infty}^{\infty}rK(r,y_1,z_1)K(r,y_2,z_2)dz_1dz_2\right)^{\frac{1}{2}}$$

$$\times\left(\int_{-\infty}^{\infty}\int_{-\infty}^{\infty}rK(r,y_1,z_1)K(r,y_2,z_2)\,|\,z_1-y_1\,|^2\,dz_1dz_2\right)^{\frac{1}{2}}=\left(\overline{A}\left(1;r,y_1,y_2\right)\right)^{\frac{1}{2}}\cdot\left(\overline{A}\left(\phi_{2,y_1};r,y_1,y_2\right)\right)^{\frac{1}{2}}\qquad(2)$$

for $(y_1,y_2)\in R^2$ and $0<r<1$. We have (see [5]):

$$\overline{A}(1;r,y_1,y_2)=\frac{2r}{1+r^2}\exp\left(-\frac{1}{2}\cdot\frac{1-r^2}{1+r^2}\left(y_1^2+y_2^2\right)\right),$$

$$\overline{A}\left(\phi_{2,y_i};r,y_1,y_2\right)=\frac{2r}{1+r^2}\left(\frac{1-r^2}{1+r^2}+\frac{(r-1)^4}{\left(1+r^2\right)^2}y_i^2\right)\exp\left(-\frac{1}{2}\cdot\frac{1-r^2}{1+r^2}\left(y_1^2+y_2^2\right)\right),\ i=1,2.$$

From this and (2) we obtain (1) for $i=1$. Analogously, we calculate (1) for $i=2$.

2. Rate of convergence

In this section, we give an order of approximation of function of two variables in the space L^p.

We achieve this using the modulus of continuity $\omega(f;\delta_1,\delta_2)$, $\delta_1,\delta_2>0$ of $f\in L^p(R^2)$ defined as follows:

$$\omega(f;\delta_1,\delta_2)=\sup_{\substack{0<h_1\le\delta_1\\0<h_2\le\delta_2}}\Big\{\sup_{(y_1,y_2)\in R^2}\big|f(y_1+h_1,y_2+h_2)-f(y_1,y_2)\big|\Big\}.$$

First, we prove the following lemma, which we will use in the proof of the approximation theorem.

We shall apply the method used in [12].

Lemma 2 *Let* $f\in C^1(R^2)\cap L^p(R^2)$, $1\le p\le\infty$. *Therefore*

$$\left|\overline{A}\left(f;r,y_1,y_2\right)-f(y_1,y_2)\overline{A}\left(1;r,y_1,y_2\right)\right| \le\frac{2r}{1+r^2}\exp\left(-\frac{1}{2}\cdot\frac{1-r^2}{1+r^2}\left(y_1^2+y_2^2\right)\right)$$

$$\times\left\{\left(\frac{1-r^2}{1+r^2}+\frac{(r-1)^4y_1^2}{(1+r^2)^2}\right)^{\frac12}\sup_{(y_1,y_2)\in R^2}\left|\frac{\partial f(y_1,y_2)}{\partial y_1}\right|+\left(\frac{1-r^2}{1+r^2}+\frac{(r-1)^4y_2^2}{(1+r^2)^2}\right)^{\frac12}\sup_{(y_1,y_2)\in R^2}\left|\frac{\partial f(y_1,y_2)}{\partial y_2}\right|\right\}.$$

for $0<r<1$ and all $(y_1,y_2)\in R^2$.

Proof. Let $(y_1,y_2)\in R^2$. be a fixed point and $f\in C^1(R^2)\cap L^p(R^2)$. We have:

$$f(z_1,z_2)-f(y_1,y_2)=\int_{y_1}^{z_1}\frac{\partial}{\partial u}f(u,z_2)du+\int_{y_2}^{z_2}\frac{\partial}{\partial v}f(y_1,v)dv$$

for all $(z_1,z_2)\in R^2$. Let us denote:

$$\lambda_{y_1}(z_1,z_2)=\int_{y_1}^{z_1}\frac{\partial}{\partial u}f(u,z_2)du,\quad \tau_{y_2}(z_1,z_2)=\int_{y_2}^{z_2}\frac{\partial}{\partial v}f(y_1,v)dv.$$

Observe that:

$$\left|\lambda_{y_1}(z_1,z_2)\right|\le|z_1-y_1|\sup_{(y_1,y_2)\in R^2}\left|\frac{\partial f(y_1,y_2)}{\partial y_1}\right|,\ \left|\tau_{y_2}(z_1,z_2)\right|\le|z_2-y_2|\sup_{(y_1,y_2)\in R^2}\left|\frac{\partial f(y_1,y_2)}{\partial y_2}\right|. \quad (3)$$

From (3) and Lemma 1, we obtain:

$$\overline{A}\left(\left|\lambda_{y_1}\right|;r,y_1,y_2\right)\le\overline{A}\left(\left|\varphi_{1,y_1}\right|;r,y_1,y_2\right)\sup_{(y_1,y_2)\in R^2}\left|\frac{\partial f(y_1,y_2)}{\partial y_1}\right|$$

$$\leq \frac{2r}{1+r^2}\left(\frac{1-r^2}{1+r^2}+\frac{(r-1)^4 y_1^2}{(1+r^2)^2}\right)^{\frac{1}{2}} \exp\left(-\frac{1}{2}\cdot\frac{1-r^2}{1+r^2}\left(y_1^2+y_2^2\right)\right) \sup_{(y_1,y_2)\in R^2}\left|\frac{\partial f(y_1,y_2)}{\partial y_1}\right|,$$

$$\overline{A}\left(\left|\tau_{y_2}\right|;r,y_1,y_2\right) \leq \frac{2r}{1+r^2}\left(\frac{1-r^2}{1+r^2}+\frac{(r-1)^4 y_2^2}{(1+r^2)^2}\right)^{\frac{1}{2}} \exp\left(-\frac{1}{2}\cdot\frac{1-r^2}{1+r^2}\left(y_1^2+y_2^2\right)\right)$$

$$\sup_{(y_1,y_2)\in R^2}\left|\frac{\partial f(y_1,y_2)}{\partial y_2}\right|.$$

Hence:

$$\left|\overline{A}\left(f;r,y_1,y_2\right)-f(y_1,y_2)\overline{A}\left(1;r,y_1,y_2\right)\right| \leq \frac{2r}{1+r^2}\exp\left(-\frac{1}{2}\cdot\frac{1-r^2}{1+r^2}\left(y_1^2+y_2^2\right)\right)$$

$$\times\left\{\left(\frac{1-r^2}{1+r^2}+\frac{(r-1)^4 y_1^2}{(1+r^2)^2}\right)^{\frac{1}{2}} \sup_{(y_1,y_2)\in R^2}\left|\frac{\partial f(y_1,y_2)}{\partial y_1}\right| + \left(\frac{1-r^2}{1+r^2}+\frac{(r-1)^4 y_2^2}{(1+r^2)^2}\right)^{\frac{1}{2}} \sup_{(y_1,y_2)\in R^2}\left|\frac{\partial f(y_1,y_2)}{\partial y_2}\right|\right\}$$

and the proof of the lemma is completed.

We are now in a position to prove the approximation theorem.

Theorem 2 *Let* $f \in C(R^2)\cap L^p(R^2),\ 1\leq p\leq\infty$. *Therefore*

$$\left|\overline{A}(f;r,y_1,y_2)-f(y_1,y_2)\overline{A}(1;r,y_1,y_2)\right|$$

$$\leq 6\omega\left(f;\sqrt{\frac{1-r^2}{1+r^2}+\frac{(r-1)^4}{(1+r^2)^2}y_1^2},\sqrt{\frac{1-r^2}{1+r^2}+\frac{(r-1)^4}{(1+r^2)^2}y_2^2}\right)$$

for $0<r<1$ and all $(y_1,y_2)\in R^2$.

Proof. Let $(y_1,y_2)\in R^2$ be a fixed point and f_{δ_1,δ_2} be the Steklov mean defined by:

$$f_{\delta_1,\delta_2}(y_1,y_2)=\frac{1}{\delta_1\delta_2}\int_0^{\delta_1}\int_0^{\delta_2} f(y_1+u,y_2+v)dudv \quad \text{for} \quad (y_1,y_2)\in R^2,\delta_1,\delta_2>0.$$

From this definition, we conclude that:

$$f_{\delta_1,\delta_2}(y_1,y_2)-f(y_1,y_2)=\frac{1}{\delta_1\delta_2}\int_0^{\delta_1}\int_0^{\delta_2}\Delta_{u,v}f(y_1,y_2)dudv,$$

$$\frac{\partial}{\partial y_1}f_{\delta_1,\delta_2}(y_1,y_2)=\frac{1}{\delta_1\delta_2}\int_0^{\delta_2}\left(\Delta_{\delta_1,v}f(y_1,y_2)-\Delta_{0,v}f(y_1,y_2)\right)dv,$$

$$\frac{\partial}{\partial y_2} f_{\delta_1,\delta_2}(y_1,y_2) = \frac{1}{\delta_1\delta_2}\int_0^{\delta_1}\left(\Delta_{u,\delta_2} f(y_1,y_2) - \Delta_{u,0} f(y_1,y_2)\right)du,$$

where

$$\Delta_{u,v} f(y_1,y_2) = f(y_1+u, y_2+v) - f(y_1,y_2).$$

Hence, if $f \in C(R^2) \cap L^p(R^2)$, then $f_{\delta_1,\delta_2} \in C^1(R^2) \cap L^p(R^2)$. Moreover

$$\sup_{(y_1,y_2)\in R^2} \left| f_{\delta_1,\delta_2}(y_1,y_2) - f(y_1,y_2)\right| \le \omega(f;\delta_1,\delta_2),$$

$$\sup_{(y_1,y_2)\in R^2} \left| \frac{\partial}{\partial y_1} f_{\delta_1,\delta_2}(y_1,y_2)\right| \le 2\delta_1^{-1}\omega(f;\delta_1,\delta_2), \tag{4}$$

for all $\delta_1,\delta_2 > 0$. Observe that

$$\left|\overline{A}(f;r,y_1,y_2) - f(y_1,y_2)\overline{A}(1;r,y_1,y_2)\right|$$

$$\le \left|\overline{A}(f - f_{\delta_1,\delta_2};r,y_1,y_2)\right| + \left|\overline{A}(f_{\delta_1,\delta_2};r,y_1,y_2) - f_{\delta_1,\delta_2}(y_1,y_2)\overline{A}(1;r,y_1,y_2)\right|$$

$$+ \left|f_{\delta_1,\delta_2}(y_1,y_2) - f(y_1,y_2)\right|\cdot\overline{A}(1;r,y_1,y_2), \quad (y_1,y_2)\in R^2, \delta_1,\delta_2 > 0.$$

From Lemma 2 and (4) we obtain

$$\left|\overline{A}(f_{\delta_1,\delta_2};r,y_1,y_2) - f_{\delta_1,\delta_2}(y_1,y_2)\overline{A}(1;r,y_1,y_2)\right|$$

$$\le \frac{2r}{1+r^2}\exp\left(-\frac{1}{2}\cdot\frac{1-r^2}{1+r^2}\left(y_1^2+y_2^2\right)\right)\left\{2\delta_1^{-1}\omega(f;\delta_1,\delta_2)\left(\frac{1-r^2}{1+r^2} + \frac{(r-1)^4 y_1^2}{(1+r^2)^2}\right)^{\frac{1}{2}}\right.$$

$$\left. + 2\delta_2^{-1}\omega(f;\delta_1,\delta_2)\left(\frac{1-r^2}{1+r^2} + \frac{(r-1)^4 y_2^2}{(1+r^2)^2}\right)^{\frac{1}{2}}\right\}$$

$$\le 2\omega(f;\delta_1,\delta_2)\left\{\delta_1^{-1}\left(\frac{1-r^2}{1+r^2} + \frac{(r-1)^4 y_1^2}{(1+r^2)^2}\right)^{\frac{1}{2}} + \delta_2^{-1}\left(\frac{1-r^2}{1+r^2} + \frac{(r-1)^4 y_2^2}{(1+r^2)^2}\right)^{\frac{1}{2}}\right\}.$$

Using (4) we have:

$$\left|f_{\delta_1,\delta_2}(y_1,y_2)-f(y_1,y_2)\right|\cdot\overline{A}(1;r,y_1,y_2)\le\overline{A}(1;r,y_1,y_2)\omega(f;\delta_1,\delta_2)\le\omega(f;\delta_1,\delta_2)$$

and

$$\left|\overline{A}(f-f_{\delta_1,\delta_2};r,y_1,y_2)\right| \le\int_{-\infty}^{\infty}\int_{-\infty}^{\infty}rK(r,y_1,z_1)K(r,y_2,z_2)\,|\,f(z_1,z_2)-f_{\delta_1,\delta_2}(z_1,z_2)\,|dz_1\,dz_2$$

$$\le\sup_{(y_1,y_2)\in R^2}\left|f_{\delta_1,\delta_2}(y_1,y_2)-f(y_1,y_2)\right|\int_{-\infty}^{\infty}\int_{-\infty}^{\infty}rK(r,y_1,z_1)K(r,y_2,z_2)dz_1\,dz_2$$

$$\le\overline{A}(1;r,y_1,y_2)\omega(f;\delta_1,\delta_2)\le\omega(f;\delta_1,\delta_2).$$

Finally, we get:

$$\left|\overline{A}(f;r,y_1,y_2)-f(y_1,y_2)\overline{A}(1;r,y_1,y_2)\right|$$

$$\le 2\omega(f;\delta_1,\delta_2)\left\{1+\delta_1^{-1}\left(\frac{1-r^2}{1+r^2}+\frac{(r-1)^4}{(1+r^2)^2}y_1^2\right)^{\frac{1}{2}}+\delta_2^{-1}\left(\frac{1-r^2}{1+r^2}+\frac{(r-1)^4}{(1+r^2)^2}y_2^2\right)^{\frac{1}{2}}\right\}$$

for all $(y_1,y_2)\in R^2,\delta_1,\delta_2>0.$ Choosing:

$$\delta_1=\left(\frac{1-r^2}{1+r^2}+\frac{(r-1)^4}{(1+r^2)^2}y_1^2\right)^{\frac{1}{2}},\quad \delta_2=\left(\frac{1-r^2}{1+r^2}+\frac{(r-1)^4}{(1+r^2)^2}y_2^2\right)^{\frac{1}{2}},$$

we obtain the desired estimation for $\overline{A}$.
From Theorem 2, we can derive the following result.

Corollary 1 *Let* $f\in C(R^2)\cap L^p(R^2),\ 1\le p\le\infty$. *Then it holds*

$$\left|\overline{A}(f;r,y_1,y_2)-f(y_1,y_2)\right|\le 6\omega\left(f;\sqrt{\frac{1-r^2}{1+r^2}+\frac{(r-1)^4}{(1+r^2)^2}y_1^2},\sqrt{\frac{1-r^2}{1+r^2}+\frac{(r-1)^4}{(1+r^2)^2}y_2^2}\right)$$

$$+|\,f(y_1,y_2)\,|\cdot\left|\overline{A}(1;r,y_1,y_2)-1\right|$$

for $0<r<1$ and all $(y_1,y_2)\in\mathsf{R}^2$.

References

[1] Bergh J., Löfström J., *Interpolation Spaces. An Introduction*, Springer-Verlag, Berlin, Heidelberg, New York 1976.

[2] DeVore R.A., Lorentz G.G., *Constructive Approximation*, Springer, Berlin 1993.

[3] Ditzian Z., Totik V., *Moduli of Smoothness*, Springer, New York 1987.

[4] Gosselin J., Stempak K., *Conjugate expansions for Hermite functions*, Illinois J. Math. 38 1994, 177-197.

[5] Krech G., *A note on the Poisson integral for Hermite expansions of functions of two variables*, J. Appl. Anal. (submitted).

[6] Krech G., *On the rate of convergence theorem for the alternate Poisson integrals for Hermite and Laguerre expansions*, Ann. Acad. Paedagog. Crac. Stud. Math. 4, 2004, 103-110.

[7] Krech G., *On some approximation theorems for the Poisson integral for Hermite expansions*, Analysis Math. 40, 2014, 133-145.

[8] Krech G., Wachnicki E., *Approximation by some combinations of the Poisson integrals for Hermite and Laguerre expansions*, Ann. Univ. Paedagog. Crac. Stud. Math. 12, 2013, 21-29.

[9] Muckenhoupt B., *Poisson integrals for Hermite and Laguerre expansions*, Trans. Amer. Math. Soc. 139, 1969, 231-242.

[10] Özarslan M.A., Duman O., *Approximation properties of Poisson integrals for orthogonal expansions*, Taiwanese J. Math. 12, 2008, 1147-1163.

[11] Szegö G., *Orthogonal polynomials*, Amer. Math. Soc. Colloq. Publ. 33, Amer. Math. Soc., Providence, R.I., 1939.

[12] Toczek G., Wachnicki E., *On the rate of convergence and the Voronovskaya theorem for the Poisson integrals for Hermite and Laguerre expansions*, J. Approx. Theory 116, 2002, 113-125.

TECHNICAL TRANSACTIONS | **CZASOPISMO TECHNICZNE**
FUNDAMENTAL SCIENCES | NAUKI PODSTAWOWE
3-NP/2014

ANNA MILIAN*

SIMPLE CHOOSER OPTIONS WITH MAPLE

OPCJE SIMPLE CHOOSER Z MAPLE

A b s t r a c t

This paper discusses Monte Carlo simulations of the Black-Scholes model. It is introduced with the simple example of the pricing of 'European call options on a no-dividend stock and the simulation results are compared with an analytical solution. Monte-Carlo methods are then used to price simple chooser options. Moreover, it is shown that the distribution of rate of the return from investment in simple chooser options is significantly dependent on the strike price. The presented simulation is performed using MAPLE.

Keywords: simple chooser options, Black-Scholes model, Monte Carlo method

S t r e s z c z e n i e

W artykule rozważa się zastosowanie metody Monte Carlo do modelu Blacka-Scholesa. Wstęp stanowi przykład wyceny europejskiej opcji kupna na akcje bez dywidendy i porównanie wyniku symulacji z rozwiązaniem analitycznym. Metodą Monte Carlo wyceniono opcję *simple chooser*. Pokazano istotną zależność rozkładu prawdopodobieństwa stopy zwrotu z tych opcji od ich ceny wykonania.

Słowa kluczowe: opcje simple chooser, model Blacka-Scholesa, metoda Monte Carlo

* Institute of Mathematics, Faculty of Physics, Mathematics and Computer Science, Cracow University of Technology; amilian@pk.edu.pl.

1. Introduction

An option is a contract between a buyer (holder) and a seller (writer) that gives the buyer the right, but not the obligation, to buy or to sell the underlying asset at an agreed price at a later date. The agreed price in the contract is called the strike price; the date is referred to as the expiration date. There are two basic kinds of options – calls and puts. A call stock option gives the holder the right to buy a specified quantity of stock at the strike price on or before the expiration date. The writer of the call option has the obligation to sell the underlying asset if the holder of the call option decides to exercise his right to buy. A put option gives the holder the right to sell a specified quantity of the underlying stock at the strike price on or before the expiration date. The writer of the put option has the obligation to buy the underlying asset at the strike price if the holder decides to exercise his right to sell. The style of an option refers to when that option is exercisable. An American option may be exercised at any time prior to the expiration date. A European option may be exercised only at the expiration date. The Monte Carlo simulation is a valuable and flexible computational tool in financial theory and practice [3, 4]. In this paper, we demonstrate how it can be applied to analyse chooser options. We price the options using Monte Carlo methods combined with the analytical Black-Scholes solution, relating to the case of the European call option, available through the MAPLE command. Using crude Monte Carlo, the distribution of the rate of return from investments in chooser options is examined. The simulations are performed using MAPLE. We use the Black-Scholes model to describe the price of the underlying asset. The following assumptions were made to derive the Black-Scholes model: there are no riskless arbitrage opportunities; there are no transaction costs; there are no dividends during the life of an option; security trading is continuous; the risk-free rate of interest and the stock price volatility are constant; the price of the underlying asset follows a geometric Brownian process

2. Model description

The Black-Scholes model is used, this is the most popular valuation model for options. The model is based on the assumptions that markets are arbitrage free and the price S of the underlying asset follows a geometric Brownian motion:

$$S_t = S_0 \exp\left(\left(r - \frac{1}{2}\sigma^2\right)t + \sigma W_t\right), t \in [0,T], \tag{1}$$

where:

- $W = \{W_t, t \in [0,T]\}$ – a standard Brownian motion under the risk-neutral probability P, r denotes the risk-free interest rate,
- S_0 – the stock price at time 0,
- T – the time to maturity of the option (expiry date),
- $\sigma > 0$ – the stock price volatility.

An estimation of future volatility σ can be obtained from historical prices of stocks as the standard deviation of the stock return, by assuming that the recent realized level of volatility will continue in the future. Another estimation can be computed from current option prices (implied volatility). The estimation of σ has been widely studied in [1] and is not discussed

in this paper. Volatility is expressed in the percentage of the underlying asset price, and for stocks, it is typically between 15% and 60%.

Under the assumption of no arbitrage, the price of a generic derivative security can be expressed as the expected value of its discounted payouts. This expectation is taken with respect to the risk-neutral measure. Then today's price of a stock option that pays at some time t according to a F_t – measurable payoff function $f(t)$, is:

$$E\left(e^{-rt} f(t)\right) \tag{2}$$

Let S_T denote the price of the underlying asset at the expiry date T, and K denote the strike price. The pay-off is given by:

$$f(T) = \left(S_T - K\right)^+ = C\left(S_0, K, T\right)$$

for a call option, and by:

$$f(T) = \left(K - S_T\right)^+ = P\left(S_0, K, T\right)$$

for a put option. A closed form formula for pricing the above options is the Black-Scholes formula:

$$c = S_0 N\left(d_1\right) - K e^{-rT} N\left(d_2\right),$$

$$p = K e^{(-rT)} N(-d_2) - S_0 N(-d_1),$$

$$\text{where } d_1 = \frac{\ln\left(\frac{S_0}{K}\right) + \left(r + \frac{1}{2}\sigma^2\right)T}{\sigma\sqrt{T}},$$

$$d_2 = \frac{\ln\left(\frac{S_0}{K}\right) + \left(r - \frac{1}{2}\sigma^2\right)T}{\sigma\sqrt{T}},$$

c is the price of a call option, p is the price of a put option and N is the cumulative probability function for a standard normal distribution [6].

Analytical solution

The call option price can be computed in MAPLE, as the analytical solution, based on the Black-Scholes model. It is available through MAPLE command:

> *with (finance)*:

*S*0 := 50 : *K* := 49 : r := 0.07 : σ := 0.3 : τ := 199:

c := evalf $\left(blackscholes\left(S0, K, r, \frac{\tau}{365}, \sigma\right)\right)$;

where τ denotes 199 days to maturity.

Monte Carlo Simulation

For the purpose of introduction, the evaluation of the price by the Monte Carlo simulation is also presented. Moreover, we compare the computed result with the analytical solution presented above.

Independent replications $S_T^{(i)}$ of the terminal stock price under the risk–neutral measure can be generated from formula (1). By the Strong Law of Large Numbers we have:

$$\frac{1}{n}\sum_{i=1}^{n} f\left(S_T^{(i)}\right) \to E\left(f(T)\right), n \to \infty, a.s.$$

An unbiased estimator of the price of European call option is given by:

$$C = \frac{1}{n}\sum_{i=1}^{n} e^{-rT} \max(S_T^{(i)} - K, 0), \tag{3}$$

where:

$$S_T^{(i)} = S_0 \exp\left(\left(r - \frac{1}{2}\sigma^2\right)T + \sigma x_i\right), i = 1 \ldots n, \tag{4}$$

T is the option's maturity and $\{x_i\}$ are independent samples from the normal distribution with mean 0 and standard deviation $\sqrt{T}$.

As we can see below, the difference between the exact and Monte Carlo results is about 0.01:

$d := \exp\left(-\frac{r \cdot \tau}{365}\right)$:

$N := 10^5$

$X :=$ *Random Variable* $\left(Normal\left(0, \sqrt{\frac{\tau}{365}}\right)\right)$:

$x :=$ *Sample* (X, N):

$L := 0$:

for i **to** N **do**

$$p[i] := \max\left(S0 \cdot \exp\left(\frac{\left(r - \frac{1}{2} \cdot \sigma^2\right) \cdot \tau}{365} + \sigma \cdot x[i]\right) - K, 0\right):$$

$L := L + p[i]$

end do:

$$c := \frac{d \cdot L}{N};$$

Monte Carlo simulations are never exact and one always has to take the sample standard deviation into account. With 100 independent Monte Carlo calculations of c, the standard deviation of the price sample and mean are around 0.03 and 5.8514 respectively. Hence

5.8514±0.006 forms the boundary for the 95% confidence interval for the price. We present a histogram of the sample of *c*, based on 100 simulations:

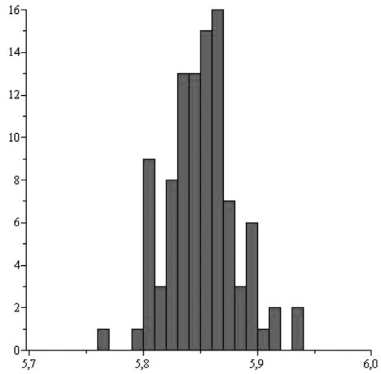

Fig. 1. Histogram of price of European call option based on 100 simulations

3. Analysis of simple chooser options

In this paper, the main attention is focused on the analysis of simple chooser options. The Monte Carlo simulation aimed at the pricing of simple chooser options and the examination of the distribution of the rate of return from the options is described. Chooser options have been traded since July 1990 with the initial contracts traded by Bankers Trust [5]. They are purchased in the present, but are chosen to be either put or call at some specified future date. Their holder has the right to decide at some specific point in time t($t < T$), whether the options will finally be put or call. Hence they are sometimes named 'you-choose' or 'as-you-like' options. Chooser options are suitable when strong volatility of the underlying asset is expected but investors are not certain about the direction of the change. In the case of a rising value of the underlying asset over a period of time, the holder of the option will choose the call option because it will have a higher value than the put option. When the underlying asset falls up, the choice will be the put option. Once this choice has been made at time t, the option stays as either a call or a put to maturity. If the strike prices of the call and the put are the same, just as their expirations, such an option is referred to as a simple chooser. We will continue to call them briefly as chooser options.

3.1. Pricing chooser options

Let us denote:
$T - t$ time to maturity,
S_t stock price at t,
$C(S_t, K, T-t)$ premium of European call option,
$P(S_t, K, T-t)$ premium of European put option.

At time t, the investor will choose the call option if:

$$C(S_t, K, T-t) > P(S_t, K, T-t),$$

otherwise, he will choose the put option [2].

By the put-call parity:

$$C(S_t, K, T-t) - P(S_t, K, T-t) = S_t - K\exp\left[-r(T-t)\right]$$

the above inequality is equivalent to:

$$S_t > K\exp\left[-r(T-t)\right].$$

Hence the value of the chooser option at time t equals:

$$ch(t) = \max\left(C(S_t, K, T-t), P(S_t, K, T-t)\right) =$$

$$C(S_t, K, T-t) + \max\left(K\exp\left[-r(T-t)\right] - S_t, 0\right). \tag{5}$$

The value of the option at time 0, when the choosing time is t, is equal to:

$$v(t) = \exp(-rt)\,E\left[C(S_t, K, T-t) + \max\left(K\exp\left[-r(T-t)\right] - S_t, 0\right)\right]. \tag{6}$$

In [5], the relationships between the choice date and the chooser price, and between the chooser price and its strike price were examined.

Applying (6), we can price the European simple chooser option by simulation.

Example. Here we use the Monte Carlo method with $n = 100000$ simulations to price the chooser option where a maturity T is one year, the underlying asset price S_0 is 50, $r = 10\%$, $\sigma = 20\%$, $k = 50$ and $t = 0.25$ and $t = 0.25$. We simulate values of S_t and use the analytical result for $C(S_t, K, T-t)$ calculated by MAPLE command *blackscholes* $(S_t, K, r, T-t, \sigma)$. We obtain the price $\nu(t) = 7.01983862$. The algorithm is as following:

Set sum = 0
for I = 1 to $i = 1$ to n
generate S_t
set sum = sum + $C(S_t, K, T-t)$ + max($Kexp(-rt)$ – St, 0)
end
set $v(t) = (\text{sum}/n)\exp(-rt)$

3.2. Rate of return

Using the Monte Carlo method, we can also analyse the profit function, which determines the profit for the holder of a chooser option on the expiry date. To obtain this goal, we have to know the values of the payoff function. We express a payoff function of the option in the following way:

$$f(T) = 1_A \max(S_T - K, 0) + 1_B \max(K - S_T, 0) \tag{7}$$

where $A = \{S_t > K \exp[-r(T-t)]\}, B = \{S_t < K \exp[-r(T-t)]\}$.

Let U and W be independent, normally distributed random variables with mean 0 and variance t and $T - t$ respectively:

$$X = S_0 \exp\left(\left(r - \frac{1}{2}\sigma^2\right)t + \sigma U\right), \quad Y = \exp\left(\left(r - \frac{1}{2}\sigma^2\right)(T-t) + \sigma W\right).$$

By (1) we have $S_t = XY$. Independent samples X and Y are generated. By definition of chooser options, if $X > K \exp[-r(T-t)]$ then $f(T) = \max(S_T - K, 0)$, lse $f(T) = \max(K - S_T, 0)$. Independent replications $f^{(i)}(T), i = 1 \ldots n$ give us not only the estimation of the chooser price:

$$ch(T) = \exp(-rT)\frac{1}{n}\sum_{i=1}^{n} f^{(i)}(T)$$

at $t = 0$, but also the sample of rate of return R, expressed in percentage:

$$R^{(i)}(T) = \frac{\exp(-rT) f^{(i)}(T) - ch(T)}{ch(T)} * 100\%, i = 1, \ldots, n.$$

3.3. Simulation of rate of return

Figure 2 presents eight different histograms and medians of the rate of return dependent on K, based on $n = 10^4$ simulations each case, where a maturity T is one year, the underlying asset price S_0 is 50, $r = 10\%$, $\sigma = 30\%$, $t = 0.6$. The mean is equal to 0 each case.

As can be seen, a data set of the rate of return is unimodal and positively skewed, the long tail is on the right-hand side, when $K \leq S_0$. The situation reverses when $K > S_0$. A data set of the rate of return is bimodal. The right-hand tail of the distribution decreases with an increased K. Figure 3 plots the median of rate of return against the strike price.

From the investor's point of view, the most interesting case is when the median rate of return is the biggest. As can be seen in Figure 3, the worst case is for $K = 50$ and the best is for $K = 90$. Let us compare the probabilities corresponding to different value ranges of the rate of return R. The simulation results are presented in Table 1.

Let us observe that in the case of strike price $K = 50$, the probability of relative loss exceeding 50% is equal to 0.39 while in the case where $K = 90$, the probability equals only 0.15. Interestingly, for $K = 50$, the probability that relative gain exceeds 50% is equal to 0.25, while for $K = 90$ it is only 0.12. Hence, for $K = 50$, large gains and large losses have the highest probabilities. The opposite situation occurs in the case of $K = 90$, the highest probabilities have small gains and small losses. As presented, the Monte Carlo simulation proves to be very useful for the analysis of the investment risk.

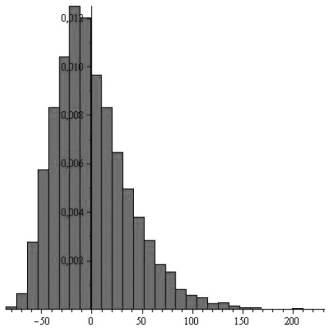

K = 10, Median = –5.05

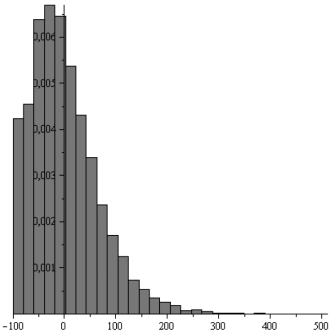

K = 30, Median = –9.9

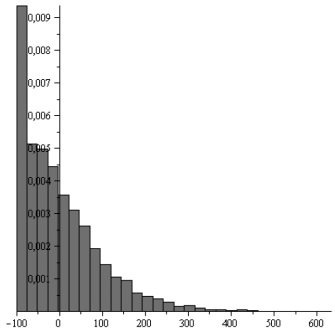

K = 40, Median = –21.09

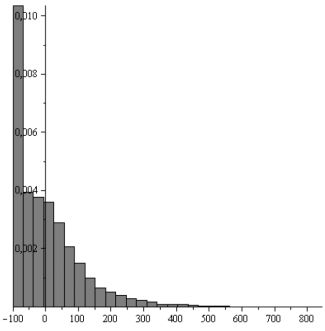

K = 50, Median = –22.66

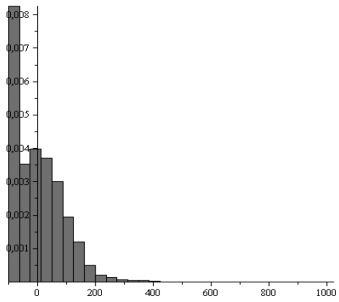

K = 60, Median = –8.21

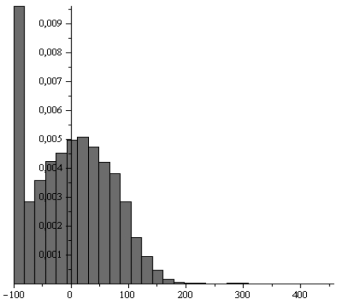

K = 70, Median = 1.05

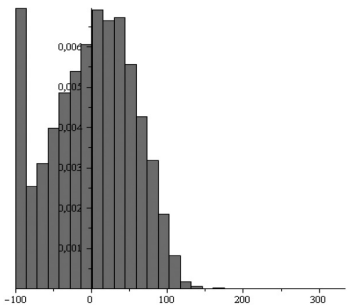

K = 80, Median = 4.86

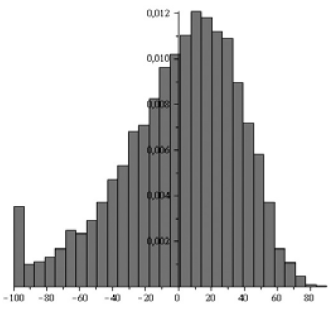

K = 90, Median = 5.83

Fig. 2. Histograms and medians of rate of return

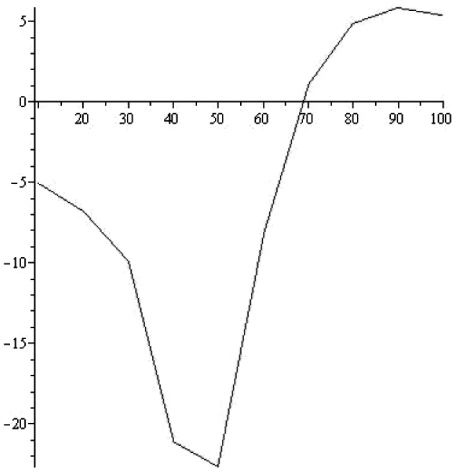

Fig. 3. Median of rate of return

Table 1

Approximated distributions of rates of return for strike price $K = 50$ and $K = 90$

	$K = 50$	$K = 90$
$P\ (R \leq -75\%)$	0.3	0.08
$P(-75\% < R \leq -50\%)$	0.09	0.07
$P(-50\% < R \leq -25\%)$ Wpisz tutaj równanie. –25%)	0.1	0.12
$P\ (-25\% < R \leq 0\%)$	0.1	0.18
$P\ (0\% < R \leq 25\%)$	0.09	0.23
$P\ (25\% < R \leq 50\%)$	0.07	0.2
$P\ (50\% < R \leq 75\%)$	0.06	0.1
$P\ (R > 75\%)$	0.19	0.02

4. Conclusions

The Monte Carlo simulation is useful in determining the distribution of the rate of return from investments in options. Knowledge of this distribution helps in determining investment risk. As demonstrated in Figures 2 and 3, and in Table 1, in the case of chooser options, the distribution and consequently, the level of risk, is significantly dependent on the strike price.

References

[1] Corrado C., Miller T., *A Note on a Simple, Accurate Formula to Compute Implied Standard Deviation*, Journal of Banking &Finance vol. 20, 1996, 593-603.
[2] Cuthbertson K., Nitzsche D., *Financial Engineering Derivatives and Risk Management*, John Wiley and Sons, LTD, New York 2003.
[3] Glasserman P., *Monte Carlo Methods in Financial Engineering*, Springer, New York 2004.
[4] Korn R., Korn E., Kroisandt G., *Monte Carlo Methods and Models in Finance and Insurance*, CRC Press, Taylor & Francis Group, New York 2010.
[5] Martinkute-Kauliene R., *Exotic Options: A Chooser Options and its Pricing*, Business, Management and Education, vol. 10 (2), 2012, 289-301.
[6] Weron A., Weron R., *Inżynieria finansowa. Wycena instrumentów pochodnych. Symulacje komputerowe. Statystyka rynku*, WNT, Warszawa 1999.

PHYSICS

FIZYKA

TECHNICAL TRANSACTIONS | **CZASOPISMO TECHNICZNE**
FUNDAMENTAL SCIENCES | NAUKI PODSTAWOWE
3-NP/2014

ROBERT GĘBAROWSKI*

MONTE CARLO SIMULATIONS OF THE ISING MODEL ON A SQUARE LATTICE WITH RANDOM GAUSSIAN INTERACTIONS

SYMULACJE MONTE CARLO MODELU ISINGA NA SIECI KWADRATOWEJ Z ODDZIAŁYWANIAMI LOSOWYMI O ROZKŁADZIE GAUSSA

Abstract

The paper shows Monte Carlo simulations of the Ising model on a square lattice with no external magnetic field. In particular, the uncertainty of the spin coupling interactions in the Ising model has been considered. The influence on the phase transition of the Gaussian noise in the spin coupling values has been demonstrated.

Keywords: Ising model, Monte Carlo simulations, Gaussian noise

Streszczenie

W artykule przedstawiono symulacje Monte Carlo modelu Isinga na sieci kwadratowej przy braku zewnętrznego pola magnetycznego. W szczególności rozważono niepewność wartości energii sprzężenia oddziałujących spinów w modelu Isinga. Zademonstrowano wpływ na przejście fazowe obecności szumu gaussowskiego w wartościach stałej sprzężenia oddziałujących spinów.

Słowa kluczowe: model Isinga, symulacje Monte Carlo, szum gaussowski

* Institute of Physics, Faculty of Physics, Mathematics and Computer Science, Cracow University of Technology, Poland; rgebarowski@pk.edu.pl.

1. Introduction

The Ising model, named after Ernst Ising [1] and studied at least 5 years earlier (in early 1920s) by Lenz [2], offers an excellent testing ground for studies of the physics of classical and quantum phase transitions. Despite being subject of numerous, brilliant and extensive research studies over nearly a century, the Ising model still poses some big challenges. For example, the analytical solution for the 2D Ising model with no field was obtained by Onsager [3, 4] in 1944, but up until now, an analytical solution has remained unknown for the case with an external magnetic field. Thus, in many cases, feasible ways to study the model include experiments with quantum simulators with hundreds of spins [5] and numerical methods (Monte Carlo simulations) for finite-size lattices with even more spins included [6–8]. The universality of the Ising model goes far beyond the modelling of purely physical phenomena such as: classical and quantum phase transitions; binary alloys; magnetic properties of condensed-matter materials; strong and long-range correlations; complex systems. Just to give an example, it has been shown by Bornholdt [6], that microscopic models based on the Ising model have a capacity of reproducing complex behavior of real financial and economic markets. Thus, it proves that this model allows for the genuine interdisciplinary research in physics, econophysics and also across other areas of fundamental and applied sciences.

The purpose of this paper is to investigate the two-dimensional (2D) Ising model by means of Monte Carlo simulations. In view of recent progress in engineering two-dimensional Ising interactions in a trapped-ion quantum simulator [5], an important research question arises. Namely, to what extent an uncertainty of the engineered interaction in a real experimental situation may influence the phase transition in the model. In order to provide at least a partial answer to this question, random Gaussian noise is introduced into the Ising interaction coupling constant.

The paper is organized as follows. In the next section, the Ising model is briefly presented. In Section 3, the results are presented for the case of constant interaction coupling energy. This allows for some justification for the applied numerical implementation of the Metropolis algorithm, as such results are fairly standard in the literature. Then, a variant of the model is proposed for which the interaction may vary according to the normal distribution with the mean and standard deviation fixed. Finally, the results are summarized and some conclusions are drawn.

2. The Model

Let us consider 2D Ising model [1, 2, 4], where $N = L^2$ spins $\sigma = \pm 1$ are located in regularly spaced sites of a square lattice $L \times L$. In general, such spins can interact with each other with some coupling energy J (in principle, interactions and thus couplings could depend on interacting spin σ_{ij}, σ_{jk} locations in the lattice). Apart from internal interactions within such an ensemble of spins, one could also take into account interactions of each spin with the external magnetic field. However, for the purpose of the following discussion, let us simplify the model considering the case with no magnetic field and include only equal interactions between nearest neighbors in the square lattice. Hence the Hamiltonian H of the system reads:

$$H = -J \sum_{\{ij,kl\}} \sigma_{ij}\sigma_{kl}$$

where

J – the coupling between interacting nearest-neighbor spins ,
σ_{ij} – the spin $\sigma_{ij} = \pm 1$ located in the site (i, j) of the lattice $(1 \le 1, j \le L)$,
$\{ij, kl\}$ – denotes summation only over pairs of the nearest-neighbor sites (i, j) and (k, l) of the lattice.

In the model studied, the usual periodic boundary conditions for the lattice are adopted. This means that any spin has 4 nearest neighbors in the square lattice and for example: $\sigma_{L+1,j} \equiv \sigma_{1,j}$ or $\sigma_{i,L+1} \equiv \sigma_{i,1}$ (the lattice is 'wrapped around').

It is well known that the 2D system exhibits a phase transition between the disordered phase (a paramagnetic state) and the ordered phase (a ferromagnetic state). The order parameter for this transition is simply the total system magnetization M per spin:

$$m = \frac{M}{N} = \frac{1}{N} \sum_{i,j} \sigma_{ij}$$

For a system at a given temperature T, an expectation value $<A>$ of any observable A in the system with spin micro-configurations σ_α on the lattice is evaluated according to probabilities $P(\sigma_\alpha)$, assigned by the canonical ensemble:

$$< A > = \sum_\alpha P(\sigma_\alpha)\, A(\sigma_\alpha)\,, \quad P(\sigma_\alpha) = \frac{1}{Z} e^{-E(\sigma_\alpha)/(k_B T)}$$

where:

Z – the partition function,
$E(\sigma_\alpha)$ – the energy of the microstate σ_α,
k_B – Boltzmann's constant.

In the Monte Carlo numerical simulation, such expectation values could be obtained through the Metropolis algorithm (see e.g. [7, 8] for a description of details of the implementation of Metropolis algorithm's).

It also transpires (see e.g. [7, 8]) that the magnetic susceptibility χ (a linear response of the magnetization to the magnetic field) is related to the total magnetization M fluctuations:

$$\chi = \frac{1}{N k_B T} \left(\langle M^2 \rangle - \langle M \rangle^2 \right)$$

The critical temperature T_C for the order-disorder transition in the 2D Ising model in the limit of an infinite lattice (the so-called thermodynamic limit, with a total spin number $N \to \infty$), without an external magnetic field, can be found exactly analytically [3, 4]:

$$\frac{k_B T_C}{J} = \frac{2}{\ln\left(1 + \sqrt{2}\right)} \approx 2.2691853$$

An interesting issue is related to the so-called finite-size lattice scaling at the critical temperature [3, 7, 8]. A ratio of any two quantities which have the same finite-size scaling at T_C should be lattice-size independent. Especially useful are the Binder ratios [8] defined in the following way (q is an integer):

$$B_q = \frac{\langle m^{2q} \rangle}{\langle |m| \rangle^{2q}}$$

Therefore, once we have obtained expectation values of the square of the magnetization and the absolute value of the magnetization itself, the first Binder ratio B_1 can be easily found.

3. Results

Monte Carlo simulations of the Ising model using the Metropolis algorithm were performed according to the implementation described by other authors (see [7, 8] for details). Typically, in the present simulations, 50000 Monte Carlo sweeps (MCS) were discarded for equilibration and there were 100 bins used, each with 50000 MCS to obtain expectation values of $\langle m^2 \rangle$, $\langle |m| \rangle$ and χ with estimates of their errors. Figure 1 shows magnetic susceptibility dependence on temperature for lattice sizes L = 16, 32, 64, 128. The data for L = 128 have been obtained with only 20 bins, so Monte Carlo error bars are more pronounced near the critical temperature (its position is denoted by the dashed vertical line) than for smaller lattices studied here (where errors are comparable to data point sizes on the plot). The coupling here is taken to be constant ($J = J_0 = 1.0$).

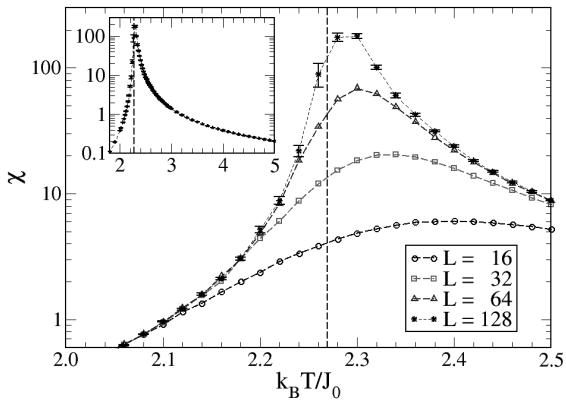

Fig. 1. The magnetic susceptibility χ versus temperature T. Note the logarithmic scale for χ. The dashed vertical line shows the position of the critical temperature T_C. The inset shows the shape of the magnetic susceptibility χ for the lattice of size L = 128 for the given range of temperatures

The corresponding analysis of the Binder ratio is shown in Figure 2. Note, that as expected, the first Binder ratio B_1 is independent of the lattice size at T_C. The inset in Figure 2 shows that in more detail. The horizontal dotted line represents the asymptotic value $\frac{\pi}{2}$

of B_1 for temperatures T much greater than T_C ($T >> T_C$) (for evidence, see [7, 8]). Thus, the results discussed and illustrated in Figures 2 and 3 validate the numerical methods used for the present study to some extent.

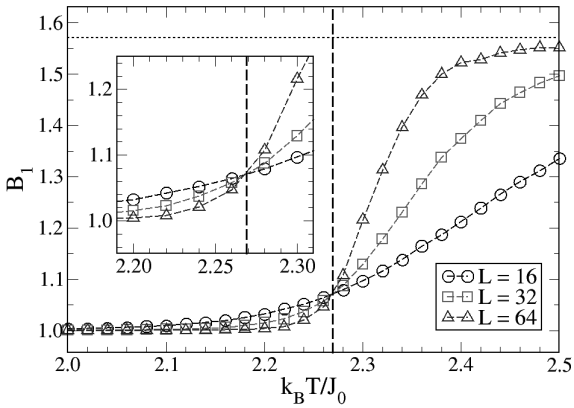

Fig. 2. The Binder ratio B_1 for the studied 2D Ising model ($J = J_0 = 1.0$). The inset shows the Binder ratio scaling in the vicinity of the critical temperature (indicated by the dashed vertical line). The horizontal dotted line indicates the asymptotic value of the Binder ratio

Finally, let us now consider the influence of the Gaussian noise in the value of the interaction coupling. It is assumed that the coupling $J = J_0$ is known with some uncertainty ΔJ_0 ($J = J_0 \pm \Delta J_0$). In the Monte Carlo simulations, the values of coupling energy are now allowed to vary slightly with subsequent MCS (but at any given MCS, they are fixed). The coupling energies are randomly drawn from the Gaussian (normal) distribution with the mean J_0 and the standard deviation ΔJ_0, so that $J = J_0 \pm \Delta J_0 = 1.0 \pm 0.1$ (this corresponds to a relative uncertainty of 10% in the value of the coupling energy). The results for the Binder ratio are shown in Figure 3 – note the shift in the value of the effective critical temperature with respect to the previously discussed case (Fig. 2). The new value of the effective critical temperature T_C' of the phase transition in the noisy system is significantly lower than in the case of noise absence, and in rescaled units, it equals approximately:

$$\frac{k_B T_C'}{J_0} \approx 2.22.$$

In order to understand this phenomenon at least qualitatively, one may regard noise in the coupling energy to be equivalent to the thermal energy in the system with no external field. This additional thermal energy allows for the system to undergo a phase transition at a lower temperature, which otherwise would be too low for the system with no noise (uncertainty) in the spin coupling interaction.

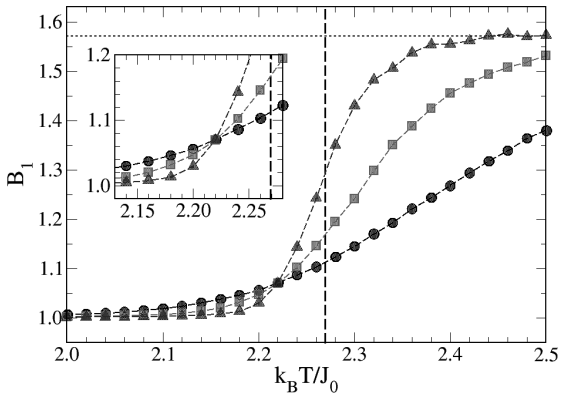

Fig. 3. The Binder ratio B_1 for the studied 2D Ising model with randomly varied coupling J, which is drawn from Gaussian probability distribution with average J_0 and standard deviation $\Delta J_0 = 1.0$

4. Conclusions

In this paper, the 2D Ising model on a square lattice with no external field was considered for various lattice sizes and spin numbers, ranging up to $N = 128^2 = 16\,384$ spins in the complex system. The results of present Monte Carlo simulations are in good agreement with earlier studies and some analytical, exact results. A novel approach has been put forward to consider the influence of the uncertainty of the spin coupling interaction on the effective critical temperatures in the system. This may have an application when comparing experimental results with some phase transition theory predictions. In particular, the results obtained in the present study give some indication regarding possible effects which may arise due to uncertainties of the system parameters in real experimental situations. Another possible application of this noisy 2D Ising model with Gaussian noise adopted would be to represent some many-body corrections or long-range spin correlations which are beyond the description within the standard Ising model, where only the interactions of pairs of spins are taken into account.

The author would like to acknowledge the use of the services and computer resources provided by the Academic Computer Center CYFRONET AGH in Kraków (Akademickie Centrum Komputerowe CYFRONET AGH, Grant No. MNiSW/IBM_BC_HS21/PK/033/2014, "Teoria złożoności rynków finansowych").

References

[1] Ising E., *Beitrag zur Theorie des Ferromagnetismus*, Zeitschrift für Physik, vol. 31, 1925, 253-258.

[2] Lenz W., *Beitrag zum Verständnis der magnetishen Erscheinungen in festen Körpern*, Zeitschrift für Physik, vol. 21, 1920, 613-615.

[3] Onsager L., *Crystal Statistics I. A Two Dimensional Model with an Order-Disorder Transition*, Physical Review, vol. 65, 1944, 117-149.

[4] Baxter R.J., *Exactly Solved Models in Statistical Mechanics*, Academic Press, New York 1982.

[5] Britton J.W., Sawyer B.C., Keith A.C., Wang C.-C.J., Freericks J.K., Uys H., Biercuk M.J. and Bollinger J.J., *Engineering two-dimensional Ising interactions in a trapped-ion quantum simulator with hundreds of spins*, Nature, vol. 484, 2012, 489-492.

[6] Bornholdt S., *Expectation Bubbles in a Spin Model of Markets: Intermittency from Frustration across Scales*, International Journal of Modern Physics C, vol. 12 (5), 2001, 667-674.

[7] Sandvik A.W., *Computational Studies of Quantum Spin Systems*, [in:] A. Avella, F. Mancini (Eds.), *Lectures on the Physics of Strongly Correlated Systems XIV*, AIP Conference Proceedings, vol. 1297, 2010, 135-338.

[8] Binder K., *Finite Size Scaling Analysis of Ising Model Block Distribution Functions*, Zeitschrift für Physik B vol. 43, 1981, 119-140. Binder K., *Applications of Monte Carlo Methods to Statistical Physics*, Reports on Progress in Physics, vol. 60, 1997, 487-559.

TECHNICAL TRANSACTIONS | **CZASOPISMO TECHNICZNE**
FUNDAMENTAL SCIENCES | NAUKI PODSTAWOWE
3-NP/2014

ANDRZEJ OSAK*

RELAXATION CURRENTS IN THE NON-MORPHOTROPIC REGION OF PZT-PFS FERROELECTRIC CERAMICS

PRĄDY RELAKSACYJNE W OBSZARZE POZAMORFOTROPOWYM FERROELEKTRYCZNEJ CERAMIKI PZT-PFS

Abstract

Studies on the dielectric relaxation currents in the non-morphotropic region of PZT-PFS are presented. Transient polarization and depolarization currents were measured at different poling fields (0.02–20 kV/cm) and different temperatures (77–473 K). The activation energies were calculated. The defect dipole complex (Fe_{TiZr}–$V_{Ö}$) and reorientation cluster dipole models are proposed to explain the observed relaxation behaviour in PZT-PFS.

Keywords: ferroelectric ceramics, PZT-PFS, relaxation currents

Streszczenie

W artykule przedstawiono badania prądów realaksacji dielektrycznej w PZT-PFS dla składów leżących poza morfotropową granicą faz. Zostały zmierzone prądy polaryzacji i depolaryzacji dla różnych wartości pola polaryzacji (0.02–20kV/cm) i temperatur (77–473 K). Wyznaczono energie aktywacji dla różnych próbek. Dla wyjaśnienia relaksacyjnego charakteru zjawisk w PZT-PFS został zaproponowany model oparty o zespoły defektów dipolowych (Fe_{TiZr}–$V_{Ö}$) i reorientacje klasterów dipoli.

Słowa kluczowe: ceramika ferroelektryczna, PZT-PFS, prądy relaksacji

* Institute of Physics, Faculty of Physics Mathematics and Computer Science, Cracow University of Technology; andrzej.osak@if.pk.edu.pl.

1. Introduction

Study of transient decaying currents is a very useful method for the determination of slow polarization and depolarization processes in ferroelectric materials. Such a study provides some insights into the microscopic mechanisms of polarization and depolarization processes and can explain aging, memory effects, domain wall motion, and the dynamics of dipoles, ions and electrons [1–4].

The results of measurements of the polarization and depolarization currents in the morphotropic region have previously been described in [5]. The present paper reports some additional studies on depolarization currents in the non-morphotropic region. Details of the experimental procedure and sample characterization are presented in [5].

Samples with circular silver electrodes with an area of 0.36 cm^2 and thickness 0.5 mm are used in all experiments. The samples $Pb[(Fe_{1/3}Sb_{2/3})_xTi_yZr_z]O_3$ with $x + y + z = 1$, $x = 0.1$ and $y = 0.43$ and $y = 0.47$ compositions were subjected to an electric field and the decaying current was measured under different strengths of the applied field. After poling, the applied field was removed and the sample was short circuited via a current-measuring 6517A Keithley electrometer until the reverse depolarization current had decayed.

2. Results

The relaxation behavior in PZT+PFS was studied for various poling fields, polarization times and temperatures. Fig. 1 shows the time dependence of the depolarization currents which were recorded after various poling times, i.e. 10^2, 10^3 and 10^4 s. The results are shown as the log-log scale plots. Initially, there was little difference between the curves, but at longer times, that difference increased. The depolarization current curves for polarization times 10^4 s and longer have tendency to coincident.

In Fig. 2a, the depolarization current for different poling field measured at 298 K, are plotted. It is evident that at a low poling field, one observes a linear dependence relaxation current in the probe field, whereas for higher poling fields, a rapid increase of nonlinearity appears and, simultaneously, the depolarization time becomes longer than 10^4 s. In Fig. 2b, the time dependences of depolarization currents, measured at 77 K, are shown. At lower poling fields, the depolarization currents are proportional to the electric field strength, but at higher fields, a non-linear behaviour is observed. However, the onset of the non-linear dependence begins at lower *poling* fields than in the case of higher temperature (298 K).

In Fig. 3, the polarization J_p, steady state J_s and depolarization J_d currents are presented for sample with $y = 0.47$. The charging currents at any time are the sum of the current due to both the decaying polarization current and the steady state conduction current:

$$J_c = J_p + J_s \tag{1}$$

At 298 K, the decaying currents are given for poling fields 0.02 (plot C) and 5 kV/cm (plot A). For low poling fields (0.02 kV/cm), the polarization and depolarization currents have approximately the same values at the same time (see Fig. 3, plot C, curves J_p and J_d). Whereas for higher fields 5 kV/cm, the depolarization current is lower than the polarization current (see Fig. 3, plot A curves J_p and J_d). At higher temperature (453 K), for the 0.02 kV/cm poling

field, the decaying polarization and depolarization currents have almost equal values at the same time (see Fig. 3, plot B, curves J_p and J_d) and the observed curves are mirror images of each other. Typical examples of the depolarization currents, measured under a low poling field (0.02 kV/cm) over the time period 1–10^4 s for selected temperatures for samples $y = 0.43$ and $y = 0.47$, are shown in Figs. 4a and 4b, respectively. The shape of the relaxation currents presented in Figs. 4a and 4b indicates the existence of two time-dependent relaxation processes, both obeying the well-known Jonscher-Dissado-Hill fractional power law:

$$J(t) = \frac{A(t)}{\left(\frac{\tau}{\tau_0}\right)^n + \left(\frac{\tau}{\tau_0}\right)^m} \tag{2}$$

where $\tau_0 = \omega_0^{-1}$ is the relaxation time for which the loss peak appears.

The relaxation of depolarization currents proceed faster, i.e. over a time shorter than the relaxation time τ_0 with the form t^{-n} and slower at times longer than τ_0 with the form t^{-m} [7]. Values of the exponents n and m, depending on temperature, are listed in Table 1. The insets in Figs. 4 a and b show the temperature dependence of the log τ_0^{-1} vs 1000/T. The activation energies calculated from the slop slope of this dependence are listed in Table II, along with the activation energies obtained from the electric conduction.

3. Discussion

1. The polarization and depolarization current decays at low (~0.02 kV/cm) and high poling fields (~20 kV/cm) as well as for different poling time were measured. The results presented in Fig. 1 show that, for a short poling time, only relaxation processes with short relaxation times are developed. Poling times of at least the order 10^4 s are needed to initiate all various polarization processes with long relaxation times, both at high and low temperatures. For a weak poling field (~0.2 kV/cm), there is no difference between polarization and depolarization currents, as shown in Fig. 3, plots B and C. This means that the reorientation of dipoles and domain wall motion is reversible and that the ferroelectric under study behaves as a linear dielectric. The onset of irrevertiable motion of the domain walls begins at higher fields [8]. In this range of poling field, the depolarization current at any time is less than the polarization current (see Fig. 3, plot A) and the remnant polarization is induced. At very high poling fields (20 kV/cm; Fig. 2a), the space charge appears providing an additional contribution to the total discharge current [5, 6].

2. The properties of the PZT compounds are strongly altered by point defects. In the case of $Pb(Zr,Ti)O_3$ modified by FeSb ions, randomly distributed Ti^{4+}, Zr^{4+}, Fe^{3+} ions on the B site of the perovskite structure are created. The group of octahedrons with identical B site ions $(BO_6)_n$ gives rise to a micro-region (cluster) with a large number of locally interacting dipoles. The nanometer size clusters with various composition have dipole moments undergoing the thermal fluctuation between equivalent positions. Between clusters, some coupling interaction occurs leading to partial long-range regularity. Longer relaxation times are associated with relaxation due to the cooperative motion of the group of clusters (micro-regions) [10, 11]. The observed, in initial time, the power law dependence $J_p(t) \sim t^{-n}$ may be

explained take into account dipol-dipol and ion-ion interactions. As it was shown in paper [12] such interaction leads to the generation low-energy correlated states. The density of this low-energy excitation gives rise to the infrared divergence response function t^{-n}.

3. In the case of PZT with Fe^{3+} ions, three Fe_{TiZr}–$V_{Ö}$ defect complexes could be formed depending on whether the oxygen atoms were removed or not [13, 14]. The energy barriers for reorientation of these defect complexes depend on the position of oxygen vacancies with respect to iron atoms [13, 14]. In the tetragonal phase of the PZT, there are two types of oxygen atoms – the oxygen atoms bonded to two Ti atoms in ab planes [O(2)] and the oxygen atoms in the O-Ti-O chains in c directions [O(1)]. Therefore, one may expect three kinds of defect complexes. The Debye-type relaxation peaks (see Figs. 4a and b), observed, in both samples, can be attributed to the reorientation defect complexes formed by the oxygen vacancies. Activation energies obtained from relaxation times (see Table 2) approximately equals to the energy barrier of the defect dipole rotation calculated in paper [13, 14].

Table 1

Values of power exponents n and m for samples with $y = 0.43$ and $y = 0.47$

$y = 0.43$			$y = 0.47$		
T [K]	n	m	T [K]	n	m
298	0.72	1.17	298	0.73	1.19
343	0.68	1.18	423	0.72	1.22
398	0.62	1.19	473	0.70	1.28

Table 2

Activation energies obtained from the measurements of relaxation times E_r and electrical conduction E_c [15]

composition	E_r [eV]	E_c [eV]
$y = 0.43$	0.34	0.37
$y = 0.47$	0.16	0.17

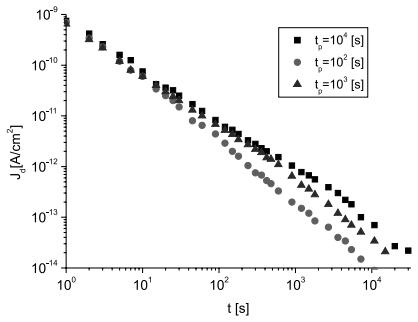

Fig. 1. Time-dependence of depolarization currents (J_d) for various poling times (t_p) measured at 298 K for sample with $y = 0.47$. Poling field: 0.02 kV/cm

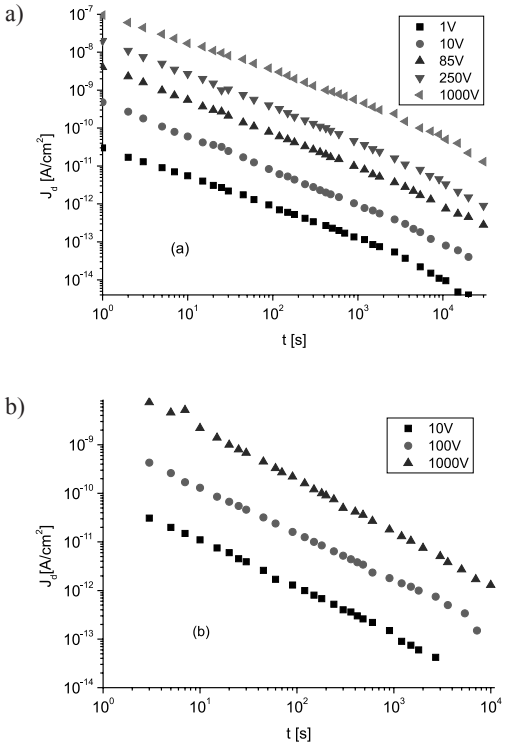

Fig. 2. Depolarization currents (J_d) for different poling fields for sample with $y = 0.47$ measured at 258 K (a) and 77 K (b)

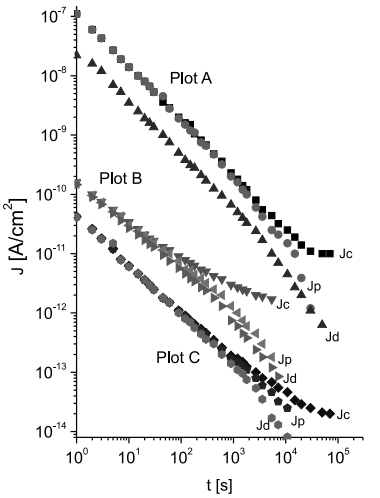

Fig. 3. Charging (J_c), polarization (J_p) and depolarization (J_d) current densities for sample with $y = 0.47$. Plot A: temperature 298 K, poling field 5 kV/cm; plot B: temperature 453 K, poling field 0.02 kV/cm; plot C: temperature 298 K, poling field 0.02 kV/cm

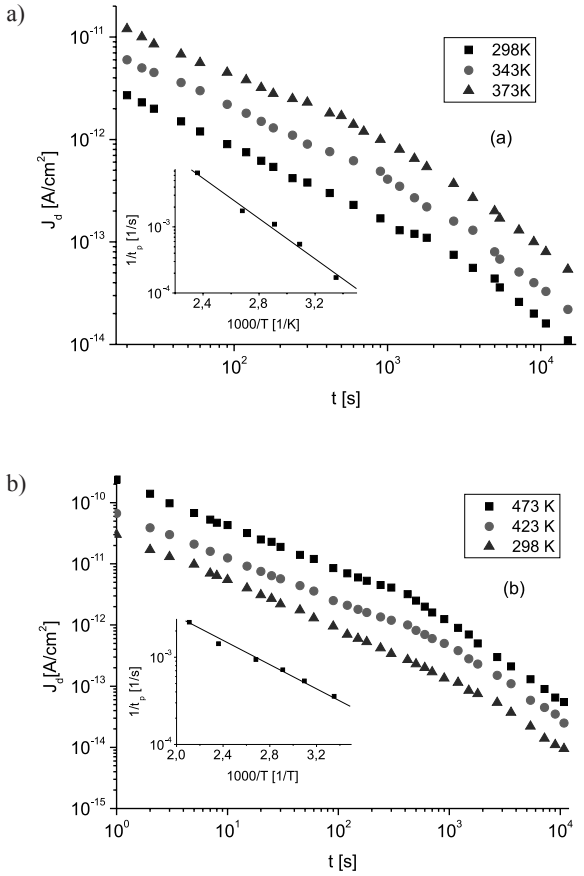

Fig. 4. Depolarization current density (J_d) under low poling field (0.02 kV/cm) at different temperatures for samples with $y = 0.47$ (a) and $y = 0.43$ (b). The insert shows the $\log 1/\tau_p$ vs. 1000/T dependence

References

[1] Rabe K.M., Dawber M., Lichtensteiger C., Ahn C.H., *Modern physics of ferroelectrics: essential background*, [in:] Rabe K.M., Ahn C.H., Triscone J-M. (Eds.), *Physics of Ferroelectrics A Modern Perspective*, Springer, Berlin–Heidelberg–New York 2007, 1-30.

[2] Paruch P., Giamarchi T., Triscone J-M., *Nanoscale Studies of Domain Walls in Epitaxial Ferroelectric Thin Films*, [in:] Rabe K. M., Ahn C. H., Triscone J-M. (Eds.): *Physics of Ferroelectrics A Modern Perspective*, Springer, Berlin, Heidelberg, New York 2007, 339-360.

[3] Carl K., Härdtl K.H., *Electrical After-Effects in Pb(TiZr)O_3 ceramic*, Ferroelectrics, vol. 17, 1978, 473-486.

[4] Kircher O., Bohmer R., *Aging, rejuvenation and memory phenomena in a lead-based relaxor ferroelectric*, Eur. Phys J., vol. 26, 2002, 329-338.

[5] Osak A., *Relaxation currents in morphotropic region of* $Pb[(Fe_{1/3}Sb_{2/3})_xTi_y\ Zr_z]O_3$ *ferroelectric ceramics*, Phase Transitions, vol. 86 (9), 2012, 1-6.

[6] Shiguang Yan, Chaoling Mao, Genshui Wang, Chunhaua Yao, Fei Cao, Xilian Dong, *Temperature and voltage stress dependent dielectric relaxation process of the doped* $Ba_{0.67}Sr_{0.33}TiO_3$ *ceramics*, Applied Physics Letters, vol. 103, 2013, 112908.

[7] Jonscher A.K., *Dielectric relaxation in solids*, Chelsea Dielectric Press, London 1983.

[8] Tosima S., Nishikawa M., *Critical field variation for domain wall motion in ferroelectric/ferroelastic* $Gd_2(MoO_4)_3$, J. Appl. Phys., vol. 48, 1977, 3169-3170.

[9] Thomas N.W., *A now framework for understunding relaxor ferroelectrics*, J. Phys. Chem. Solids, vol. 51, 1990, 1419-1431.

[10] Dissado L.A., Hill R.M., *Dielectric behaviour of materials undergoing dipole aligment transitions*, Phil. Mag. B, vol. 41, 1980, 625-642.

[11] Jonscher A.K., Jurlewicz A., Weron K., *Stochastic schems of dielectric relaxation in corelated cluster systems*, Contemporary Physics, vol. 44, 2003, 329-339.

[12] Ngai K.L. White C.T., *Frequency dependence of dielectric loss in condensed matter*, Phys. Rev. B, vol. 20, 1979, 2475-2486.

[13] Maraton P., Elsässar, *Switching of substitutional-iron oxygen vacancy deffect complex in ferroelectric* $PbTiO_3$ *from first principles*, Phys. Rev. B, vol. 83, 2011, 020106.

[14] Jakes P., Erden E., Eichel R.A., Li Jin, Damjanowic D., *Position of defects with respect to domain walls in* Fe^{3+}*-doped* $Pb[Zr_{0.52}Ti_{0.48}]O_3$ *piezoelectric ceramics*, Appl. Phys. Letts, vol. 98, 2011, 072907.

[15] Osak A.P., Ptak W.S., Osak W., Strzałkowska C., *Dielectric and electric properties of polycrystalline* $Pb[(Fe_{1/3}Sb_{2/3})_xTi_yZr_z]O_3$, Ferroelectrics, vol. 154, 1994, 247-252.

TECHNICAL TRANSACTIONS | **CZASOPISMO TECHNICZNE**
FUNDAMENTAL SCIENCES | NAUKI PODSTAWOWE
3-NP/2014

ADAM SZMAGLIŃSKI, GRZEGORZ CZAJKOWSKI*

OPTIMAL INVESTMENT HORIZONS FOR THE MAIN INDICES OF THE WARSAW STOCK EXCHANGE

OPTYMALNE HORYZONTY INWESTYCYJNE DLA GŁÓWNYCH INDEKSÓW WARSZAWSKIEJ GIEŁDY PAPIERÓW WARTOŚCIOWYCH

Abstract

The investment horizon is the smallest time interval when an asset crosses a fixed value of the return level. For a given return level, the investment horizon distribution is created by putting the investment horizons into a histogram. We fit probability distribution function to the histogram. The maximum of the function is called the optimal investment horizon. We performed the analysis of some indices of the Warsaw Stock Exchange for WIG, WIG20, mWIG40 and shares of KGHM and MBK. For these assets, we found the coefficients of linear proportion between the optimal investment horizons and the logarithm of their return levels.

Keywords: econophysics, financial markets, inverse statistics

Streszczenie

Horyzont inwestycyjny jest najmniejszym odcinkiem czasu, w którym dana inwestycja przekroczyła ustalony poziom zwrotu. Dla danego poziomu zwrotu tworzymy rozkład horyzontu inwestycyjnego, składając horyzonty inwestycyjne w histogram. Maksymalna wartość dopasowanej funkcji rozkładu prawdopodobieństwa jest optymalnym horyzontem inwestycyjnym. Przeprowadziliśmy analizę dla niektórych indeksów Warszawskiej Giełdy Papierów Wartościowych WIG, WIG20, mWIG40, sWIG80 oraz akcji KGHM i MBK. Dla wymienionych instrumentów finansowych wyznaczyliśmy współczynniki proporcji liniowej pomiędzy optymalnymi horyzontami inwestycyjnymi i logarytmami poziomów zwrotu.

Słowa kluczowe: ekonofizyka, rynki finansowe, odwrócona statystyka

* Institute of Physics, Faculty of Physics, Mathematics and Computer Science, Cracow University of Technology, Poland; aszmag@op.pl, g.czajkowski@yahoo.pl.

1. Introduction

The character of price movements was described quantitatively by the random walk hypothesis proposed by Bachelier [1]. However, the nature of these movements better reflects the random walk hypothesis for the logarithm of the price $s(t) = \ln(S(t))$ [2]. According to this assumption, the distribution of the returns of an asset is effectively described by a Gaussian distribution [3–5].

A large amount of financial data is recorded for financial studies and benchmarking. An important and common task in studying the data is calculating the distribution of returns over a fixed time period Δt. The distribution measures gains or losses at time $t + \Delta t$ produced by the investment made at time t.

Many empirical studies for small values of Δt argue that the price changes are much larger than expected from the Gaussian distribution. The distributions have so-called fat tails [3–6]. For larger values of Δt the distribution of returns converges to the Gaussian distribution [7–10]. The analogue distribution is found for turbulence in air and fluids [11]. The statistics of financial markets were compared with turbulent fluids [4, 12–14].

The inversion of the standard return-distribution problem was proposed by Simonsen, Jensen and Johansen [15–17]. They studied the probability distribution of waiting times needed to reach a fixed return value ρ for the first time [11].

Another kind of investigation on waiting times and price movements was proposed in [18]. There were studied the frequency of occurrences of subsequent movements' proportions in price and time. Their proportions are effectively described by the generalized Gamma probability distribution.

2. Investment horizons

The first passage time problem was described in [19]. The solution to the Brownian motion problem is analytically provided by the Gamma distribution in [20, 21]:

$$p(t) = \frac{1}{\sqrt{\pi}} \frac{|a|}{t^{3/2}} e^{-a^2/t}, \tag{1}$$

where a is proportional to the return level ρ.

The overall growth of the economy modulated with times of recession influences financial time series $s(t)$ with a positive drift over long time scales. In the presence of such a drift, we cannot use the Brownian motion model to describe these series. For this reason, we should use so-called deflated asset prices $\tilde{s}(t)$ for reducing the effect of this drift. The drift $d(t)$ we describe with a 1000-day moving average for stock indices and a 250-day moving average for shares due to their higher volatility. These two periods naturally correspond to four calendar years and one calendar year respectively. For our analysis, we use logarithmic prices with subtracted drift $\tilde{s}(t) = s(t) - d(t)$. The prepared data for the WIG index and the MBK shares is depicted in Fig. 1. and Fig. 2.

The log-return over a time interval Δt of an asset of price $S(t)$ at time t reads:

$$r_{\Delta t}(t) = \ln \frac{S(t + \Delta t)}{S(t)}, \tag{2}$$

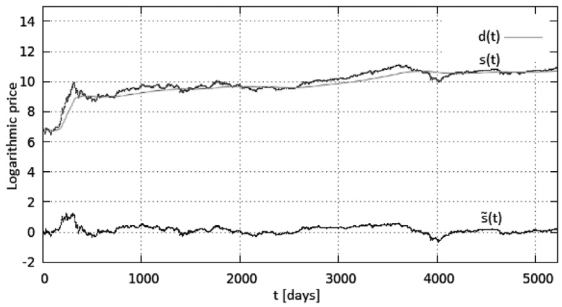

Fig. 1. Daily logarithmic closure prices of the WIG index over years 1991–2013

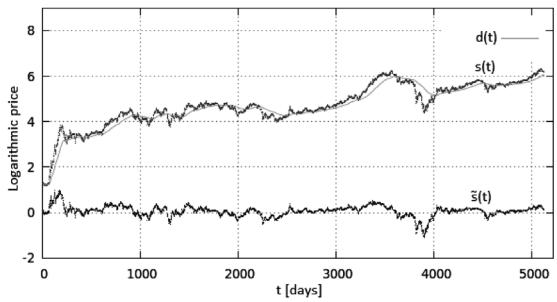

Fig. 2. Daily logarithmic closure prices of the MBK shares over years 1991–2013

For a return level ρ at time t, the *investment horizon* $\tau_p(t)$ is the smallest time interval Δt that satisfies the relation $r_{\Delta t}(t) \geq \rho$. For a fixed return level, we put the investment horizons in the histogram. In this way, we obtain the investment horizon distribution $p(\tau_p)$. Due to the empirical logarithmic stock price process is not the Brownian [3–6], we fit generalized Gamma distribution to the histogram:

$$p(t) = \frac{\nu}{\Gamma(\alpha/\nu)} \frac{|\beta|^{2\alpha}}{(t+t_0)^{\alpha+1}} \exp\left\{-\left(\frac{\beta^2}{t+t_0}\right)^{\nu}\right\}. \tag{3}$$

The distribution (3) reduces to the Gamma distribution (1) for parameters $\alpha = \beta = 0.5$, $\nu = 1$ and $t_0 = 0$.

The maximum of the distribution (3) defines the *optimal investment horizon*:

$$\tau_\rho^* = \beta^2 \left(\frac{\nu}{\alpha+1}\right)^{1/\nu} - t_0 \tag{4}$$

According to (1) for geometric Brownian processes we have relation $\tau_\rho^* \sim \rho^2$. The empirical data generate slightly different dependence, as we will see in the next section.

3. Discussion and results

The analysis was performed originally by Simonsen et al. in [15], it was also used for the WIG and some stock companies quoted in the Warsaw Stock Exchange (WSE) [22–24]. In this paper, we continue the investigation described in [25] for indices and companies quoted in the WSE. For the return level ρ = 0.10 in Fig. 3 and Fig. 4, we present $p(\tau_\rho)$ – the probability distribution function (pdf) of the investment horizons measured in trading days τ_ρ. As one can expect from the higher volatility of the share prices of MBK compared to WIG, the optimal investment horizon was $\tau_\rho^* = 4.52$ for MBK and $\tau_\rho^* = 11.33$ for WIG. The probability of reaching the return level for MBK is two times larger than for the WIG index in the area of the optimal investment horizon. The values of the optimal investment horizons for indices and shares we analyzed are placed in Table 1.

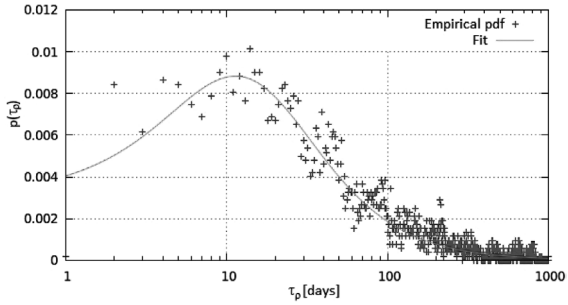

Fig. 3. The probability distribution function of the investment horizons of WIG measured in trading days, for the return level ρ = 0.10

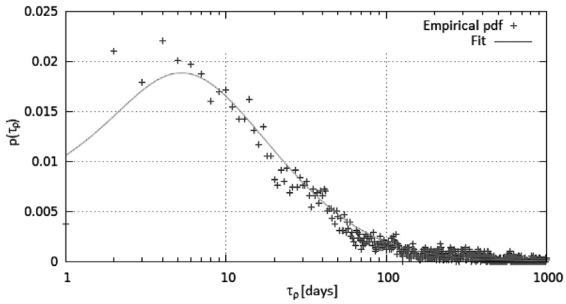

Fig. 4. The probability distribution function of the investment horizons of MBK measured in trading days, for the return level ρ = 0.10

We compare results with the DJIA index, which has a few times larger values of τ_ρ^* in comparison with indices quoted in WSE. This higher volatility is a feature of the WSE, rather than of emerging stock markets [22]. Among the main indices on the WSE, mWIG40 has the highest value of the optimal investment horizon. mWIG40 is composed of 40 medium-sized companies.

We also analyzed KGHM, the company with the highest capital in WIG20. Another company is MBK (former BRE Bank), which has been quoted in WIG20 since its beginning. Companies have much shorter values of τ_ρ^* than indices. The reason for this is in their higher volatility than the volatility of indices. The index is a weighted sum of the companies and every price movement of each company is only partially reflected in the change of the index.

Table 1

Optimal investment horizons for return levels ρ = 0.05, 0.10, 0.15 and the exponent of the return level γ

Name	ρ = 0.05	ρ = 0.10	ρ = 0.15	γ
DJIA	10.97	36.15	63.04	1.55
WIG	4.33	11.33	18.23	1.25
WIG20	3.33	9.66	15.27	1.34
mWIG40	6.82	20.27	40.07	1.60
sWIG80	4.82	12.93	22.21	1.35
KGHM	–	5.55	11.51	1.52
MBK	–	4.52	8.60	1.57

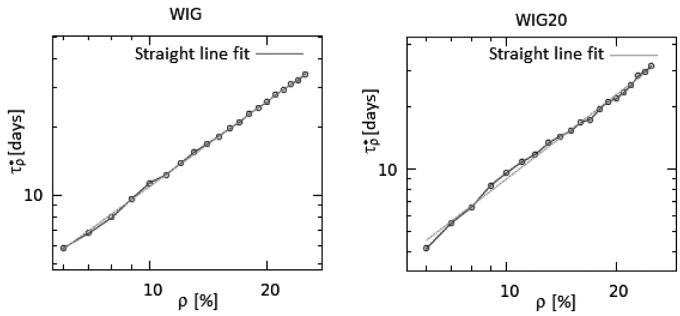

Fig. 5. The optimal investment horizon of two main indices on the WSE as a function of the log-return level ρ

Another important feature we investigate is the proportion:

$$\tau_\rho^* \sim \rho^\gamma \tag{5}$$

The Brownian motion model with $\gamma = 2$ is inconsistent with empirical results [15]. For higher return values ρ, we fitted γ parameter as in Fig. 5. and Fig. 6. We find $\gamma < 2$ in the range 1.35–1.60 as shown in Table 1. For smaller return values ρ, we observed higher values of τ_ρ^* (not shown in the picture) than we could expect from (5).

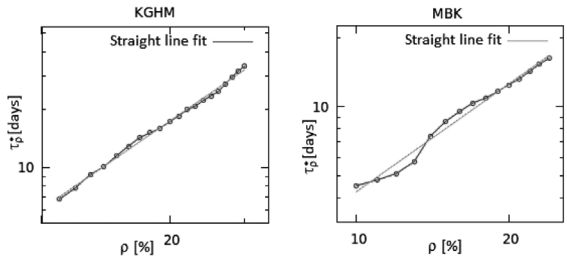

Fig. 6. The optimal investment horizon of two companies as a function of the log-return level ρ.

4. Conclusions

In this work, we analyzed the main indices quoted in the WSE which constitute the benchmark for some capital funds. The distributions and the optimal investment horizons can be applied for estimating the most probable time period for realization of the return level. The analogue passage time distributions are applied in turbulence of fluids, where they are called inverse structure functions.

The lower values of γ parameter indicate that the prices are more stable and connected with the real value of the asset than the expectation of the geometrical Brownian hypothesis which is generally accepted for capital markets [3, 4].

References

[1] Bachelier L., *Théorie de la Spéculation*, Annales de l'Ecole normale superiure, 1900.
[2] Samuelson P., *Economics: The Original 1948 Edition*, McGraw-Hill/Irwin.
[3] Bouchaud J.P., Potters M., *Theory of Financial Risks: From Statistical Physics to Risk Management*, Cambridge University Press, Cambridge, 2000.
[4] Mantegna R.N., Stanley H.E., *An Introduction to Econophysics: Correlations and Complexity in Finance*, Cambridge University Press, Cambridge, 2000.
[5] Hull J., *Options, Futures and other Derivatives*, Prentice-Hall, London 2000.
[6] Mandelbrot B.B., *J. Business*, vol. 36 No. 4, 1963, 394-419.
[7] Drożdż S., Kwapień J., Grümmer F., Ruf F., Speth J., *Acta Phys. Pol. B*, vol. 34, 2003, 4293-4306.
[8] Rak R., Drożdż S., Kwapień J., *Physica A*, vol. 374, 2007, 315-324.
[9] Drożdż S., Forczek M., Kwapień J., Oświęcimka P., Rak R., *Physica A*, vol. 383, 2007, 59-64.
[10] Kwapień J., Drożdż S., *Physics Reports*, vol. 515, 2012, 115-226.
[11] Jensen M.H., *Phys. Rev. Lett.*, vol. 83, 1999, 76-79.
[12] Mantegna R.N., Stanley H.E., *Nature*, vol. 383, 1996, 587-588.
[13] Ghashghaie S., Breymann W., Peinke J., Talkner P., Dodge Y., *Nature*, vol. 381, 1996, 767-770.
[14] Friedrich R., Peinke J., Renner Ch., *Phys. Rev. Lett.*, vol. 84, 2000, 5224-5227.

[15] Simonsen I., Jensen M.H., Johansen A., *Eur. Phys. J. B*, vol. 27, No. 4, 2002, 583-586.
[16] Jensen M.H., Johansen A., Simonsen I., *Physica A*, vol. 234, 2003, 338-343.
[17] Jensen M.H., Johansen A., Petroni F., Simonsen I., *Physica A*, vol. 340, 2004, 678-684.
[18] Szmagliński A., *Acta Phys. Pol. A*, vol. 123, 2013, 621-623.
[19] Redner S., *A Guide to First Passage Process*, Cambridge, New York 2001.
[20] Ding M., Yang W., *Phys. Rev. E*, vol. 52, 1995, 207-213.
[21] Rangarajan G., Ding M., *Phys. Lett. A*, vol. 273, 2000, 322-330.
[22] Karpio K., Załuska-Kotur M., Orłowski A., *Physica A*, vol. 375, 2007, 599-604.
[23] Załuska-Kotur M., Karpio K., Orłowski A., *Acta Phys. Pol. B*, vol. 37, 2006, 3187-3192.
[24] Grudziecki M., Gnatowska E., Karpio K., Orłowski A., Załuska-Kotur M., *Acta Phys. Pol. A*, vol. 114, 2008, 569-574.
[25] Czajkowski G., Eng. Th. *Investment Horizon Distribution for Main Indices of Warsaw Stock Exchange*, Kraków 2014.

TECHNICAL TRANSACTIONS | **CZASOPISMO TECHNICZNE**
FUNDAMENTAL SCIENCES | NAUKI PODSTAWOWE
3-NP/2014

WŁODZIMIERZ WÓJCIK*

THE STRUCTURE OF NEUTRON STARS WITH LOCALIZED PROTONS

STRUKTURA GWIAZD NEUTRONOWYCH ZE ZLOKALIZOWANYMI PROTONAMI

Abstract

Strongly asymmetric nuclear matter becomes unstable with respect to proton localization above a specific critical nuclear density. For equation of state of Akmal, Pandharipande and Ravenhall the Tolman-Oppenheimer-Volkoff equations were solved and the radius of the spherical shell of a neutron star within which proton localization takes place was found.

Keywords: strongly asymmetric nuclear matter, proton localization, neutron stars

Streszczenie

Silnie asymetryczna materia jądrowa wykazuje niestabilność związaną z lokalizacją protonu powyżej krytycznej gęstości. Dla równania stanu Akmala, Pandharipande i Ravenhalla zostały rozwiązane równania Tolmana-Oppenheimera-Volkoffa i został wyznaczony promień powłoki gwiazdy neutronowej, wewnątrz której ma miejsce lokalizacja protonów.

Słowa kluczowe: silnie asymetryczna materia jądrowa, lokalizacja protonu, gwiazdy neutronowe

* Institute of Physics, Faculty of Physics, Mathematics and Computer Science, Cracow University of Technology, Poland; puwojcik@cyf-kr.edu.pl.

1. Introduction

The structure of neutron stars is both interesting and complex and is a problem to be solved. A few years ago, the model with star matter having localized protons was proposed [1–5]. In high-density matter with a low proton fraction, the coupling of proton impurities with the density waves in neutron matter could lead to the localization of protons in the potential wells associated with the neutron density inhomogeneities. Such instability is a universal phenomenon in high density matter, although the proton localization threshold density depends on the equation of state [6].

This paper is organized as follows. In Section 2, there is a brief discussion of some of the features of the Akmal-Pandharipande-Ravenhall (APR) Hamiltonian [7] and the ingredients involved in their construction. In Section 3, the Tolman-Oppenheimer-Volkoff equations [8] are presented. In Section 4, these are solved with the APR equation of state and the radius of the shell below which protons in neutron stars are localized is calculated.

2. Akmal-Pandharipande-Ravenhall equation of state

The A18+δv+UIX* parametrization of the APR equation of state was chosen for nuclear interaction. In this approach, the Jastrow wave function is assumed and the expectation value of the Hamiltonian is cluster-expanded. Subsequently, parts of the higher-order cluster terms are resummed up by the Fermi Hypernetted Chain (FHCN) method [9]. Akmal, Pandharipande and Ravenhall performed the FHCN calculation [8] with Argonne v18 (Av18) two-body potential [10] and the Urbana IX* (UIX*) three-body potential [11] with boost correction. The obtained energy density reads:

$$
\begin{aligned}
&\mu(n_N,n_P)=\left(\frac{1}{2m_N}+\left(\left(p_3+p_5\right)n_N+p_3n_P\right)e^{-p_4\left(n_N+n_P\right)}\right)\frac{3}{5}\left(3\pi^2\right)^{\frac{2}{3}}n_N^{\frac{5}{3}}+\\
&\left(\left(\frac{1}{2m_P}+\left(\left(p_3+p_5\right)n_P+p_3n_N\right)e^{-p_4\left(n_N+n_P\right)}\right)\frac{3}{5}\left(3\pi_2\right)^{\frac{2}{3}}n_P^{\frac{5}{3}}+4n_Nn_P\left(p_1+p_2(n_N+n_P)+\right.\right.\\
&\left.p_6(n_N+n_P)^2+\left(p_{10}+p_{11}(n_N+n_P)\right)e^{-p_9^2(n_N+n_P)^2}\right)-\\
&(n_N-n_P)^2\left(\frac{p_{12}}{n_N+n_P}+p_7+p_8(n_N+n_P)+p_{13}e^{-p_9^2(n_N+n_P)^2}\right)-\\
&4n_Nn_P(n_N+n_P-p_{19})\left(p_{17}+p_{21}(n_N+n_P-p_{19})\right)e^{p_{18}(n_N+n_P-p_{19})}-\\
&(n_N-n_P)^2(n_N+n_P-p_{20})\left(p_{15}+p_{14}(n_N+n_P-p_{20})\right)e^{p_{16}(n_N+n_P-p_{20})},
\end{aligned}
\tag{1}
$$

where the neutron and the proton densities fulfil the following conditions $n_N + n_P > p_{19}$ or: $n_N + n_P > p_{20}$. The parameters have the following values: $p_1 = 337.2$ MeVfm^3; $p_2 = -382.0$ MeVfm^6; $p_3 = 89.8$ MeVfm^5; $p_4 = 0.457$ fm^3; $p_5 = -59.0$ MeVfm^5; $p_6 = 19.1$ MeVfm^9; $p_7 = 214.6$ MeVfm^3; $p_8 = -384.0$ MeVfm^6; $p_9 = 6.4$ fm^3;

p_{10} = 69.0 MeVfm^3; p_{11} = –33.0 MeVfm^6; p_{12} = 0.35 MeV; $p_{13} = p_{14} = p_{21} = 0$;
p_{15} = 287.0 MeVfm^6; p_{16} = –1.54 fm^3; p_{17} = 157.0 MeVfm^6; p_{18} = –1.45 fm^3;
p_{19} = 0.32 fm^{-3}; p_{20} = 0.195fm^{-3}.

3. Tolman-Oppenheimer-Volkoff equations

The structure of spherically symmetrical non-rotating neutron stars is described by the celebrated the Tolman-Oppenheimer-Volkoff (TOV) equations [12], which form a coupled set of first-order differential equations of the following form:

$$\frac{dP}{dr} = -\frac{G\rho m}{r^2}\left(1+\frac{P}{\rho c^2}\right)\left(1+\frac{4\pi r^3 P}{mc^2}\right)\left(1-\frac{2Gm}{rc^2}\right)^{-1}, \tag{2}$$

$$\frac{dm}{dr} = 4\pi r^2 \rho, \tag{3}$$

where:

$P(r)$ – denotes the pressure (at radius r),
$\varrho(r)$ – mass density,
$m(r)$ – the mass enclosed within the radius r,
G – the gravitational constant,
c – the speed of light.

For a given fluid element in the star, hydrostatic equilibrium is attained by adjusting the pressure gradient to exactly balance the gravitational pull.

The second equation defines the total mass contained in the sphere of radius r. Thus at $r = 0$, m must be zero and at $r = R$, m is the total mass M of the star. The unknowns in these two equations are ϱ, P and m – hence, a third equation is needed to close the system. This third equation is the equation of state (EOS) $P = P(\varrho)$. Thus, the input to the calculations is the EOS and the output yields the masses of neutron stars as a function of their radius for a given central density. Given the stellar radius R, which is defined by zero pressure at the stellar surface, the gravitational mass is as follows:

$$M(R) = 4\pi \int_0^R \rho(r) r^2 dr. \tag{4}$$

In hydrostatic equilibrium the neutron star is perfectly balanced by the action of two forces – gravity and pressure. The pressure gradient is negative so the pressure decreases monotonically with distance until it vanishes at the edge of the star. The pressure at the center must be enormous in order to be able to support the full weight of the star. This implies that models of the EOS will have to encompass high and low density ranges. This is an example of how the microscopic physics (EOS) can potentially be 'observed' from astrophysical data, namely from the mass and radius of the star.

4. The results

The aim of this work was to compare the energies of two phases. The energetically favorable ground state of matter is found by comparing the energy of a normal phase E_0 with uniform density and a phase with localized protons E_L. Based on our papers [1–5] we calculate $\Delta E = E_L - E_0$ versus neutron density n_N (Fig. 1) and we establish that above n_L = 0.819 fm^{-3}, protons in neutron matter for the A18+δv+UIX* potential are localized.

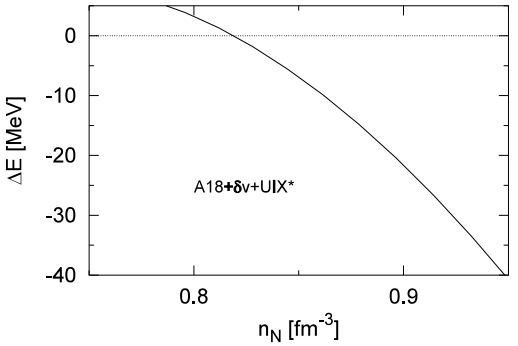

Fig. 1. Difference $\Delta E = E_L - E_0$ versus neutron density for the A18+δv+UIX* parametrization

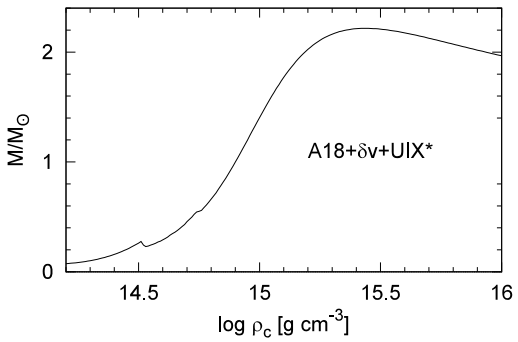

Fig. 2. Mass-central density relation for the A18+δv+UIX* equation of state

The TOV equations are solved with the A18+δv+UIX* parametrization introduced in Section 2. Fig. 2 presents the dependence of neutron star masses on the logarithm of central density. For central density above 10^{15} g cm^{-3}, we have neutron stars with masses higher than the solar mass ($M_\odot$). It transpires that the mass of the neutron star has a maximum value (Fig. 2) as a function of central density, above which the star becomes unstable and collapses to a black hole. The value of the maximum mass depends on the nuclear EOS. The considered solutions of the TOV equations with the A18+δv+UIX* equation of state is compatible with the largest mass observed up until now, which is measured to be 2.01 ± 0.04 $M_\odot$ [13].

We have also plotted (Fig. 3) the density versus the distance from the centre of the neutron star for a given central density (log ϱ_c = 15.4) and found that the radius of the neutron star equals approximately 10 km. The obtained value is compatible with the observed radii of neutron stars [12].

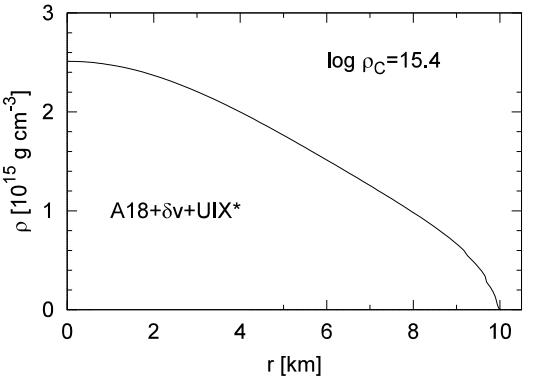

Fig. 3. Density of neutron star versus distance from centre for log ϱ_c = 15.5

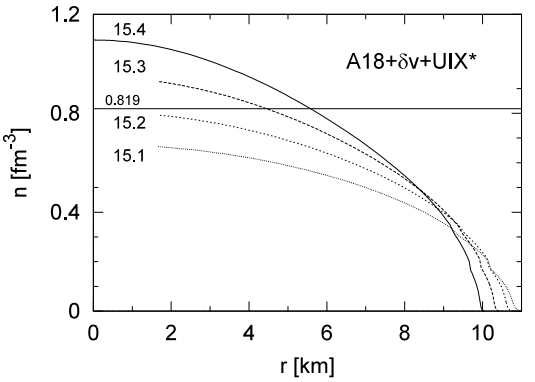

Fig. 4. Baryon number density versus distance from the centre of the neutron star. The curves are labelled by the logarithm of the central density of the star. The straight line indicates the threshold density of localization

Next, the density profiles of neutron stars were calculated. For the various central densities, changes of neutron star matter density versus distance from its centre for the A18+δv+UIX* equation of state were calculated (Fig. 4). Comparing the profile shape with the value of proton localization threshold (straight line on Fig. 1) n_L = 0.819 gives a radius of spherical shell r_L within which proton localization takes place. The curves are labelled by the logarithm of the central densities. In our case, for log ϱ_c = 15.3 we have r_L = 4.4 km (for neutron star radius R equals 10.4 km) and for log ϱ_c = 15.4 we have r_L = 5.6 km (R = 10.9 km).

5. Concluding remarks

The solution of the Tolman-Oppenheimer-Volkoff equations with the A18+δv+UIX* equation of state indicates that the structure of neutron stars is inhomogeneous – in the central area, up to r_L protons are localized and above r_L to R (radius of neutron star) protons and neutrons are delocalized.

The phase with localized protons inside neutron star cores has profound astrophysical consequences. As has been shown [14], the cooling of neutron stars proceeds in quite different ways for localized and delocalized phases. The presence of such a localized proton phase results in more satisfactory fits of the observed temperatures of neutron stars.
Further studies applying other equations of state are in progress.

References

[1] Kutschera M., Wójcik W., *Proton impurity in the neutron matter: A nuclear polaron problem*, Phys. Rev. **C47**, 1993, 1077.

[2] Kutschera M., Wójcik W., *Magnetic properties of strongly asymmetric nuclear matter*, Phys. Lett. **B223**, 1989, 11.

[3] Kutschera M., Wójcik W., *A Thomas-Fermi model of localization of proton impurities in neutron matter*, Acta Phys. Polon. **B21**, 1990, 823.

[4] Kutschera M., Wójcik W., *Self-consistent proton crystallization in dense neutron-star matter*, Nucl. Phys. **A581**, 1995, 706.

[5] Szmagliński A., Kutschera M., Stachniewicz S., Wójcik W., *The structure of a neutron star*, Monograph **389**, Cracow University of Technology, Cracow 2010.

[6] Szmagliński A., Wójcik W., Kutschera M., *Properties of localized protons in neutron star matter for realistic nuclear models*, Acta Phys. Polon. **B37**, 2006, 277.

[7] Akmal A., Pandharipande V.R., Ravenhall D.G., *Equation of state of nucleon matter and neutron star structure*, Phys. Rev. **C58**, 1998, 1804.

[8] Oppenheimer J.R., Volkoff G.M., *On massive neutron cores*, Phys. Rev. **55**, 1939, 374.

[9] Clark J.W., *Variational theory of nuclear matter*, Prog. Part. Nucl. Phys. 2, 1979, 89.

[10] Wiringa R.B., Stocks V.G.J., Schiavilla R., *Accurate nucleon-nucleon potential with charge-independence breaking*, Phys. Rev. **C51**, 1995, 38.

[11] Pudliner B.S., Pandharipande V.R., Carlson J., Wiringa R.B., *Quantum Monte Carlo calculations of $A \leq 6$ nuclei*, Phys. Rev. Lett. **74**, 1995, 4396.

[12] Shapiro S.L., Teukolsky S.A., *Black Holes, White Dwarfs and Neutron Stars*, John Wiley & Sons, New York 1983; Glendenning N.K., *Compact Stars: Nuclear Physics, Particle Physics and General Relativity*, Springer, New York 2000.

[13] Antoniadis J. et al., *A massive pulsar in a compact relativistic binary*, Science **340**, 2013, 6131.

[14] Baiko D.A., Haensel P., *Cooling neutron stars with localized protons*, Astron. Astrophys. **356**, 2000, 171.

TECHNICAL TRANSACTIONS | **CZASOPISMO TECHNICZNE**
FUNDAMENTAL SCIENCES | NAUKI PODSTAWOWE
3-NP/2014

WŁODZIMIERZ WÓJCIK*

TEMPERATURE EVOLUTION OF THERMODYNAMIC FUNCTIONS FROM SYMMETRIC TO ASYMMETRIC NUCLEAR MATTER

TEMPERATUROWA EWOLUCJA FUNKCJI TERMODYNAMICZNYCH OD SYMETRYCZNEJ DO ASYMETRYCZNEJ MATERII JĄDROWEJ

Abstract

This paper investigates thermal properties of nuclear matter using the Friedman-Pandharipande-Ravenhall equation of state. Thermodynamic quantities such as internal energy, entropy and free energy are calculated both for symmetric and asymmetric nuclear matter for temperatures ranging up to 30 MeV. A change of free energy curvature indicates the liquid-gas phase transition in nuclear matter.

Keywords: strongly asymmetric nuclear matter, proton localization, equation of state

Streszczenie

Dla równania stanu Friedmana-Pandharipande-Ravenhalla zbadano własności termiczne materii jądrowej. Dla symetrycznej i asymetrycznej materii jądrowej wyznaczono wielkości termodynamiczne, takie jak energię wewnętrzną, entropię i energię swobodną dla temperatur do 30 MeV. Zmiana krzywizny energii swobodnej wskazuje na przejście fazowe ciecz–gaz w materii jądrowej.

Słowa kluczowe: silnie asymetryczna materia jądrowa, lokalizacja protonu, równanie stanu

* Institute of Physics, Faculty of Physics, Mathematics and Computer Science, Cracow University of Technology, Poland; puwojcik@cyf-kr.edu.pl.

1. Introduction

Thermodynamic properties of nuclear matter play an important role in studies of high-energy astrophysical phenomena. The nuclear equation of state at zero temperature governs the structure of cold neutron stars, whereas the equation of state for finite temperatures is necessary for studies of many processes e.g. core collapse of supernovae, black hole formation and neutron star cooling, to name but a few. Knowledge of thermodynamic quantities is required when considering an extremely wide range of densities, temperatures and proton fractions. In order to better understand the properties of dense nuclear matter changes of thermodynamic functions such as internal energy, entropy and free energy with densities, temperatures and degree of asymmetry were evaluated.

This paper is organized as follows. In Section 2, there is a discussion on some of the features of the Friedman-Pandharipande-Ravenhall (FPR) equation of state (EOS) and explicit expressions for thermodynamic functions are given, which are presented in Section 3 for symmetric and asymmetric nuclear matter.

2. Thermodynamics of dense matter with the Friedman-Pandharipande-Ravenhall equation of state

The EOS of dense nuclear matter is an essential ingredient in modelling neutron stars. Knowledge of the EOS, particularly with arbitrary isospin asymmetry, i.e. different proton and neutron fractions, is of fundamental importance for both nuclear physics and astrophysics. The saturation density and the energy per particle of nuclear matter can be used to test properties of finite nuclear systems extrapolated to the thermodynamic limit. Moreover, the study of the EOS of asymmetric matter allows us to shed some light on the behavior of the isospin asymmetry energy. In our approach, we use the FPR model in which the density of energy as a function of neutron n_N and proton n_P densities reads [1]:

$$\varepsilon\left(n_N,n_P\right)=\left(\frac{1}{2m_N}+B_N\right)\tau_N+\left(\frac{1}{2m_P}+B_P\right)\tau_P+n_B^2\left(a_1+a_2e^{-b_1n_B}+\left(\frac{1}{2}-x\right)^2\left(a_1+a_2e^{-b_1n_B}\right)\right)+$$
$$n_Be^{-b_1n_B^2}\left(a_5+a_6n_B+\left(\frac{1}{2}-x\right)^2\left(a_7+a_8n_B\right)\right), \tag{1}$$

where $n_B=n_N+n_P$, $x=\dfrac{n_P}{n_B}$,

$$B_i=\left(a_9n_B+a_{10}n_i\right)e^{-b_3n_B},$$

$$\tau_i=\frac{3}{5}\left(3\pi^2\right)^{\frac{2}{3}}n_i^{\frac{5}{3}}\qquad i=N,P.$$

The effective proton mass is as follows:

$$\frac{1}{2m_P^*} = \frac{1}{2m_P} + a_9 n_B e^{-b_3 n_N}. \tag{2}$$

The parameters in (1) are: a_1 = 1054.0 MeV fm^3; a_2 = –1393.0 MeV fm^3; a_3 = –2316.0 MeV fm^3; a_4 = 2859.0 MeV fm^3; a_5 = –1.78; a_6 = –52.0 MeV fm^3; a_7 = 5.5 MeV; a_8 = 197.0 MeV fm^3; a_9 = 89.8 MeV fm^5; a_{10} = –59.0 MeV fm^5; b_1 = 0.284 fm^3; b_2 = 42.25 fm^6; b_3 = 0.457 fm^3.

A major advantage of the above effective interactions is that they can be used straightforwardly to make finite-temperature calculations. In our approach, it is assumed that the kinetic energy densities and baryon matter densities are the only quantities that exhibit dependence on temperature [2]:

$$\tau_i = \frac{2}{(2\pi)^2}\left(2m_i^* T\right)^{\frac{5}{2}} J_{\frac{3}{2}}\left(\eta_i\right), \qquad i = N, P, \tag{3}$$

where $\eta_i = \frac{\mu_i}{kT}$ (μ_i the chemical potential of neutrons or protons) can be derived from the baryon number density:

$$n_i = \frac{2}{(2\pi)^2}\left(2m_i^* T\right)^{\frac{3}{2}} J_{\frac{1}{2}}\left(\eta_i\right). \tag{4}$$

Eqs. (3) and (4) are written in terms of Fermi integrals:

$$J_\nu\left(\eta\right) = \int_0^\infty dx \frac{x^\nu}{1+\mathrm{e}^{x-\eta}}. \tag{5}$$

Calculated entropy per baryon is:

$$S_i = \frac{5}{3}\frac{1}{n_i}\frac{1}{4\pi^2}\left(2m_i^* T\right)^{\frac{3}{2}} J_{\frac{3}{2}}\left(\eta_i\right) - \frac{1}{2}\eta_i, \tag{6}$$

where:

m_i^* – the effective nucleon masses of neutrons and protons.

While studying the thermodynamics of dense matter, it is convenient to choose the Helmholtz free energy. From Eqs. (1) and (6), the expression for the free energy per baryon reads:

$$F = \left(\varepsilon\left(n_N, n_P, T\right) - T\left(n_N S_N + n_P S_P\right)\right)/n_B, \tag{7}$$

where the energy density $\varepsilon(n_N, n_p, T)$ depends on temperature. In the next section, we discuss the properties of internal energy, entropy and free energy in the FPR model.

3. Properties of symmetric and asymmetric nuclear matter at finite temperatures

At finite temperatures, the nuclear matter structure and properties are not as well settled as at zero temperature. In this paper, the thermodynamic properties of dense matter for the FPR equation of state are discussed. To make the discussion complete, the energy per particle, the entropy per particle and the free energy per particle are computed. Based on the calculated free energy, all other thermodynamic quantities may be obtained from standard thermodynamic relations.

In Fig. 1, the FPR equation of state for symmetric nuclear matter (proton fraction $x = 0.50$) are displayed for different temperatures $T = 0$, 10, 20 and 30 MeV.

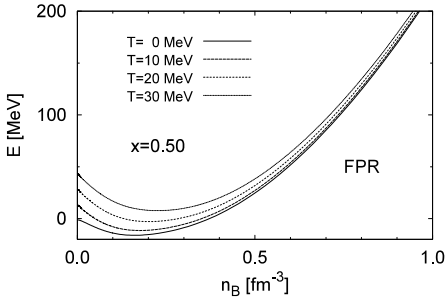

Fig. 1. Energy per nucleon versus baryon density for symmetric nuclear matter at different temperatures

For very small densities (below 0.02 fm^{-3}), one obtains the behavior of a free Fermi gas with linear temperature dependence and for increasing density, quadratic temperature dependence [3]. The entropy per baryon and the free energy per baryon for symmetric matter are shown in Fig. 2 and Fig. 3 for different temperatures. For symmetric nuclear matter, the entropy behaviour (Fig. 2) agrees very closely with the experimental results [4].

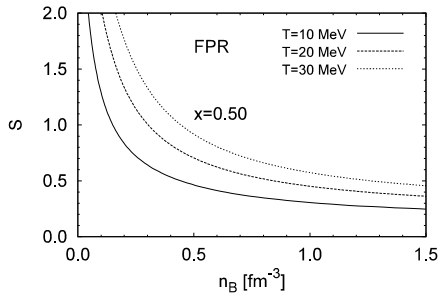

Fig. 2. Entropy per nucleon versus baryon density for symmetric nuclear matter at different temperatures

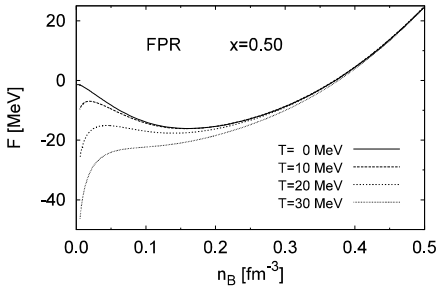

Fig. 3. Free energy per nucleon versus baryon density for symmetric nuclear matter at different temperatures

In Fig. 3, the free energy per nucleon versus baryon density exhibits an unstable region of negative curvature for lower densities below $T = 20$ MeV (cf [5]). Non-convexity of $F(n_B,T)$ with respect to n_B at a fixed temperature implies a negative isothermal compressibility K_T which violates the stability relation $K_T > 0$. In this region, the physical equation of state can be obtained by performing the Maxwell construction. This signifies the presence of a first-order phase transition. The existence of a critical temperature for nuclear matter is extremely strong evidence that, under appropriate conditions, there should be a transition between a nuclear 'liquid' and nuclear 'gas'. The physics of nuclear matter is therefore a crossover from a gas of nucleons to homogeneous matter, where nuclei and larger clusters coexist with the nucleon gas over a wide range of intermediate densities. At temperatures ($T \sim 20$ MeV) and high densities, a liquid-gas type of phase transition was first predicted theoretically by A.L. Goodman [6] and later observed experimentally in a nuclear multi-fragmentation phenomenon [7].

The case of asymmetric matter is more complex to study since there is an additional degree of freedom to consider – the isospin asymmetry, i.e. different neutron and proton fractions. Such matter plays an essential role in astrophysics, where neutron-rich systems are involved in neutron stars and type-II supernovae evolution [8].

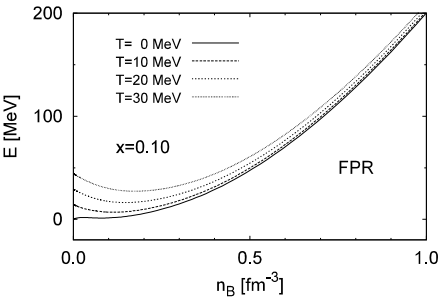

Fig. 4. Energy per nucleon versus baryon density for asymmetric nuclear matter ($x = 0.10$) at different temperatures

Fig. 5a presents the entropy density S versus baryon density for asymmetric matter (x = 0.10). This quantity is the sum of two contributions – the first from neutron entropy (Fig. 5b), and the second from proton entropy (Fig. 5c). In asymmetric nuclear matter, the contribution of S_P to total entropy is much greater than S_N – as follows clearly from relation (7).

The dependence of free energy of asymmetric nuclear matter versus baryon density (Fig. 6) shows non-convexity at temperatures below T = 10 MeV for proton fraction equaling x = 0.10. It indicates that in asymmetric nuclear matter, the phase transition occurs in much lower temperatures than in symmetric one.

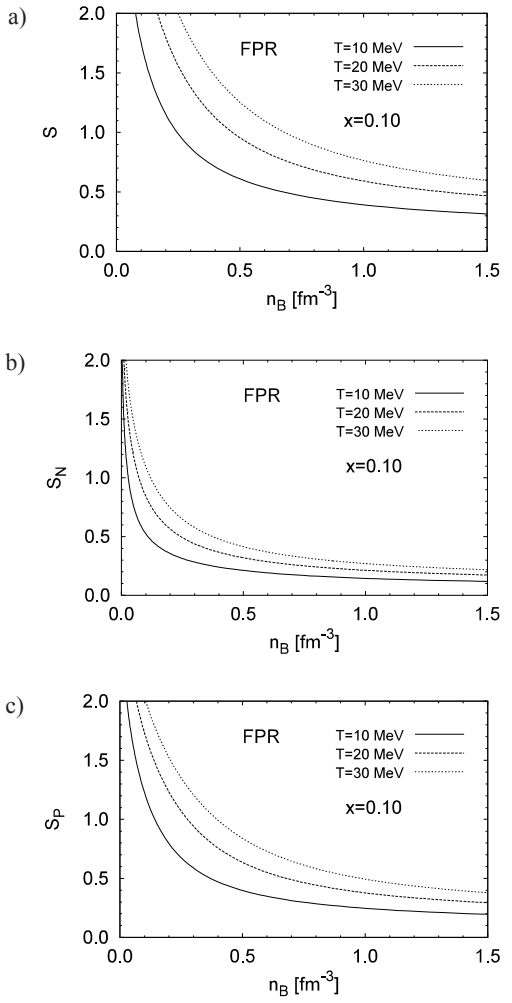

Fig. 5 a) Entropy per nucleon versus baryon density for asymmetric nuclear matter (x = 0.10) at different temperatures; b) neutron entropy contribution; c) proton entropy contribution

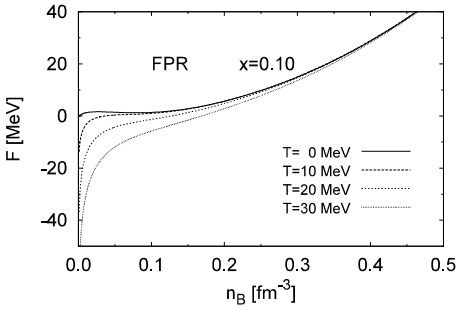

Fig. 6. Free energy per nucleon versus baryon density for asymmetric nuclear matter ($x = 0.10$) at different temperatures

In Fig. 7, changes of the free energy with densities at constant temperature $T = 10$ MeV for different asymmetry of nuclear matter are also shown. It was observed that phase transition in asymmetric nuclear matter takes place for lower densities than in symmetric nuclear matter.

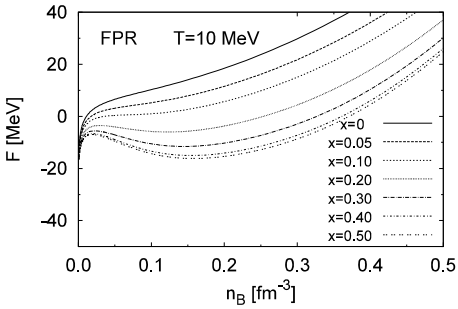

Fig. 7. Free energy per nucleon versus baryon density at $T = 10$ MeV from fully asymmetric ($x = 0$) to symmetric ($x = 0.50$) nuclear matter

4. Conclusions

The thermodynamic properties of hot, dense nuclear matter employing the Friedman-Pandharipande-Ravenhall model of nuclear interaction were investigated. Evidence of the liquid-gas phase transition both in symmetric and asymmetric nuclear matter was observed. As this paper shows the critical temperature strongly decreases with nuclear matter asymmetry. The results presented here lead to better understanding of phase diagram of nuclear matter.

References

[1] Lattimer J.M., *The equation of state of hot dense matter and supernovae*, Ann. Rev. Nucl. Part. Sci. **31**, 1981, 337.

[2] Brack M., Guet C., Håkansson H.-B., *Self-consistent* semi-classical *description of average nuclear properties – a link between microscopic and macroscopic models*, Phys. Rep. **123**, 1985, 275.

[3] Küpper W.A., Wegmann G., Hilf E.R., *Thermostatic properties of symmetric nuclear matter*, Ann. of Phys. **88**, 1974, 454.

[4] Das C., Tripathi R.K., Sahu R., *Hot nuclear and neutron matter with a density-dependent interaction*, Phys. Rev. **C145**, 1992, 2217.

[5] Karnaukhov V. et al., *Critical temperature for the nuclear liquid-gas phase transition (from multifragmentation and fission)*, Phys. Atom. Nucl. **71**, 2008, 2067.

[6] Goodman A.L., Kapusta J.I., Mekjian A.Z., *Liquid-gas instabilities and droplet formation in nuclear reactions*, Phys. Rev. **C30**, 1984, 851.

[7] Xu H.S. et al., *Isospin fractionation in nuclear multifragmentatation*, Phys. Rev. Lett. **85**, 2000, 716.

[8] Glendenning N.K., *Phase transitions and crystalline structures in neutron star cores*, Phys. Rep. **342**, 2001, 393.

TECHNICAL TRANSACTIONS | **CZASOPISMO TECHNICZNE**
FUNDAMENTAL SCIENCES | NAUKI PODSTAWOWE
3-NP/2014

WŁODZIMIERZ WÓJCIK*

TEMPERATURE DEPENDENCE OF PROTON LOCALIZATION FOR SKYRME NUCLEAR INTERACTIONS

ZALEŻNOŚĆ TEMPERATUROWA LOKALIZACJI PROTONÓW DLA ODDZIAŁYWAŃ SKYRME'A

Abstract

In this paper, our earlier approach to proton localization in neutron star matter to finite temperatures is extended. The Skyrme forces were chosen to describe interactions in nuclear matter. The dependence of threshold density on temperatures for proton localization was obtained and these results were compared with those calculated earlier for the Friedman-Pandharipande-Ravenhall potential.

Keywords: temperature dependence of proton localization, the Skyrme forces

Streszczenie

W artykule rozszerzono wcześniejsze podejście do lokalizacji protonów w materii gwiazdy neutronowej do skończonych temperatur. Wybrano siły Skyrme'a do opisu oddziaływań w materii jądrowej. Otrzymano zależność gęstości progowej od temperatury dla lokalizacji protonów i porównano te wyniki z wcześniejszymi obliczeniami dla potencjału Friedmana-Pandharipande-Ravenhalla.

Słowa kluczowe: temperaturowa zależność lokalizacji protonu, siły Skyrme'a

* Institute of Physics, Faculty of Physics, Mathematics and Computer Science, Cracow University of Technology, Poland; puwojcik@cyf-kr.edu.pl.

1. Introduction

We have shown in the earlier papers [1, 2] that in asymmetric nuclear matter, protons are localized in the core of neutron stars for realistic nuclear models. Protons that form the admixture tend to be localized above the threshold density n_{loc} depending on the model used. The localization effect occurs as a result of the interaction of protons with small density oscillations of the neutron background [2]. In paper [3], we have extended the effect of proton localization to finite temperatures for the Friedman-Pandharipande-Ravenhall potential. Here, the influence of temperature on the proton localization for another nuclear model, the Skyrme nuclear interaction, is investigated.

The plan of this paper is as follows. In Section 2, some of the features of the Skyrme forces are briefly discussed. In Section 3, model of proton admixture in neutron model is presented. In Section 4, the process of calculating entropy and free energy of nuclear matter is described. Numerical results are discussed in Section 5.

2. Skyrme forces parametrization

It was chosen to work with the Skyrme forces [4] to calculate the properties of the asymmetric nuclear matter. The Skyrme potential reads:

$$\varepsilon(n_N,n_P)=\left(\frac{1}{2m_N}+\frac{1}{4}\left(\left(1+\frac{1}{2}x_1\right)t_1+\left(1+\frac{1}{2}x_2\right)t_2\right)n_B+\frac{1}{8}\left((1+2x_2)t_2-(1+2x_1)t_1\right)n_N\right)\tau_N+$$
$$+\left(\frac{1}{2m_{\mathrm{P}}}+\frac{1}{4}\left(\left(1+\frac{1}{2}x_1\right)t_1+\left(1+\frac{1}{2}x_2\right)t_2\right)n_B+\frac{1}{8}\left((1+2x_2)t_2-(1+2x_1)t_1\right)n_P\right)\tau_P$$
$$+n_B^2\left(\frac{3}{8}t_0+\frac{1}{16}t_3n_B^{\square}\right)-\frac{1}{4}(n_N-n_P)^2\left(\left(\frac{1}{2}+x_0\right)t_0+\frac{1}{6}\left(\frac{1}{2}+x_3\right)t_3n_B^{\square}\right), \tag{1}$$

where $n_B = n_N + n_P$ (the density of baryon) and masses of nucleons are $m_P = 4.7549$ fm^{-1} and $m_N = 4.7615$ fm^{-1} .

The local kinetic energy densities of neutrons and protons for plane waves become:

$$\tau_i=\frac{3}{5}\left(3\pi^2\right)^{2/3}n_i^{5/3},\quad i=N,P. \tag{2}$$

In our calculations, the following Skyrme force parameters were used: t_0 = –1057.3 MeVfm^3; t_1 = 235.9 MeVfm^5; t_2 = –100.0 MeVfm^5; t_3 = 14463.5 MeVfm$^{3+3\gamma}$; x_0 = 0.2885; $x_1 = x_2 = 0$; x_3 = 0.2257; γ = 1. These are the Vautherin and Brink [5] parameters modified as described in [6].

3. Proton admixture in neutron matter

Protons in strong asymmetric nuclear matter tend to localize [1, 2] in potential wells which correspond to neutron matter inhomogeneities created by the protons in neutron medium. The energetically favorable ground state of asymmetric nuclear matter was found by comparing the energy of two phases: a normal phase (in Wigner-Seitz approximation) and a phase with localized protons. The cells are assumed to be spherical and the volume is $V = 1/n_P$, where the proton density $n_P = xn_N$ for a small proton fraction x. In normal phase, protons are not localized and their wave functions are plane waves. The energy of the cell reads:

$$E_0 = V\varepsilon\left(n_N, n_P\right), \tag{3}$$

where $\varepsilon(n_N, n_P)$ is the energy density. In the phase with localized protons, the energy of the Wigner-Seitz cell E_{loc} is [7]:

$$E_{\text{loc}} = \int d^3r\psi_P^*(r)\left(-\frac{\nabla^2}{2m} + \mu_P\left(n(r)\right)\right)\psi_P(r) + \int d^3r\varepsilon\left(n(r)\right) + B_N\int d^3r\left(\nabla n(r)\right)^2. \tag{4}$$

The first term is the energy of the proton confined to an effective potential well $v_{\text{eff}} = \mu_P(n(r))$. The two other terms in eq. (4) describe the contributions to the energy arising from local change of the neutron Fermi momentum and the gradient of the neutron distribution, respectively, in the Thomas-Fermi approximation. Here, $\varepsilon(n(r))$ is the local neutron matter energy per unit volume. The parameter B_N is the curvature coefficient for pure neutron matter.

We assume a simple trial form of the proton wave function:

$$\Psi_{\text{P}}(r) = \left(\frac{2\pi}{3}R_P^2\right)^{-\frac{3}{4}}\exp\left(-\frac{3r^2}{4R_P^2}\right), \tag{5}$$

where R_P is the root mean square (r.m.s.) radius of the localized proton probability distribution. We treat this quantity as a variational parameter and minimize $\Delta E = E_{\text{loc}} - E_0$. The results are presented in Section 5.

4. Entropy and free energy of nuclear matter

The internal energy density of uniform nuclear matter is given by eq. (1) and inhomogeneities one by eq. (4). The entropy densities S_i reads:

$$S_i = -k_B\sum_{\alpha}\left(n_{\alpha,i}\log n_{\alpha,i} + (1-n_{\alpha,i})\log\left(1-n_{\alpha,i}\right)\right). \tag{6}$$

Here, $n_{\alpha,i}$ are the occupation numbers of the simple-particle orbitals $\Phi_{\alpha,i}(x)$ and $i = N$ or P. Upon integration by parts, the entropy per baryon has the particularly simple form

$$S_i = \frac{5}{3}\frac{1}{n_i}\frac{1}{4\pi^2}\left(2m_i^* T\right)^{\frac{3}{2}} J_{\frac{3}{2}}\left(\eta_i\right) - \frac{1}{2}\eta_i, \tag{7}$$

where m_i^* denotes the effective nucleon masses $i = N, P$. The quantity η_i is calculated from the relation:

$$n_i = \frac{2}{(2\pi)^2}\left(2m_i^* T\right)^{\frac{3}{2}} J_{\frac{1}{2}}\left(\eta_i\right), \tag{8}$$

where Fermi integrals are defined as follows:

$$J_\nu\left(\eta\right) = \int_0^\infty dx \frac{x^\nu}{1+e^{x-\eta}} \quad . \tag{9}$$

Knowing the internal energy ε and the entropy per baryon S_i the free energy per baryon is:

$$F = \left(\varepsilon\left(n_N, n_P, T\right) - T\left(n_N S_N + n_P S_P\right)\right) / n_B \,. \tag{10}$$

At finite temperatures, the ground state is found by minimizing the free energy.

5. Proton localization in finite temperatures

The internal energy difference between the localized state of protons and the state with uniform matter $\Delta E = E_{\text{loc}} - E_0$ for the Skyrme forces was calculated. The difference ΔE as the function of variational parameter R_P for various neutron density at $T = 0$ is shown in Fig. 1.

The curves are labelled with the neutron matter density n_N. One can notice that for the Skyrme (*Sk*) interaction, a local minimum above a certain density for the proton r.m.s. radius R_P appears to strongly decrease with neutron density (Fig. 2). With increasing neutron matter density n_N, the depth of the minimum ΔE increases. Above the threshold density, the energy difference becomes negative. The negative value $\Delta E < 0$ means that the energy of

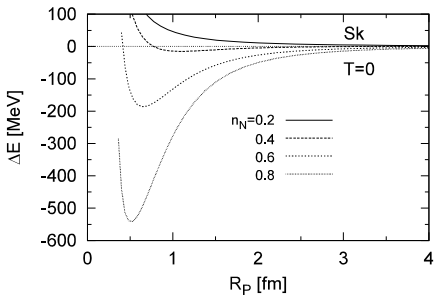

Fig. 1. The energy difference $\Delta E = E_{\text{loc}} - E_0$ as a function of the proton r.m.s. radius R_P for various neutron densities at zero temperature for the Skyrme forces

the localized proton is lower than the energy of a non-localized proton. This means that the localized proton state is preferred energetically for $n > n_{loc}$.

To investigate the influence of temperatures on proton localization, we calculate the free energy difference $\Delta F = F_{loc} - F_0$ in the same manner as in Section 2 using eq. (10). The relation ΔF versus proton radius presents Fig. 3.

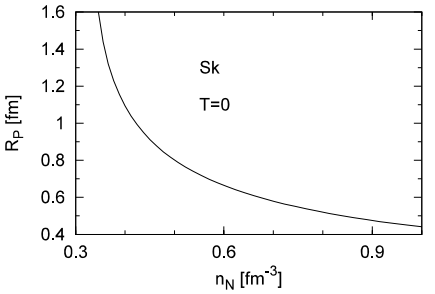

Fig. 2. The r.m.s. radius of proton wave function at zero temperature as the function of density

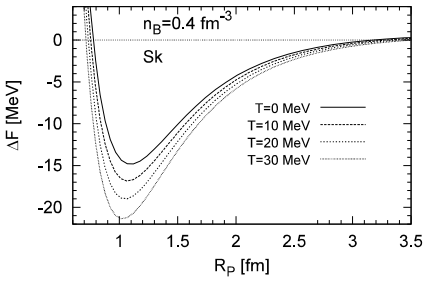

Fig. 3. The difference of free energy between the localized and delocalized states as a function of proton radius at fixed baryon density and for various temperatures

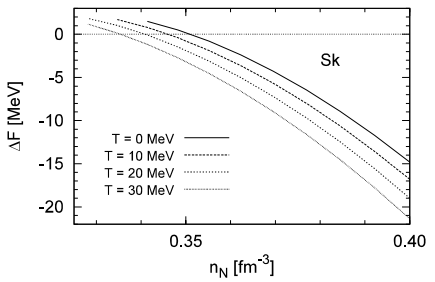

Fig. 4. The free energy difference at the minimum ΔE as a function of density at different temperatures for the Skyrme nuclear forces

When the temperature increases, the minimum value of ΔF as a function of the average neutron number density is shown in Fig. 4. A value of zero corresponds to the threshold density n_{loc} above which the state with localized proton occurs.

A strong influence of temperatures on proton localization was observed (Fig. 5). Temperature inclusion lowers the localization threshold density and diminishes the size of the proton wave function (Fig. 2). Thus, the localization is present even in the case of very high temperature. This means that temperature and baryon density cooperate to achieve proton localized state in dense asymmetric nuclear matter.

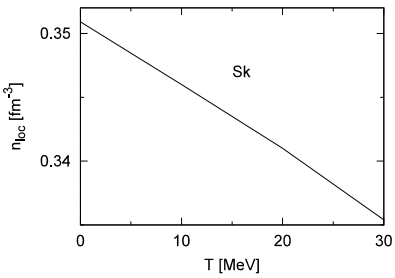

Fig. 5. The threshold density n_{loc} above which the localization is occurred as a function of the temperature of neutron matter

5. Conclusions

Finally, the results show that for low values of x, the state with localized single protons has a lower energy than a uniform configuration for $n > n_{loc}$, even for high temperatures. We have also found that the threshold localization temperature relationship for the Friedman-Pandharipande-Ravenhall parametrization [3] turns out to be surprisingly close to that which was obtained in our calculation for the Skyrme forces. This fact indicates universal character of temperature influence on the proton localization in dense nuclear matter.

References

[1] Kutschera M., Wójcik W., *Magnetic properties of strongly asymmetric nuclear matter*, Phys. Lett. **B223**, 1989, 11.

[2] Kutschera M., Wójcik W., *Proton impurity in the neutron matter: A nuclear polaron problem*, Phys. Rev. **C47**, 1993, 1077.

[3] Szmagliński A., Kubis S., Wójcik W., *Properties of localized protons in neutron star matter at finite temperatures*, Acta Phys. Polon. **B45**, 2014, 249.

[4] Skyrme T.H.R., *The effective nuclear potential*, Nucl. Phys. **9**, 1959, 615.

[5] Vautherin D., Brink D.M., *Hartree-Fock calculation with Skyrme interaction*, Phys. Lett. **B32**, 1970, 149.

[6] Ravenhall D.G., Bennet C.D., Pethick C.J., *Nuclear surface energy and neutron star matter*, Phys. Rev. Lett. **28**, 1972, 978.

[7] Kutschera M., Wójcik W., *Self-consistent proton crystallization in dense neutron-star matter*, Acta Phys. Polon. **B21**, 1990, 823.

COMPUTER SCIENCE

INFORMATYKA

TECHNICAL TRANSACTIONS | **CZASOPISMO TECHNICZNE**
FUNDAMENTAL SCIENCES | NAUKI PODSTAWOWE
3-NP/2014

MATEUSZ BARAN*

MULTIVARIATE FUNCTION APPROXIMATION USING SPARSE GRIDS AND HIGH DIMENSIONAL MODEL REPRESENTATION – A COMPARISON

PRZYBLIŻANIE FUNKCJI WIELU ZMIENNYCH PRZY UŻYCIU SIECI RZADKICH I HIGH DIMENSIONAL MODEL REPRESENTATION – PORÓWNANIE

Abstract

In many areas of science and technology, there is a need for effective procedures for approximating multivariate functions. Sparse grids and cut-HDMR (High Dimensional Model Representation) are two alternative approaches to such multivariate approximations. It is therefore interesting to compare these two methods. Numerical experiments performed in this study indicate that the sparse grid approximation is more accurate than the cut-HDMR approximation that uses a comparable number of known values of the approximated function unless the approximated function can be expressed as a sum of high order polynomials of one or two variables.

Keywords: Sparse Grids, Approximation, Numerical experiments, Metamodelling, Curse of dimensionality

Streszczenie

W wielu obszarach nauki i technologii potrzebne są efektywne metody aproksymacji funkcji wielu zmiennych. Sieci rzadkie i cut-HDMR (High Dimensional Model Representation) są dwoma alternatywnymi podejściami do aproksymacji funkcji wielu zmiennych. Interesujące jest zatem porównanie tych dwóch metod. Eksperymenty numeryczne przeprowadzone w ramach niniejszych badań wskazują, że aproksymacja sieciami rzadkimi jest bardziej dokładna niż aproksymacja cut-HDMR wykorzystująca porównywalną liczbę znanych o ile aproksymowana funkcja nie może być wyrażona jako suma wielomianów wysokiego stopnia jednej lub dwóch zmiennych.

Słowa kluczowe: Sieci Rzadkie. Aproksymacja, Eksperymenty numeryczne, Metamodelowanie, Przekleństwo wymiarowości

* Institute of Teleinformatics, Faculty of Physics, Mathematics and Computer Science, Cracow University of Technology, Poland; mbaran@pk.edu.pl.

1. Introduction

The approximation of multivariate functions is a remarkably hard problem due to the so-called 'curse of dimensionality' [1]. However, the effective approximation of high-dimensional functions is the only solution in numerous practical problems from virtually all branches of science and technology. In particular such an approximation is an essential element of the so-called metamodelling [2, 3] (see also [4] for a discussion of metamodelling of high-dimensional problems, [5] for a comparison of a few metamodelling techniques and [6] for an example of the usage of sparse grids in metamodelling).

Examples of the application of high-dimensional approximation in science and engineering include ionosphere modelling [7], quantum mechanics [8], materials science [9], structural engineering [10], electrochemistry [11] and nuclear reactor modelling [12].

Sparse grids offer a method of function approximation where instead of one dense grid, we have a number of sparser grids and a linear combination is used [13]. The method is also known under other names such as the (discrete) blending method [14], the Boolean method [15] and hyperbolic cross approximation [16].

HDMR (High Dimensional Model Representation) approximation is a different approach that hinges on the fact that many high-dimensional functions can be efficiently approximated by sums of low-dimensional functions. The concept is attributed to Sobol [17]. The method is described in [18, 19]. Reference [20] describes many variants of HDMR approximation.

This paper compares the above two methods for the approximation of multivariate functions. In Section 2, a basic theory of sparse grid and cut-HDMR methods is described. Section 3 describes the performed numerical experiments. Section 4 summarizes the obtained results.

2. Theory of sparse grids and cut-HDMR

2.1. Sparse grids

Let us start with a one-dimensional interpolation. Consider a function $f:[0,1]^M \to \mathbb{R}$. We need a sequence $\left\{U^i\right\}_{i=1}^{\infty}$ of interpolating operators, each one providing a better approximation than the previous one. The formula for operator U^i, which interpolates on nodes $\left\{x_1^i, x_2^i, \ldots, x_{m_i}^i\right\}$, can be written as

$$U^i(f)(x) = \sum_{j=1}^{m_i} f\left(x_j^i\right) a_j^i(x). \tag{1}$$

Functions $a_j^i(x)$ depend on the interpolation nodes and interpolation type. For Lagrange interpolation, the functions are given by [21]:

$$a_j^i(x) = \prod_{1 \le k \le m_i, k \ne j} \frac{x - x_k}{x_j - x_k}. \tag{2}$$

An M-dimensional approximation corresponds to the tensor product of operators $U^{i_1}, U^{i_2}, \ldots, U^{i_M}$ as follows:

$$U^{i_1} \otimes \ldots \otimes U^{i_M}(f)(x_1, x_2, \ldots, x_M) = \sum_{j_1=1}^{m_{i_1}} \ldots \sum_{j_M=1}^{m_{i_M}} f\left(x_{j_1}^{i_1}, \ldots, x_{j_M}^{i_M}\right) a_{j_1}^{i_1}(x_1) \ldots a_{j_M}^{i_M}(x_M) \quad (3)$$

(see [22]). The interpolating operator for a kth variable is U^{i_k}. The calculation of the interpolant requires computing the interpolated function at $m_{i_1} m_{i_2} \ldots m_{i_M}$ nodes. In polynomial or spline interpolation, we select a single grid corresponding to a single tensor product of operators. In sparse grid approximation, we combine multiple grids.

The central idea in sparse grid approximation is Smolyak's formula [13]. This formula represents a linear combination of interpolants on many grids. The sparse grid interpolation operator is defined by a linear combination of operators from Eq. (3):

$$A(q, M) = \sum_{q-M+1 \le |\boldsymbol{i}| \le q} (-1)^{q-|\boldsymbol{i}|} \binom{M-1}{q-|\boldsymbol{i}|} U^{i_1} \otimes \ldots \otimes U^{i_M}. \quad (4)$$

The operator (4) has two arguments: the first (q) describes the density of the grid and the second (M) is the number of variables. The sum of components of index $\boldsymbol{i} = \{i_1, i_2, \ldots, i_M\}$ is denoted by $|\boldsymbol{i}| = \sum_{j=1}^{M} i_j$. Figure 1 shows two examples of two-dimensional sparse grids.

One can choose different approximation spaces for the sparse grid approximation. The simplest choice is a space constructed from so-called hat functions [23] but this space is rarely used in practice. Instead, commonly used sparse grids are based on polynomial or piecewise-polynomial functions.

One important feature of all sparse-grid methods is that one-dimensional basis functions $\psi_{i_j}(x_j)$ are combined into M-dimensional basis functions $\psi_{\boldsymbol{i}}(\boldsymbol{x})$ defined as:

$$\psi_{\boldsymbol{i}}(\boldsymbol{x}) = \prod_{j=1}^{M} \psi_{i_j}(x_j). \quad (5)$$

In Eq. (5), j is the number of independent variables and i_j is a parameter to distinguish different one-dimensional functions of that variable. A sparse grid approximant is constructed as a linear combination of the multivariate basis functions $\psi_{\boldsymbol{i}}(\boldsymbol{x})$ for different values of $\boldsymbol{i} = \{i_1, i_2, \ldots, i_M\}$.

A motivating feature of sparse grids with polynomial interpolation is the fact that formula $A(M + k, M)$ exactly reproduces multivariate polynomials up to order k [22]. Full grid approximation by operators from Eq. (3) on the other hand, exactly reproduces monomial $x_1^{m_{i_1}} x_2^{m_{i_2}} \ldots x_M^{m_{i_M}}$ of order $m_{i_1} m_{i_2} \ldots m_{i_M}$ but not monomial $x_1^{m_{i_1}+1}$ of order $m_{i_1} + 1$.

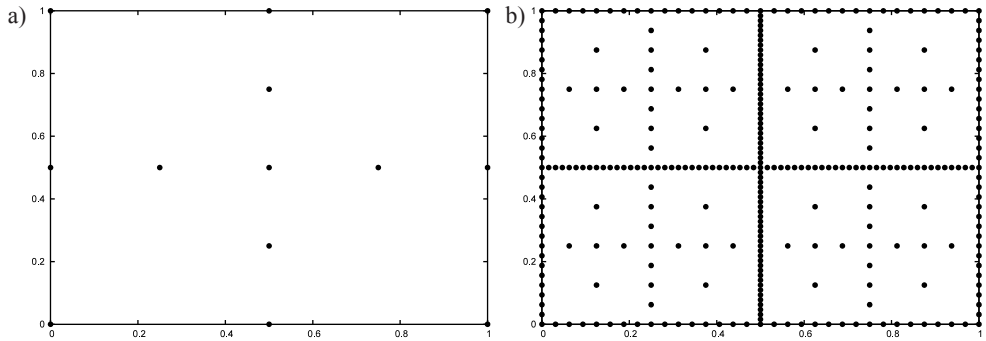

Fig. 1. Two-dimensional sparse grids with q equal to 3 (a) and 7 (b). Both examples use equidistant one-dimensional nodes

2.2. Cut-HDMR approximation

An approximated M-variate function $f(\boldsymbol{x})$ can be written as a sum of the constant term, functions of one variable, etc.

$$f(\boldsymbol{x}) = f_0 + \sum_{1\le i\le M} f_i(x_i) + \sum_{1\le i<j\le M} f_{i,j}(x_i, x_j) + \ldots + f_{1,2,\ldots,M}(x_1, x_2, \ldots, x_M). \tag{6}$$

The choice of functions $f_0, f_i, f_{i,j}$ etc. is not unique. By retaining only a few initial terms in the expansion (6) one obtains an HDMR approximation. The maximum dimension of the domain of functions used in the approximation is called the order of the approximation, for example, the first-order approximation consist only of a constant f_0 and one-dimensional functions f_i.

In the cut-HDMR variant of the method, a reference point **r** is selected and used to determine the terms of expansion (6) in the following way:

$$f_0 = f(\boldsymbol{r}), \tag{7}$$

$$f_i(x_i) = f(x_1, \ldots, x_{i-1}, r_i, x_{i+1}, \ldots, x_M) - f_0, \tag{8}$$

$$f_{i,j}(x_i, x_j) = f(x_1, \ldots, x_{i-1}, r_i, x_{i+1}, \ldots, x_{j-1}, r_j, x_{j+1}, \ldots, x_M) - f_i(x_i) - f_j(x_j) - f_0, \tag{9}$$

etc.

For analytic functions f this approximation can be compared to the multidimensional Taylor expansion at point $\boldsymbol{r}$:

$$f(\boldsymbol{x}) = f(\boldsymbol{r}) + \sum_{i=1}^{M} \frac{\partial f(\boldsymbol{r})}{\partial x_i}(x_i - r_i) + \sum_{i=1}^{M}\sum_{j=1}^{M} \frac{\partial^2 f(\boldsymbol{r})}{\partial x_i \partial x_j}(x_i - r_i)(x_j - r_j) + \ldots. \tag{10}$$

Regrouping the terms in Eq. (10) gives expressions for the cut-HDMR terms. As each cut-HDMR term corresponds to many Taylor expansion terms, cut-HDMR usually offers a better approximation than the Taylor expansion. The cut-HDMR approximation is, like the Taylor expansion, local. However, in certain subspaces, the approximation is exact (i.e. there is no error). They are called cut subspaces and depend solely on the expansion point (cut point, anchor point) and the order of the expansion. In agreement with Eqs. (7) to (9), first order cut subspaces are straight lines of the form

$$\{(r_1,\ldots,r_{i-1},x_i,r_{i+1},\ldots,r_M):x_i\in\mathbb{R}\},1\le i\le M \tag{11}$$

and second order cut subspaces are planes described by

$$\{(r_1,\ldots,r_{i-1},x_i,r_{i+1},\ldots,r_{j-1},x_j,r_{j+1},\ldots,r_M):x_i,x_j\in\mathbb{R}\},1\le i<j\le M\,. \tag{12}$$

For the purpose of representing a cut-HDMR expansion on a computer, a method of interpolating the low-variate functions is necessary. Typically, first degree spline interpolation is used. The approximated function is calculated on grids spanning the cut subspaces. This is an improvement over interpolation in the whole $\mathbb{R}^M$, as fewer values of the approximated function need to be known. The number N of values of function f, that need to be stored decreases from K^M (assuming K interpolation nodes for each independent variable), to the value

$$N=\binom{M}{l}(K-1)^{l-1}+\binom{M}{l-1}(K-1)^{l-2}+\ldots+\binom{M}{1}(K-1)+1 \tag{13}$$

for an lth order expansion. For each l the value N given by Eq. (13) is a polynomial in M. Equation (13) can be obtained by counting the number of points that lie in an lth order cut subspace, but not in an $l-1$st order cut subspace, adding points that lie in an $l-1$st order cut subspace, but not in an $l-2$nd order cut subspace etc. In this way no point is counted twice.

The choice of the cut point r is an important issue. Wang [24] proposed an automatic method of selecting the best cut point. A low-discrepancy sequence of points $\left\{x^i:x^i\in[0,1]^M\right\}_{i=1}^{p}$ is selected and each point is taken tentatively as a cut point of the HDMR decomposition. The error of the expansion is calculated as

$$e(f,f_L)=\frac{1}{\sigma^2(f)}e_2(f,f_L) \tag{14}$$

where:

f – the approximated function,

f_L – the approximant.

The point with the lowest error is finally selected as the cut point. The variance $\sigma^2(f)$ of function f is defined as [25]:

$$\sigma^2(f)=\int_{[0,1]^M}\left(f(\boldsymbol{x})\right)^2d\boldsymbol{x}-\left(\int_{[0,1]^M}f(\boldsymbol{x})d\boldsymbol{x}\right)^2 \tag{15}$$

and the function e_2 is given by

$$e_2(f, f_L) = \int_{[0,1]^M} \left(f(\boldsymbol{x}) - f_L(\boldsymbol{x})\right)^2 d\boldsymbol{x}\,. \tag{16}$$

It can be observed that since the variance is a constant positive number that does not depend on the approximation, the function f_L minimizing $e_2(f, f_L)$ minimizes $e(f, f_L)$ as well.

2.3. Theoretical comparison of sparse grids and cut-HDMR

Sparse grids and cut-HDMR method use two different approaches for the approximation of multivariate functions. Both of these methods try to overcome the curse of dimensionality. The cut-HDMR method approximates a given function by a number of low-dimensional functions. The sparse grids method combines the results of interpolation using a number of grids to give a better approximation.

The methods utilize different assumptions about an approximated function. The sparse grids method assumes that high-order terms of the Taylor expansion of an approximated function are negligible. Cut-HDMR approximation assumes that terms of the Taylor expansion involving more than a few (typically one or two) variables are negligible.

3. Numerical experiments

A number of numerical experiments were carried out to compare the sparse grid approximation with the cut-HDMR approximation. Six functions defined on the cube $[0, 1]^M$ were selected for the experiments. Results presented below refer to the following functions f_1 to f_4:

$$f_1(\boldsymbol{x}) = \frac{\log\left(\sum_{i=1}^{M} 2x_i + 1\right)}{\log(2M+1)}, \tag{17}$$

$$f_2(\boldsymbol{x}) = \sum_{i=1}^{M} (2x_i - 1)^{20}, \tag{18}$$

$$f_3(\boldsymbol{x}) = \sum_{i=1}^{M}\sum_{j=1}^{M} (2x_i - 1)^{10} (2x_j - 1)^{10}, \tag{19}$$

$$f_4(\boldsymbol{x}) = e^{2x_M - 1} x_1 + \sum_{i=1}^{M-1} e^{2x_i - 1} x_{i+1}\,. \tag{20}$$

For other functions, similar results were obtained.

The above test functions have been selected with the aim of objectively test both approximation methods, without favouring any one of them. Assuming the approximated function is analytical, sparse grids behave poorly when there are high degree terms in the Taylor expansion of the approximated function at a given point. The functions f_1 and f_4 fulfill

these requirements. On the other hand, cut-HDMR effectively approximates high degree terms as long as they are monomials of no more variables than the order of the expansion (functions f_2, f_3 and f_4).

A few different one-dimensional node placements were tested for sparse grids:

- equidistant nodes $x_k = \frac{k}{m-1}, k = 0,1,\ldots,m-1,$
- extrema of the Chebyshev polynomials together with endpoints

$$x_k = 0.5 - 0.5\cos\left(\frac{\pi k}{m-1}\right), k = 0,1,\ldots,m-1,$$

- roots of the Legendre polynomials $P_n(x) = \frac{1}{2^n n!}\frac{d^n}{dx^n}\left[\left(x^2-1\right)^n\right]$ mapped to the interval [0, 1].

The first node placement was selected for its simplicity; the second, because it eliminates the Runge effect [26]. Their implementation was obtained from the code of the TASMANIAN sparse grid package [27]. The values of the parameter q in Eq. (4) that were used are 3, 4, 5, 6, 7, 8 and 9.

Figure 2 shows the relationship between the absolute approximation error calculated as:

$$ERR(f, f_L, G) = \max_{\boldsymbol{x}\in G}\left|f(\boldsymbol{x}) - f_L(\boldsymbol{x})\right|, \tag{21}$$

and the number N of points at which the function needs to be calculated. Grid G, which is the third argument of the error function (21), is a Cartesian product of M sets of k equally spaced points between 0 and 1:

$$G(M,k) = \prod_{n=1}^{M}\left\{0, \frac{1}{k-1}, \ldots, \frac{k-2}{k-1}, 1\right\}, \tag{22}$$

In the experiments, $M = 4$ and $k = 19$ were assumed. The first and second order cut-HDMR approximations were used. The error (21) was estimated on grid $G(4, 8)$. The cut-HDMR approximation used a first order spline interpolation or a Hermitian piecewise cubic interpolation employing first function derivatives approximated by three-point finite differences to represent functions of one or two arguments.

The method proposed by Wang [24] was used to determine the best placement of the cut points by minimizing expression (16). Sobol sequence [28] was used both for picking up candidates for the cut points and for the Quasi-Monte Carlo integration needed in Eq. (16). In both cases, 1000 points from the Sobol Sequence were taken. The coefficients needed for calculation of the Sobol sequence were obtained from the web page http://web.maths.unsw.edu.au/~fkuo/sobol/new-joe-kuo-6.21201 (accessed 2014-04-01). The details of the Sobol sequence generation can be found in [29].

Plot (a) in Fig. 2 shows errors for a function that cannot be expressed as a sum of functions of at most two arguments. As a result, the error of the cut-HDMR expansion reaches a minimum of approximately 0.11 and cannot become lower. At the same time, the sparse grids can achieve much lower errors.

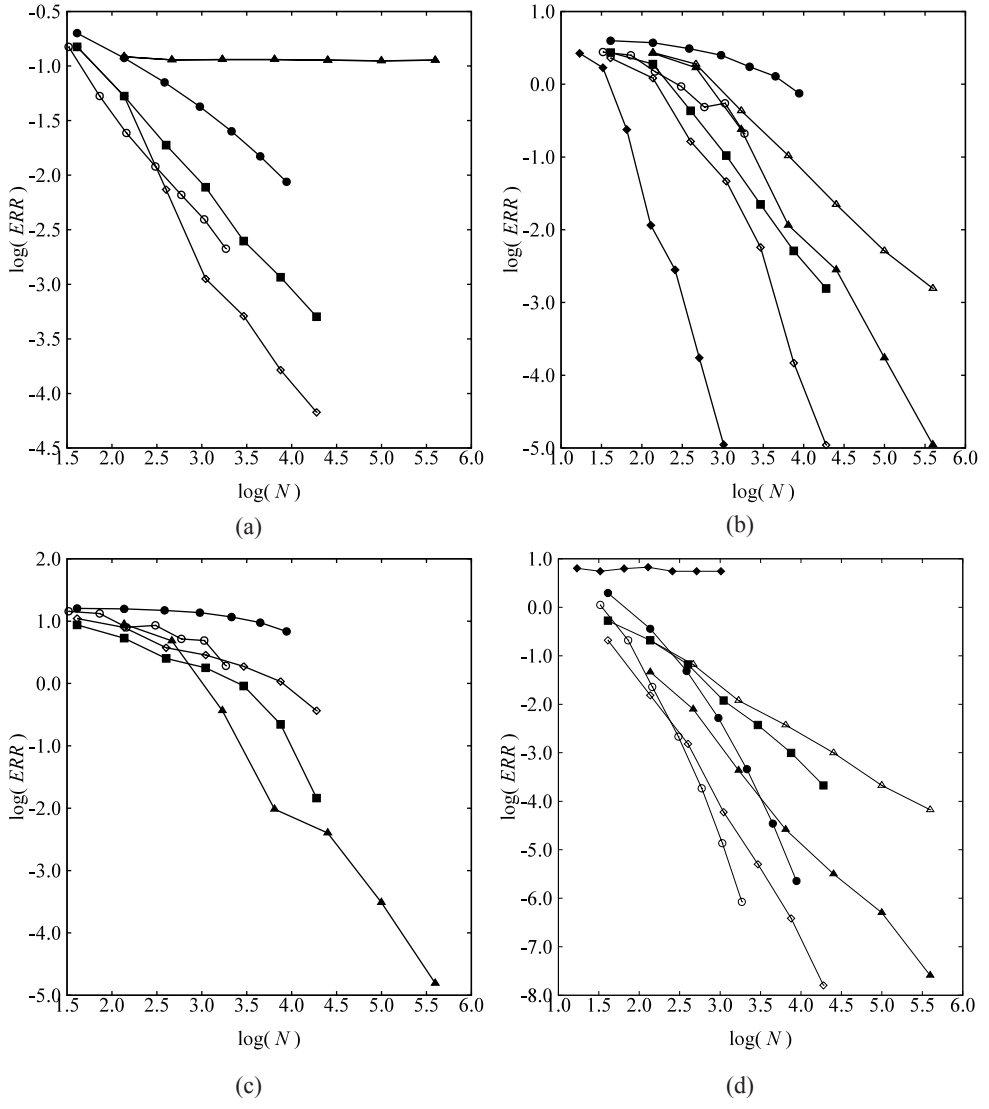

Fig. 1. Absolute approximation error as dependent on the number N of known values of function f employed by the approximation. Plot (a) – function f_1, (b) – function f_2, (c) – function f_3 (d) – function f_4. Notation: (■) – sparse grids with equidistant nodes and first-order spline interpolation, (◊) – sparse grids with equidistant nodes and third-order spline interpolation, (○) – sparse grids with nodes at the extrema of Chebyshev polynomials and with Lagrange interpolation, (●) – sparse grids with nodes at the roots of Legendre polynomials and with Lagrange interpolation, (Δ) – second order cut-HDMR with first-order spline interpolation, (▲) – second order cut-HDMR with piecewise third-order polynomial interpolation, (♦) – first order cut-HDMR with piecewise third-order polynomial interpolation

Plot (b) in Fig. 2 shows errors for a function that can be expressed as a sum of functions of one argument. In this case, the error of the expansion (6) truncated to order 2 is zero so that only the interpolation error remains and cut-HDMR approximation can be arbitrarily accurate. The variant with a higher order of interpolating polynomials shows significantly lower errors than the one that uses only first-order spline interpolation. The variant of sparse grids using third-degree piecewise polynomial interpolation has the lowest error of all sparse grid methods. The cut-HDMR decomposing only to functions of 0 and 1 variable (using third-degree piecewise polynomial interpolation) has the lowest error among all other methods.

Plot (c) in Fig. 2 shows errors for a function that can be expressed as a sum of functions of at most two variables. This function is characterized by high correlations between variables and is relatively fast-changing so that the error of the expansion (6) truncated to order 2 is zero again. The second-order cut-HDMR has the lowest errors in the range of N where the logarithm of the error is lower than 0.

Plot (d) in Fig. 2 shows errors for a function that can be represented as a sum of functions of two arguments but is relatively slow-changing. In this case, two types of sparse grid approximation have the lowest errors.

4. Conclusions

In this study, two methods of approximating multivariate functions were compared – sparse grids and cut-HDMR. The comparison regarded the accuracy of both methods defined as the maximum absolute error of approximation. In most cases, sparse grids appear more accurate than the cut-HDMR method that employs a comparable number of known values of the approximated function. However, the cut-HDMR approximation has lower errors when the function is fast-changing and can be exactly represented as a sum of functions of at most one or two variables.

In conclusion, sparse grids are recommended over cut-HDMR for approximating multivariate functions. Cut-HDMR approximation should only be used when the sparse grids method cannot achieve desired accuracy using the assumed number of known values of the approximated function.

References

[1] Donoho D.L., *Aide-Memoire. High-Dimensional Data Analysis: The Curses and Blessings of Dimensionality*, presented at the Mathematical Challenges of 21st Century, Los Angeles 2000.

[2] Barton R.R., *Metamodels for Simulation Input-output Relations*, [in:] *Proceedings of the 24th Conference on Winter Simulation*, New York 1992, 289-299.

[3] Barton R.R., *Metamodeling: a state of the art review*, [in:] *Simulation Conference Proceedings, 1994. Winter*, 1994, 237-244.

[4] Shan S., Wang GG., *Metamodeling for High Dimensional Simulation-Based Design Problems*, J. Mech. Des., vol. 132, no. 5, 051009-1-051009-11, May 2010.

[5] Jin R., Chen W., Simpson T.W., *Comparative studies of metamodelling techniques under multiple modelling criteria*, Struct Multidisc Optim, vol. 23, no. 1, Dec. 2001, 1-13.

[6] Klimke A., Pye C.J., *Sparse Grid Meta-Models for Model Updating*, [in:] *Proceedings of the IMAC-XXVII*, Orlando 2009.
[7] Schoendorf J., Rabitz H., Li G., *A fast and accurate operational model of ionospheric electron density*, Geophysical Research Letters, vol. 30, no. 9, 2003.
[8] Geremia J., Weiss E., Rabitz H., *Achieving the laboratory control of quantum dynamics phenomena using nonlinear functional maps*, Chemical Physics, vol. 267, no. 1–3, Jun. 2001, 209-222.
[9] Zabaras N., *An Information-Theoretic Multiscale Framework With Applications to Polycrystalline Materials*, Cornell University, Ithaca NY, Materials Process Design and Control Laboratory, Feb. 2010.
[10] Chowdhury R., Rao B.N., *Assessment of high dimensional model representation techniques for reliability analysis*, Probabilistic Engineering Mechanics, vol. 24, no. 1, Jan. 2009, 100-115.
[11] Bieniasz L.K., Rabitz H., *High-Dimensional Model Representation of Cyclic Voltammograms,* Anal. Chem., vol. 78, no. 6, Mar. 2006, 1807-1816.
[12] Balu A.S., Rao B.N., *Reliability analysis using high dimensional model representation for mixed uncertain variables*, IOP Conf. Ser.: Mater. Sci. Eng., vol. 10, no. 1, Jun. 2010, 012014.
[13] Smolyak S., *Quadrature and interpolation formulas for tensor products of certain classes of functions*, Soviet Mathematics, Doklady, vol. 4, 1963, 240-243.
[14] Gordon W.J., *Blending-Function Methods of Bivariate and Multivariate Interpolation and Approximation*, SIAM Journal on Numerical Analysis, vol. 8, no. 1, Mar. 1971, 158-177.
[15] Delvos F.J., Schempp W.J., *Boolean Methods in Interpolation and Approximation*. Longman Higher Education, 1989.
[16] Shen J., Wang L.-L., *Sparse Spectral Approximations of High-Dimensional Problems Based on Hyperbolic Cross*, SIAM J. Numer. Anal., vol. 48, no. 3, Jul. 2010, 1087-1109.
[17] Sobol I.M., *Sensitivity Estimates for Nonlinear Mathematical Models*, Mathematical Modelling and Computational Experiment, vol. 1, no. 4, 1993, 407-414.
[18] Rabitz H., Aliş Ö.F., *General foundations of high-dimensional model representations*, Journal of Mathematical Chemistry, vol. 25, no. 2–3, Jun. 1999, 197-233.
[19] Rabitz H., Aliş Ö.F., Shorter J., Shim K., *Efficient input-output model representations*, Computer Physics Communications, vol. 117, no. 1-2, Mar. 1999, 11-20.
[20] Li G., Wang S.-W., Rabitz H., *High Dimensional Model Representation (HDMR): Concepts and Applications*, 2000.
[21] Quadling D.A., *Lagrange's Interpolation Formula*, The Mathematical Gazette, vol. 50, no. 374, Dec. 1966, 372.
[22] Barthelmann V., Novak E., Ritter K., *High dimensional polynomial interpolation on sparse grids*, Advances in Computational Mathematics, vol. 12, no. 4, Mar. 2000, 273-288.
[23] Griebel M., *Sparse grids and related approximation schemes for higher dimensional problems*, 2005.
[24] Wang X., *On the approximation error in high dimensional model representation*, [in:] *Proceedings of the 40th Conference on Winter Simulation*, Miami, Florida 2008, 453-462.

[25] Sobol I.M., *Theorems and examples on high dimensional model representation*, Reliability Engineering & System Safety, vol. 79, no. 2, Feb. 2003, 187-193.

[26] Runge C., *Über empirische Funktionen und die Interpolation zwischen äquidistanten Ordinaten*, Zeitschrift für Mathematik und Physik, vol. 46, 1901, 224-243.

[27] Stoyanov M., *User Manual: TASMANIAN Sparse Grids*, Oak Ridge National Laboratory, One Bethel Valley Road, Oak Ridge, Tennessee 37831, ORNL REPORT, Aug. 2013.

[28] Sobol I.M., *On the distribution of points in a cube and the approximate evaluation of integrals*, USSR Computational Mathematics and Mathematical Physics, vol. 7, no. 4, 1967, 86-112.

[29] Joe S., Kuo F.Y., *Remark on Algorithm 659: Implementing Sobol's Quasirandom Sequence Generator*, ACM Trans. Math. Softw., vol. 29, no. 1, Mar. 2003, 49-57.

TECHNICAL TRANSACTIONS | CZASOPISMO TECHNICZNE
FUNDAMENTAL SCIENCES | NAUKI PODSTAWOWE
3-NP/2014

ARTUR NIEWIAROWSKI, MAREK STANUSZEK*

PARALLELIZATION OF THE LEVENSHTEIN DISTANCE ALGORITHM

ZRÓWNOLEGLENIE ALGORYTMU ODLEGŁOŚCI EDYCYJNEJ LEVENSHTEINA

Abstract

This paper presents a method for the parallelization of the Levenshtein distance algorithm deployed on very large strings. The proposed approach was accomplished using .NET Framework 4.0 technology with a specific implementation of threads using the System. Threading.Task namespace library. The algorithms developed in this study were tested on a high performance machine using Xamarin Mono (for Linux RedHat/Fedora OS). The computational results demonstrate a high level of efficiency of the proposed parallelization procedure.

Keywords: Levenshtein distance, Levenshtein-Damerau distance, edit distance, very large strings, parallel computing, threads, high performance computing, Microsoft .NET Framework 4.0, mono-project

Streszczenie

Artykuł przedstawia metodę zrównoleglenia algorytmu analizy odległości edycyjnej Levenshteina dedykowaną bardzo dużym ciągom tekstowym. Zaproponowane rozwiązanie zostało zaimplementowane na platformie .NET Framework 4.0 z uwzględnieniem metod dostępnych w przestrzeni nazw System.Threading.Task. Zastosowane algorytmy przetestowano na komputerze wysokiej wydajności, w oparciu o narzędzia Xamarin Mono (dla SO Linux RedHat/Fedora). Otrzymane wyniki pokazują znacząco zwiększoną wydajność obliczeń dla przedstawionych w artykule rozwiązań.

Słowa kluczowe: odległość edycyjna Levenshteina oraz Levenshteina-Damerau, odległość edycyjna, duże ciągi tekstowe, obliczenia równoległe, wątki, obliczenia wysokiej wydajności, Microsoft .NET Framework 4.0, mono-project

* Institute of Computer Science, Faculty of Physics, Mathematics and Computer Science of Cracow University of Technology; aniewiarowski@pk.edu.pl, mareks@riad.pk.edu.pl.

1. Introduction

The Levenshtein distance [6] between two strings of characters is equal to the minimum number of insertions, deletions and substitutions of characters required to convert one string into the second string. The Levenshtein distance has applications in many areas, e.g. text analysis (detection of plagiarism) [3, 13], spell-checking in text processors [7], web mining (search engine robots) [9, 10], bioinformatics (Levenshtein-Damerau distance for DNA structure analysis [8, 11]), etc.

The algorithm for Levenshtein distance calculation creates a matrix (Levenshtein matrix) where its last element (Fig. 1) constitutes a solution. The asymptotic computational complexity of the algorithm assumes the order $O(NM)$, where N and M denote the lengths of the text strings (i.e. the number of characters in each strings).

Difficulties occur when long strings have to be analyzed (e.g. millions of characters in one string). In such cases, the Levenshtein matrix is complex, and to attain the final results, more time is required. Moreover, it is more complicated to allocate such large matrices in standard development environments. The problem of analysis of very long strings may occur when, for example, the same fragments of a book (whole terms or words instead of consecutive characters in the original algorithm [2, 12]) have to be compared or when DNA chains (Levenshtein-Damerau distance [8, 11]) are analyzed.

In this experiment, it was decided to design both the Levenshtein as well as the Levenshtein-Damerau algorithms with Microsoft .NET Framework [14] and run developed applications under Linux OS with the use of Xamarin Mono Project [5]. Such project environments allowed for an additional validation of efficiency and of speed of the proposed algorithms.

2. Description of the Levenshtein distance algorithm

The Levenshtein distance K for two strings is the minimum number of operations –insertion, deletion and substitution required to convert one term (string) into the other. The Levenshtein distance K is equal to the $d[M, N]$ element of the so-called Levenshtein matrix d:

$$K = d[M, N] = LevenshteinDistance\ (String1, String2)$$

The main idea of the Levenshtein distance algorithm (*LevenshteinDistance* function) is described by the following pseudo-code:

```
input variables: char Text1[0..M-1], char Text2[0..N-1]
         declare: int d[0..M, 0..N]
         for i from 0 to M
              d[i, 0] := i
            for j from 0 to N
              d[0, j] := j

         for i from 1 to M
               for j from 1 to N
       if substring of Text1 at (i – 1) = substring of Text2 at (j – 1) then
```

```
                cost := 0 else cost := 1
                d[i, j] :=
                    Minimum(d[i - 1, j] + 1,
                    d[i, j - 1] + 1,
                    d[i - 1, j - 1] + cost)
            end for (variable j)
        end for (variable i)


    return d[M, N];
```

where:

d	–	Levenshtein matrix of the size N+1, M+1, formed for two terms: *Text1* and *Text2*,
M, N	–	lengths of two terms respectively,
$d[i, j] - (i, j)$	–	element of Levenshtein matrix d,
Minimum	–	a function to calculate a minimum of three variables,
cost	–	variable that gets values either 0 or 1.

The deference between the Levenshtein and the Levenshtein-Damerau distance algorithms is shown below as a part of the relevant pseudo-code with the definition of elements of the Levenshtein-Damerau matrix z:

```
   z[i, j] :=
        Minimum(d[i - 1, j] + 1,
        z[i, j - 1] + 1,
        z[i - 1, j - 1] + cost)

   if i > 1 and j > 1 and substring of Text1 at (i-1) = substring
of Text2 at (j – 2) and substring of Text1 at (i-2) = substring of
Text2(j-1]) then
        z[i, j] := Minimum(z[i, j], z[i - 2, j - 2] + cost)
```

The Levenshtein-Damerau distance D is the minimum number of operations (insertion, deletion, substitution) required to change one term into the other, this is similar to the standard Levenshtein procedure, but additionally, it is necessary to account for the number of transpositions of neighboring characters. Consequently, the Levenshtein-Damerau distance between two sequences D is equal to the $z[M, N]$ element of the suitable Levenshtein-Damerau matrix z:

$$D = z[M, N] = LevensteinDamerauDistance\ (Text1,\ Text2)$$

The figures below and the pseudo-codes above show that the value of element $[i, j]$ of matrix d in the current iteration is calculated based on the values: $d[i - 1, j]$, $d[i, j - 1]$ and $d[i - 1, j - 1]$ for the Levenshtein distance and additionally, $z[i - 2, j - 2]$ for the Levenshtein-Damerau distance. This means that each of these values must be calculated in the previous iterations of the algorithm.

		y	e	s	t	e	r	d	a	y
	0	1	2	3	4	5	6	7	8	9
t	1	1	2	3	3	4	5	6	7	8
o	2	2	2	3	4	4	5	6	7	8
m	3	3	3	3	4	5	5	6	7	8
o	4	4	4	4	4	5	6	6	7	8
r	5	5	5	5	5	5	5	6	7	8
r	6	6	6	6	6	6	5	6	7	8
o	7	7	7	7	7	7	6	6	7	8
w	8	8	8	8	8	8	7	7	7	8

Fig. 1. Levenshtein matrix d, constructed for terms: yesterday and tomorrow[1]

		G	G	C	C	T	C	C
	0	1	2	3	4	5	6	7
T	1	1	2	3	4	4	5	6
C	2	2	2	2	3	4	4	5
C	3	3	3	2	2	3	4	4
A	4	4	4	3	3	3	4	5
A	5	5	5	4	4	4	4	5
T	6	6	6	5	5	4	5	5
A	7	7	7	6	6	5	5	6

Fig. 2. Levenshtein-Damerau matrix **z**, constructed for deoxyribonucleic acid (DNA) sequences: TCCAATA and GGCCTCC (where: T – thymine, A – adenine, G – guanine, C – cytosine)

Table 1

Examples of Levenshtein distance between two strings

No.	string 1	string 2	Levenshtein distance
1	Car	Cars	1
2	University	Universities	3
3	Tom is writing a letter	Tom is writin letters	4

Table 1 shows an example of the results of calculations of the Levenshtein distances using the conventional algorithm. In the first example, we need to add one character in string1 or remove one character in string2 to transform one string into the other. In the second example, we need to substitute one character and add two characters (string1) or substitute

[1] The application for both Levenshtein and Levenshtein-Damerau matrices calculations is available from the web site: www.pk.edu.pl/~aniewiarowski/publ/levenMatrix.exe.

one character and remove two characters (string2). In the last example, we need to remove four characters (‘g’, ‘a’, ‘s’ and space) in string1 or add four characters in string2.

3. Numerical implementation of parallelization algorithm[2]

As was depicted above, difficulties occur when strings of millions of characters have to be analyzed. In such cases, the Levenshtein matrix becomes very large and more time is required to compute all its elements. Table 2 shows examples of time consumption requirements in the case of complex Levenshtein matrices calculation (without any parallelization procedure implemented). The whole series of experiments was performed on a computer with parameters: 32GB RAM; two physical processors (Intel(R) Xeon(R) CPU E5-2620 0 @ 2.00GHz, 24 threads).

Table 2

Time consumption in the case of complex Levenshtein matrices calculation

No.	Length of string 1	Length of string 2	Number of elements of Levenshtein matrix	Computation time [sec.] (high performance computer)	Computation time [sec.] (standard PC)[1]
1	5 000	5 000	25 000 000	0.724	3.385
2	10 000	10 000	100 000 000	2.520	13.400
3	30 000	30 000	900 000 000	22.020	105.502
4	32 000	32 000	1 024 000 000	25.040	172.879
5	40 000	40 000	1 600 000 000	out of memory exception	out of memory exception

In Fig. 3, a graphical interpretation of the proposed solutions for large strings is presented. One very large matrix is built from the smaller component matrices resulting from the structure of the analyzed substrings. Each component matrix (i.e. values from last column and last row) is calculated and some of their values are transmitted to the next small matrix where they become initial values. This procedure reiterates through all component matrices. Each component matrix is calculated by the parallelized threads (1, 2 .. n) with the use of an array of locks algorithm where a younger thread (e.g. $n - 1$) waits for an older one (e.g. $n - 2$). Matrices which will not be used anymore are removed from the memory.

The pseudo-code below Fig. 3 describes a part of the function *LevDistDecomposition* where the input strings *Text1* and *Text2* are decomposed for the smaller substrings. Based on two subsequent substrings the component matrices are calculated and their final boundary elements are collected in two one-dimensional arrays: *arrVertical* and *arrHorizontal*. Next, these arrays are transmitted to the new small matrix in which they stay as the initial values for further calculations. Finally, the algorithm returns the Levenshtein distance as the result.

[2] All the results for the described algorithms were calculated with the use of a 64-bit console application (written in C# language) available on website: www.pk.edu.pl/~aniewiarowski/publ/ LevParallelCS.exe.

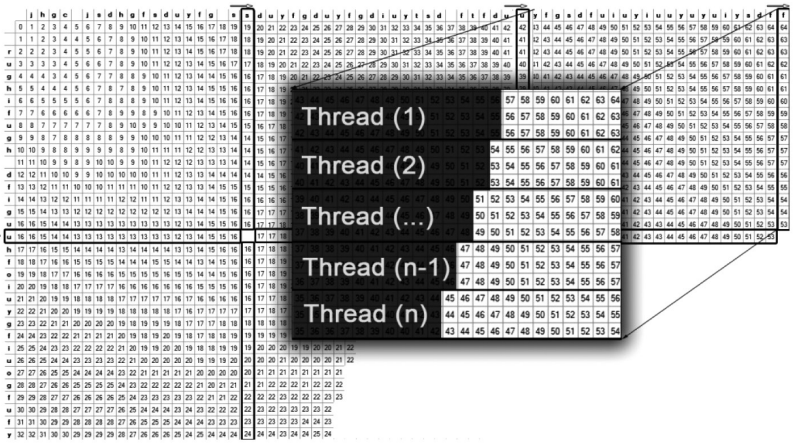

Fig. 3. Parallelization procedure of the Levenshtein distance matrix decomposition

```
input variables: char Text1[0..M-1], char Text[0..N-1], number of
parts, number of parallel threads
declare: part_rangeX[0..number of ranges of horizontal parts], part_
rangeY[0..number of ranges of vertical parts] as structure of int from
and int to
declare: results_of_matrix[0..number of ranges of horizontal parts,
0..number of ranges of vertical parts] as structure of int[]
arrVertical[0..length of Text1] and int[] arrHorizontal[0..length of
Text2]

for vm from 0 to M do arrVertical[vm]:=vm
for vn from 0 to N do arrHorizontal[vn]:=vn

for mx from 1 to number of ranges of horizontal parts (i.e. number of
elements of part_rangeX)
    for my from 1 to number of ranges of vertical parts (i.e. number
of elements of part_rangeY)
      results_from_matrix[mx, my] :=
        LevDistParallelParts(
        substring of Text1 at (part_rangeX[mx-1].from-1,
         part_rangeX[mx-1].to - part_rangeX[mx-1].from+1),
        substring of Text2 at (part_rangeY[my-1].from-1,
         part_rangeY[my-1].to - part_rangeY[my-1].from+1),
        number of parallel Threads,
        results_from_matrix[mx - 1, my].arrVertical,
        results_from_matrix[mx, my - 1].arrHorizontal
       )
       clear results_from_matrix[mx - 1, my].arrVertical
       clear results_from_matrix[mx, my - 1].arrHorizontal
end for (variable my)
end for (variable mx)

return the last element of arrVertical (or arrHorizontal) of the last
element of result_from_matrix
```

In the pseudo code-above, some designations are taken:
LevDistParallelParts – function for calculation of the component matrices,
results_from_matrix – two-dimensional array, collects elements of one-dimensional arrays: arrVertical and arrHorizontal,
part_rangeX, part_rangeY – one-dimensional arrays with elements representing the range of calculated component matrices,
arrVertical, ***arrHorizontal*** – one-dimensional arrays of results, input parameters for *LevDistParallelParts* function.

Additional complex operations, required for the implementation of the parallelization procedure are presented precisely in the pseudo-code in appendix A.

4. Results

In the present research, the *Microsoft .NET* technology was used (C# language) [14][3]. The proposed algorithm was tested with *mono-project* (cross platform, open source .NET development framework) [5] and *OS Fedora Linux*. The obtained results are presented in Fig. 4. The diagram shows the relationship between the length of analyzed strings (additionally described by the number of parts of the main matrix – right-hand legend in Fig. 4) and the number of parallel

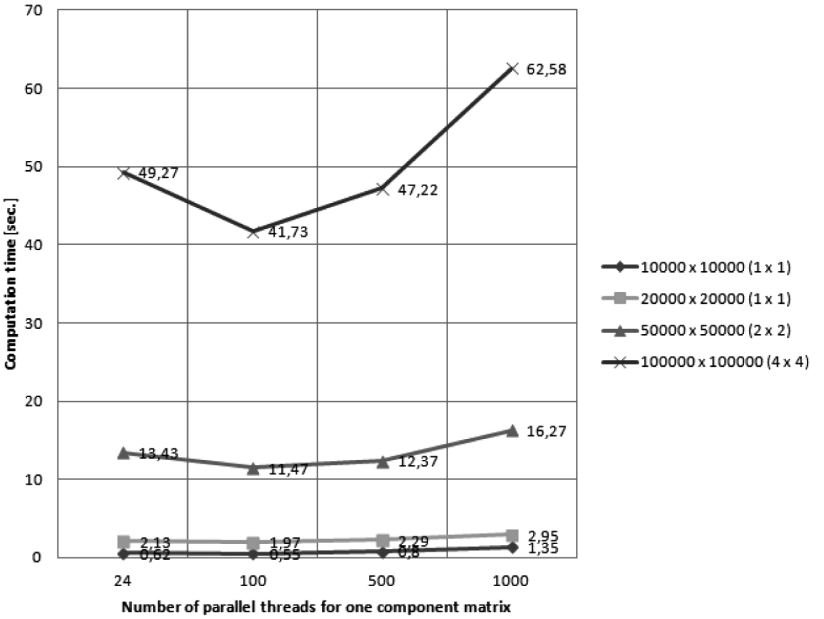

Fig. 4. Correlations between length of strings and computation time for different numbers of parallel threads for one component matrix

[3] Some details of .NET's threads and parallel technologies are presented in [15].

threads for one component matrix. As can be seen, the final computation time strongly depends on string sizes and on the number of parallel threads. In the presented examples, the best optimal results were obtained for about 100 threads applied for the component matrix in all cases of partitioning. For other numbers of threads, the parallelized parts of the component matrix were too large or too small and the procedure of threads construction was not cost-effective.

In Fig. 5, the relationship between the number of parts of a large decomposed matrix ($1 \cdot 10^{12}$ elements) and the computation time is presented. The obtained results show that the speed of calculations strongly depends on the number of parts (i.e. sizes of component matrices) of the decomposed matrix as well. This effect influences the main decomposition algorithm (in function *LevDistDecomposition*), in which the one-dimensional array of results becomes the input data for the next iteration, and some old data are removed from memory. If there are too many parts, the transfer of partial results (and other operations) will be too frequent.

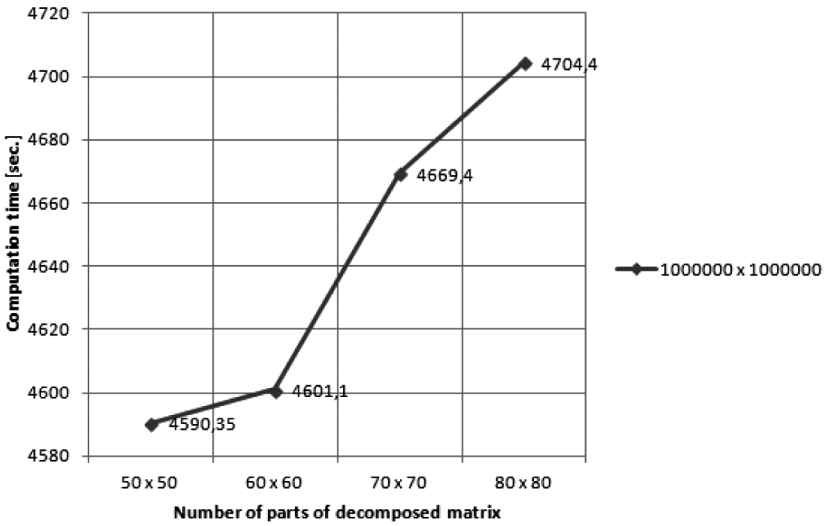

Fig. 5. Relationship between number of parts (blocks) of decomposed matrix and computation time for string size of $1 \cdot 10^6 \times 1 \cdot 10^6$

The results obtained for strings depicted with the Levenshtein matrix of $4 \cdot 10^{12}$ elements, are presented in Tab. 3. It turns out that for parts 50×50 and 60×60, the component matrices were too large and the system could not allocate them in memory.

In Fig. 6, the consumption times of computations of the Levenshtein distance for very long strings with the use of optimized parameters (the best values of number of parallel threads for one component matrix and number of parts of decomposed main matrix) are presented. It is worth underlining that the calculation time versus the string's length grows approximately according to the power function.

Next, the calculation times of the Levenshtein distance for very long texts with or without the parallelization procedure were compared. Different length texts were analyzed and the obtained results are presented in Tab. 4 and Fig. 7.

Table 3

Computation times for two long strings according to number of blocks of main matrix

String sizes	Number of parallel threads for component matrix	Number of parts of main matrix	Computation time [sec.]
1 000 000 × 1 000 000	100	50 × 50	4 590.35
1 000 000 × 1 000 000	100	60 × 60	4 601.1
1 000 000 × 1 000 000	100	70 × 70	4 669.4
1 000 000 × 1 000 000	100	80 × 80	4 704.4
2 000 000 × 2 000 000	100	50 × 50	out of memory exception
2 000 000 × 2 000 000	100	60 × 60	out of memory exception
2 000 000 × 2 000 000	100	70 × 70	17 360.4
2 000 000 × 2 000 000	100	80 × 80	17 630.58

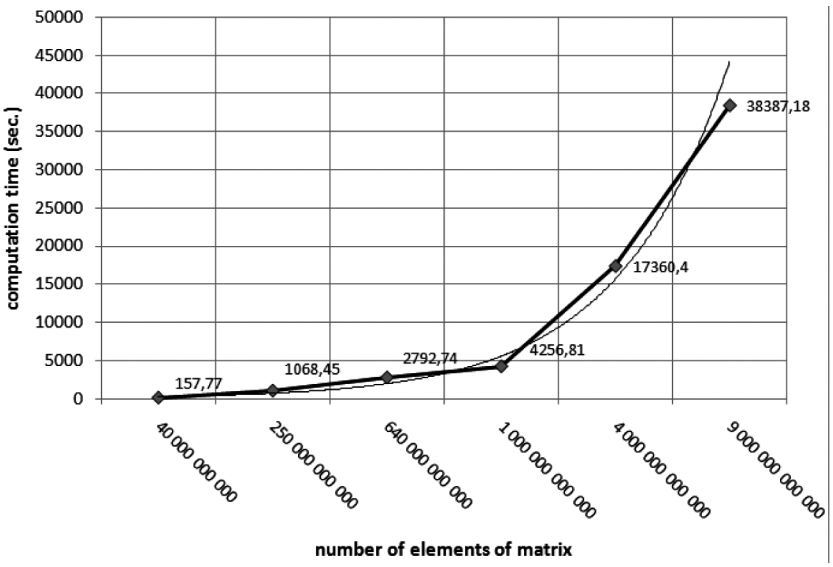

Fig. 6. Computation times of calculations for very long strings using matrix decomposition with the parallelization procedure

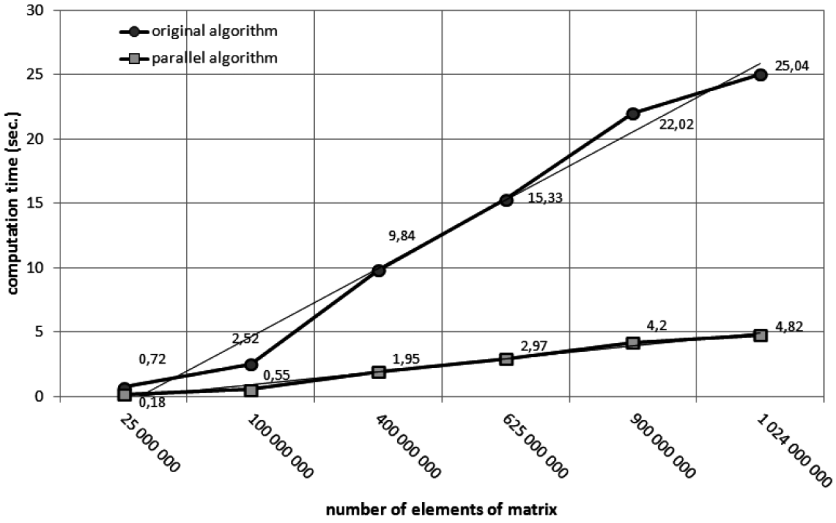

Fig. 7. Computation times of calculations of long strings using Levenshtein distance algorithm with and without parallelization for one decomposed matrix

Based on Fig. 7, it can be seen that the parallelized Levenshtein distance algorithm is about 4–5 times faster than that without the parallelization procedure applied.

Table 4

Computation times of Levenshtein distance algorithm with or without parallel procedure

Chars in text *A*	Chars in text *B*	Comp. time [sec.] – with parallel procedure	Comp. time [sec.] – no parallel procedure
5 000	5 000	0.18	0.72
10 000	10 000	0.55	2.52
20 000	20 000	1.95	9.84
25 000	25 000	2.97	15.33
30 000	30 000	4.20	22.08
32 000	32 000	4.82	25.04
33 000	33 000	out of mem. exception	out of mem. exception

Figure 8 presents the computation times of DNA sequences for one decomposed Levenshtein-Damerau matrix with the use of assumed (100) number of parallel threads. As can be seen, the parallelized algorithm is again about 4-5 times faster than the algorithm not being parallelized. DNA sequences consist of chars T, A, G, C (described in Fig. 2).

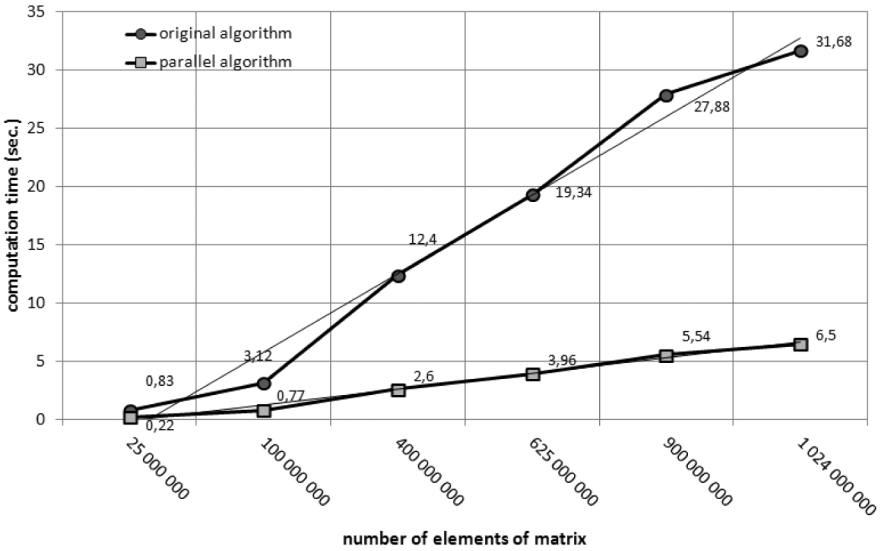

Fig. 8. Computation times of calculations of DNA sequences using Levenshtein-Damerau algorithm with and without the parallelization procedure for one decomposed matrix

5. Conclusions and further work

The research presented in this paper results in a method for the parallelization of the Levenshtein distance algorithm. Its implementation allows for the improvement of the speed of calculating the similarity measure of two long strings. In the presented examples, a high efficiency of the proposed techniques was achieved and very good results on a high-performance computer were confirmed [4].

The algorithm proposed in the paper was implemented in the mechanism of automatic selection of promotors and reviewers of diploma thesis within the system "Diplomas' Manager". This system was implemented at the Faculty of Physics, Mathematics and Computer Science of the Cracow University of Technology[4] as a tool for diploma thesis management. The solution was also implemented within the anti-plagiarism system of "Diplomas' Manager" and high efficiency in the case of searches for plagiarism was achieved.

In our future research, efforts will be undertaken towards improving the Levenshtein-Damerau algorithm for analyzing very long DNA sequences by decomposing the main matrix in accordance with the proposed algorithms. Moreover, the MPI technology will be implemented for computing each part of a large matrix. Furthermore, the introduction of measures of the distance between text elements (terms) in the analyzed text documents to build its internal specific characteristic and document structure is also anticipated [1].

[4] System is available on web page: https://administracja.fmi.pk.edu.pl/~dyplomy.

References

[1] Niewiarowski A., Stanuszek M., *The mechanism of identification and classification of content*, Studia Informatica, Vol. 34, 2B(112), Silesian University of Technology Press, Gliwice 2013, 205-222.

[2] Niewiarowski A., Stanuszek M., *Mechanism of analysis of similarity short texts, based on the Levenshtein distance*, Studia Informatica. Vol. 34, 1 (110), Silesian University of Technology Press, Gliwice 2013, 107-114.

[3] Niewiarowski A., *Term frequency optimization for the vector space model*, Czasopismo Techniczne, 9-M/2012, 155-165.

[4] Kobzdej P., Waligóra D., Wielebińska K., Paprzycki M., *Parallel Application of Levenshtein Distance to Establish Similarity Between Strings*, International Journal of Computer Research, Vol. 12, No. 4, 2003, 625-633.

[5] Mono-project (www.mono-project.com/What_is_Mono).

[6] Левенштейн В.И., *Двоичные коды с исправлением выпадений, вставок и замещений символов*, Доклады Академий Наук СССР 163 (4), 1965, 845-848.

[7] Wypych M., *Stochastic Spelling Correction of Texts in Polish*, Institute of Linguistics, Adam Mickiewicz University, Poznań, Poland; Speech and Language Technology. Volume 6, Poznań 2002.

[8] Damerau F.J., *A technique for computer detection and correction of spelling errors*, Communications of the ACM, 7 (3), 1964, 171-176.

[9] Runkler T.A., Bezdek J.C., *Web mining with relational clustering*, International Journal of Approximate Reasoning, Vol. 32, Issues 2–3, February 2003, 217-236.

[10] Niewiarowski A., *Działanie parsera ‚Part-of-Speech Tagging' w ujęciu mechanizmu Web Content Mining*, Wydawnictwo VI Ogólnopolskiej Konferencji Naukowej Nauka i Przemysł, Politechnika Krakowska im. Tadeusza Kościuszki, Kraków 2011, 93-100.

[11] Niewiarowski A., Stanuszek M., *Parallelize edit distance algorithm*, Proceedings. Seventh ACC Cyfronet AGH Users' Conference, Academic Computer Centre Cyfronet AGH, Zakopane 2014, 31-32.

[12] Niewiarowski A., Stanuszek M., *Performance and quality of method for short text similarity algorithm based on edit distance and thesaurus*, Proceedings. Seventh ACC Cyfronet AGH Users' Conference, Academic Computer Centre Cyfronet AGH, Zakopane 2014, 33-34.

[13] Ramos J., *Using tf-idf to determine word relevance in document queries*, Proceedings of the First Instructional Conference on Machine Learning, 2003.

[14] Campbell C., Johnson R., Miller A., Toub S., *Parallel Programming with Microsoft. NET. Design Patterns for Decomposition and Coordination on Multicore Architectures*, Microsoft Press, 2010.

[15] Niewiarowski A., *Szybko zrozumieć Visual Basic 2012*, Self Publishing. Kraków 2013, 66-73.

Appendix 1

The pseudo-code below describes part of the function *LevDistParallelParts* which provides the parallelization procedure of component matrix *dpart*. The procedure calls threads that are assigned to insert the one-dimensional array *pth*. For iteration of all elements of matrix *dpart* two loops *for*, loop in the line 16 and loop in the line 2, are required. The number of iterations within the loop in line 21 is restricted by the number of threads. Additionally, in line, 19 the automat of waiting mechanism is implemented and a loop with the array of locks *point_lock* is introduced. Based on this, the thread number *p* in loop *for* (line 16) waits for parallel thread number *p-1* (line 19) until column *i* in thread *p-1* has all values calculated.

```
 1  input variables: number of parallel threads nTh, char fragText1[0..tM-
 2  1] char fragText2[0..tN-1], initial values included in arrVertical and
    arrHorizontal arrays
 3  declare: array of threads pth[0..nTh], array arrRanges[0..tN] of
    structure int form and
 4  int to, array dpart (part of Levenshtein distance matrix)
 5
 6  calculate ranges for Y size of matrix dpart and save in arrRanges
    for i from 0 to tM
 7          d[i, 0] := arrHorizontal[i]
 8  for j from 0 to tN
 9          d[0, j] := arrVertical[j]
10
11  for p from 1 to nTh
12   pth[p] := new Thread((num) of
13   {
14   int cost
15   for i from 1 to tM
16
17      point_lock[num] = i
18      wait if i >= point_lock[num - 1]
19
20      for j from arrRanges[num - 1].from to arrRanges[num - 1].to
21
22      if substring of Text1 at (i – 1) = substring of Text2 at (j – 1)
23  then
        cost := 0  else  cost := 1
24
25      dpart[i, j] := Minimum(
26                     dpart[i - 1, j] + 1,
27                     dpart[i, j - 1] +1,
28                     dpart[i - 1, j - 1] +cost)
29
30      end for (variable j)
31   end for (variable i)
32   increment +1 of point_lock[num]
33   }
34  run thread pth[p]
35  end for (variable p)
36
37  wait for finish thread pth[nTh] (i.e. wait for all threads)
38  return structure of (array dpart[0..tM-1, tN-1], array dpart[tM-1,
39  0..tN-1])
```

In the pseudo code-above, some designations are taken:
pth – one-dimensional array of thread objects,
point_lock – one-dimensional array of locks,
arrRanges – one-dimensional array of calculated ranges of areas of component matrix,
num, p –thread number (i.e. number of part matrix),
dpart – component matrix of Levenshtein matrix **x**,
LevDistParallelParts – the Levenshtein distance obtained with the parallelization procedure.

TECHNICAL TRANSACTIONS | **CZASOPISMO TECHNICZNE**
FUNDAMENTAL SCIENCES | NAUKI PODSTAWOWE
3-NP/2014

PIOTR ZABAWA, MAREK STANUSZEK*

CHARACTERISTICS OF THE CONTEXT-DRIVEN META-MODELING PARADIGM (CDMM-P)

CHARAKTERYSTYKA PARADYGMATU META MODELOWANIA STEROWANEGO KONTEKSTEM (CDMM-P)

A b s t r a c t

The paper introduces a novel Context-Driven Meta-Modeling Paradigm (CDMM-P) and discusses its properties. The CDMM-P changes the traditional division of responsibilities within the data layer in software systems. It facilitates the interchangeable usage of both objects representing data and objects representing relationships. The decomposition of specific responsibilities results in the weakening of internal data model dependencies. This in turn allows for run-time construction of the whole data model. The proposed paradigm facilitates exceptional flexibility in the implementation of the data layer in software systems. It may be applied to domain modeling in enterprise applications as well as to the modeling of any ontology, including the construction of modeling and meta-modeling languages. As such, CDMM-P underpins a broad domain of Context-Driven Meta-Modeling Technology (CDMM-T).

Keywords: Data layer, model layer, paradigm, model parameterization, UML, entity class, pure entity class, entity relationship class, domain model, meta-model, meta-programming, meta-language

S t r e s z c z e n i e

W artykule wprowadzono nową koncepcję Paradygmatu Meta Modelowania Sterowanego Kontekstem (CDMM-P) oraz przedyskutowano jego własności. CDMM-P zmienia tradycyjny podział odpowiedzialności w warstwie danych systemów softwerowych. Ułatwia wymienne stosowanie zarówno obiektów reprezentujących dane, jak i obiektów reprezentujących relacje. Podział tych specyficznych odpowiedzialności skutkuje osłabieniem wewnętrznych zależności modelu danych. Pozwala to z kolei na konstruowanie całej warstwy danych w czasie wykonania. Proponowany paradygmat zapewnia wyjątkową elastyczność implementowania warstwy danych systemów softwerowych. Może być on stosowany do modelowania dziedzinowego aplikacji korporacyjnych i do modelowania dowolnego systemu pojęć (ontologii) z konstruowaniem języków modelowania i metamodelowania włącznie. CDMM-P stanowi podstawę szerokiej dziedziny Technologii Meta Modelowania Sterowanego Kontekstem (CDMM-T).

Słowa kluczowe: warstwa danych, warstwa modelu, paradygmat, parametryzacja modelem, UML, klasa encyjna, klasa czysto encyjna, klasa relacji encyjnej, model dziedzinowy, meta model, meta programowanie, meta język

* Institute of Computer Science, Faculty of Physics, Mathematics and Computer Science of Cracow University of Technology; pzabawa@pk.edu.pl, mareks@riad.pk.edu.pl.

1. Introduction

There is a disparity between the UML's (Unified Modeling Language) system of notions and its application to programming languages. This disparity has been known for many years. In particular, there is no the programming language that offers a built-in mechanism for management of life-time of objects, in the meaning of associative relationships defined in UML – the association, aggregation, containment. As the result, the management of an object's life-time is traditionally assumed as the responsibility of applications implemented in these languages, thus it is the programmer's responsibility.

One possible solution to this problem is the new concept of meta-modeling presented here. This concept offers several new and very useful opportunities for software construction. This solution, as well as its accompanying features, constitutes a new CDMM-P (Context-Driven Meta-Modeling Paradigm) for both software design and development. The considerations presented here apply to the software system's data layer and the main focus of attention was the associative relationships and wide spectrum of applications of CDMM-P.

The CDMM-P presented here plays an important role in software engineering – it allows for the breaking of limits in UML's mapping of associative relationships into programming languages. Moreover, it helps to break limits characteristic of all known approaches to the modeling system of notions from any application domain, including the modeling of software systems.

2. State of the art

The topic of this paper overlaps software engineering and artificial intelligence. This is the first reason why the analyzed scientific literature is so differentiated. The second is the fact that domain modeling can refer to vertical domains as well as to the construction of modeling languages – meta-languages. The last reason is new and shows that, as a consequence of CDMM-P implementation, the same notions can be implemented in enterprise applications as well as being applied in meta-modeling.

The main idea of the proposed paradigm is that information about the interconnections of entity classes is moved out from these classes and put into separate *entity relationship classes*. This way, the new responsibility distribution to the data layer is applied. Furthermore, the literature is considered in the context of the data layer only from several perspectives.

2.1. Architectural perspective

Generally speaking, there is no literature on the CDMM-P approach as long as the presented problem is analyzed within the perspective of traditional software engineering. This observation is confirmed by the contents of [29] which discusses architectural approaches to the data layer – there is no parameterization of the data layer by model. Moreover, in all available publications, such models are constructed statically through explicit embedding of relationships in interrelated classes in the form of pointers or references. More general software engineering subject reviews like [5] or [23] also confirm this observation. The same conclusion results from the literature dedicated to more detailed problems. In [34], the ADOM-UML (Application-based DOmain Modeling) is used to enrich modeling in

order to fill the gap between domain and application models, while in [35], the SDM (Semi-Automated Domain Modeling) concept is introduced to infer domain models from the former application models stored in a repository. In [28], the system for gathering information about modeling is introduced, but its meta-model has a fixed structure. In paper [7], the domain model is composed from many interrelated heterogenic project artifacts and the emphasis is put on the important role of the relationships performed in that approach. In [2], the challenge for the research is to make use of very large and very complex UML and Ecore meta-models [11]. In paper [13], the evolutionary introduction of changes to running software system without it stopping is shown. However, this goal is achieved through carrying out a priori off-line analysis. Paper [14] presents information regarding how to mix interrelated ontologies in a direct and static way. In [25], the meta-model is inferred from several models.

2.2. Ontological perspective

The notion of ontology in its technical meaning originated from artificial intelligence research. In software engineering, it can be applied to end-user domain enterprise applications (the product), to the problems of modeling and meta-modeling or to the software development process. The analysis presented below addresses all of the above perspectives with the exception of processes.

Monograph [4] contains traces of references to the concepts of open ontology, but without references to software engineering. More references to ontology can be found in [15] and [16].

Paper [10] shows how to define the domain model with the aid of ontology. Then, with the application of technologies well suited for DSL (Domain-Specific Language) construction and Magic Potion [8] like Clojure/Lisp [19, 21, 22], the compilable and executable source code in the domain-specific language for making operations on this model is created. They refer to the Semantic Web which is a kind of open ontology and does not have a meta-models hierarchy above the model layer – this is typical of OMG (Object Management Group) approaches.

Another very important publication is [24] which presents the system for ontology-based application design. The access to object's domain takes place through object-oriented paradigm, which is not new compare to [37, 30]. The cited work contains the whole IDE (Integrated Development Environment) named JOINT (Java Ontology Integrated Toolkit). It offers the ability of generating Java source code directly from the ontology.

Paper [33] is focused on the method of the application of ontology to the customization of the domain model for the needs of a particular software system. In this way, the ontology as an expression medium for OMG vertical standards is applied. In paper [12], ontology is used to infer a static class model, while in [26], a special ontology must be chosen to build OGML (Ontology Grounded MetaLanguage) meta-language on top of it.

The analysis of the "whole-part" relationship is presented in [32]. However, this analysis, based on [20], assumes that the WP (Whole-Part) relationship is defined as a class of property. This is why the analysis is so complex and needs dedicated frameworks.

In [9], the MOF-based (Meta Object Facility) MDA-compliant (Model Driven Architecture) meta-model is introduced for modeling ontologies, thus, software engineering and artificial intelligence are combined. While in paper [3], the proposed framework is integrated into several ontologies through their injection into the more general meta-ontology.

2.3. Paradigmatical perspective

Further we may analyze the literature from the paradigmatical perspective. In paper [8], the meta-modeling role, as a way of application of many paradigms at the same time, is presented, referring directly to [10]. A very interesting solution named "MagicPotion" which has already been discussed in section 2.2, is introduced there.

According to [36], meta-programming is the old concept of "using programs to manipulate other programs" and in case of Java, the meta-programming concept is supported by annotations. This paper defines the requirements of meta-programming.

2.4. DSL perspective

DSL languages are always designed in the context of a particular application domain. This domain is usually limited to the operations executed on the data layer. This is why the approach to the construction of this layer results from the way in which the DSL is perceived. This conclusion also relate to presented work.

The work reviewed in [27] shows that, independently of the approach to DSL design, the closed character of the ontology is assumed at the very beginning. This publication describes the abstract syntax of DSL as a meta-meta-model or as an Abstract Syntax Graph (ASG)/ Abstract Syntax Tree (AST), but each of these approaches closes the ontology by MOF or by grammar respectively. In publication [31], localized in the area of Computer Supported Cooperative Work (CSCW), the appropriate DSL is constructed on the basis of close ontology (Ecore). Moreover, article [6] is focused on the embedding of abstractions into domain-driven approaches (DSML – Domain Specific Modeling Languages) to DSL construction. These abstractions can be reused in many application domains. The mapping between them, and particularly between modeling languages, is implemented in the form of annotations.

2.4. Mixed perspective

There are some papers dealing simultaneously with several of the perspectives pointed out above. In [38], DSL, ontology notions and UML modeling are joined and the idea of DSL construction based on fixed static entity classes structure is presented. Paper [18] presents an approach to the change of meta-model via the application of a universal ontology introduced in [17]. Combination of the ontological approaches with meta-modeling is shown in [1]. It is dedicated to providing a better transformation from modeling of general concepts in domain languages (ontology) to models/meta-models that are MDA-compliant. However, fixed entity models are used again.

3. Decomposition of data model responsibilities

The main goal of the CDMM-P is to take the responsibility for lifetime management of the objects, inter-related through associative relationships characteristic of the data layer. This goal can be achieved through the change of responsibilities, that is the typical solution implemented for design. It transpires that the entity classes encompass too many

responsibilities. On the one hand, they map application objects to their data source and on the other hand, they store relationships that in turn define how the lifetime of related objects must be managed. At the same time, entity classes or application codes are responsible for lifetime management. However, this should be the responsibility of relations because they know their own nature best. This is why the split of both responsibilities through the introduction of the notions of pure entity (in contrast to the established notion of entity) and entity relationship is. Such a decomposition was not considered in the literature till now. Pure entity classes are responsible for the representing of data while the entity relationships are responsible for the lifetime management of pure entity class instances involved in associative relationships. The sample data models of a class named Company for both traditional and new approaches are presented in Fig. 1.

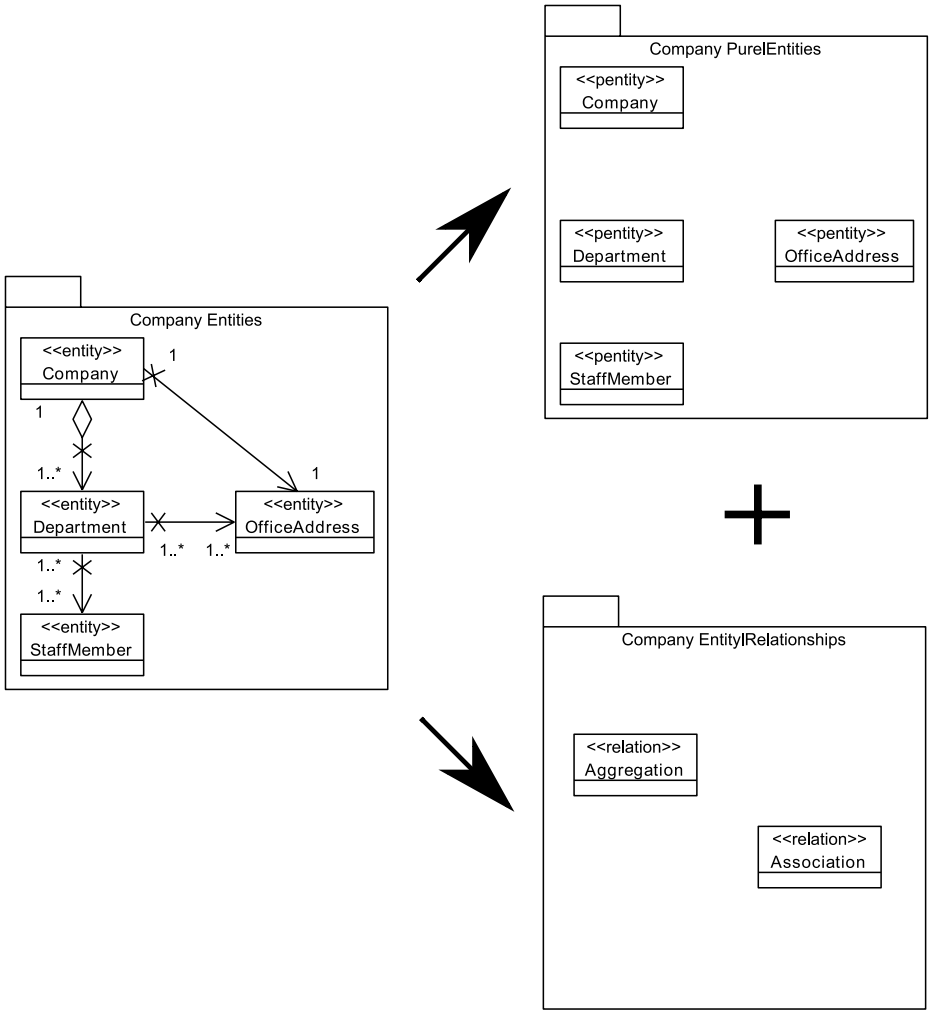

Fig. 1. Conceptual transformation from fixed entity model to context-driven entity model for sample Company model

With the introduction of this crucial modification, the application's source code and (optionally) entity classes are released from the responsibility of representing relations. In effect, it leads to the weakening of dependencies on the following borders:

- pure entity class – pure entity class,
- entity relationship – entity relationship,
- pure entity class – entity relationship.

Maximal weakening of the above dependencies can be described by not measurable but intuitive quality criterion 'weak coupling & strong-cohesion' which is commonly accepted as good design practice in software engineering. This weakening plays the key role in the CDMM-P concept. Moreover, it constitutes the starting point for reaching and achieving the goals described below.

4. Influence of responsibilities shifting on the ease of change management

The elimination of circular dependencies as well as the limitation of dependencies were introduced as good practice in software engineering. In the context of the CDMM-P, significant weakening allows for the achieving of two succeeding goals:

- maximal limitation of the scope of introduced change,
- possibility of run-time data layer change.

The first goal is quite obvious – the introduction of change into the pure entity class does not impact the entity relationship. Similarly, introduction of change into the entity relationship does not influence pure entity classes involved in this. The second goal is however, not as clear. All classes introduced by the CDMM-P can be interconnected at run-time due to the fact that they are independent of each other. Specifically, all pure entity class objects may first be loaded, and then all entity relationships between them can be created. The point here is not, however, just to interconnect existing objects, but also to store information about their classes. These allows to:

- obtain information from each *pure entity class* about the *entity relationship classes* that the *pure entity class* is involved in,
- obtain information from each *entity relationship class* about the *pure entity classes* involved in this *entity relationship*.

An XML file describing both classes and relationships can be used as the source of information about both *pure entity classes* and their relationships. Such a file can be interpreted by the implementation of the CDMM-P, which can take the form of the framework named Context-Driven Meta-Modeling Framework (CDMM-F). Such a framework will be presented in further publications. As a result of this approach, all classes involved in the model can be run-time interconnected, as depicted in Fig. 2. The class objects can be created from the CDMM-F's client level through the API (Application Programming Interface) after loading the whole data layer model from the XML file mentioned above.

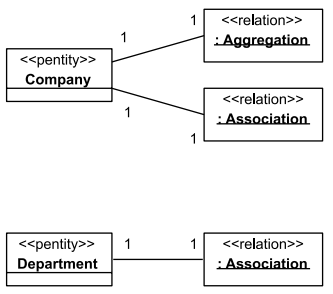

Fig. 2. Implementation-dependent context-driven entity model of a sample Company model from Fig. 1 with injected relationships

5. Parameterization of data layer by its model

The authors noticed that in the data layers of software systems, like in UML, there is a strong asymmetry in the number of available entity classes (potentially infinite) and the number of available relationships among them (three associative relationships are usually sufficient) in most domain models. It thus allows for the introduction of predefined *entity relationship classes* and for further parameterization of the data layer through *pure entity classes* defined by the user of CDMM-P. Predefined entity relationship classes are independent of user-defined *pure entity classes* thanks to the maximal weakening of dependencies in the CDMM-P. At the same time, user-defined *pure entity classes* are independent of predefined entity relationship classes. As a result, the set of entity relationship classes can be modified independently of the set of *pure entity classes*. This means that in such a situation, the relationships between any set of classes can be shaped as needed without any limits – there is nothing that closes or limits these sets. Thus, the data model can be created according to the CDMM-P on the basis of its UML model. More specifically, this model can be loaded at run-time for the purpose of the dynamic creation of the application data layer as long as the CDMM-P is used. The application of the UML class model, as a widely accepted standard, is quite obvious, but the whole structure of the data layer can be loaded from any resource describing the whole structure both sufficiently and unambiguously.

The presented method of the dynamic loading of the data model into the application, based on CDMM-P, is possible because of the dependency weakening presented above. Consequently, there is no information in the entity classes about other entity classes. According to the CDMM-P, there are no property fields in *pure entity classes* that represent entity relationships just as in entity relationship classes, there are no fields representing *pure entity classes*. *Pure entity classes* interconnecting via entity relationships in the CDMM-P do not have compile-time character but have run-time only. As a result, the data layer is parameterized at run-time by the data model.

6. Reusability consequences

The data layer creation based on CDMM-P allows for any customization of previous data models being constructed in an IT enterprise. It also significantly improves the possibilities for the reuse of former *pure entity classes* (they may be used in any relationships context) as well as the reuse of specific entity relationship classes (they may be used in any context of *pure entity classes*). Thus, the approach presented here allows for unlimited changes of the context through introducing *pure entity classes* and entity relationship classes in the data model. Moreover, this context can be established at run-time. In the result, the *pure entity classes* can be run-time changed or replaced in the application containing them. Achieving any of the goals presented here with the application of traditional approaches to software engineering is not possible.

7. Class-based perspective for non-class-based paradigm

The CDMM-P cannot be implemented in class-based versions of object-oriented technologies. Nevertheless, it should be taken into account that its potential users (developers) implement this approach only in the most popular class-based version of the object-oriented paradigm. In order to make the CDMM-P useful for the developers community, it should be matched to the way they make use of entity classes in the class-based variant of the object-oriented manner. Thus, the next goal of the CDMM-P is the ability to offer its users class-based access to CDMM-P's specific notions – *pure entity class* objects and entity relationship objects. This goal can be achieved via introduction of the additional layer with both access to entity relationship objects through the *pure entity objects* perspective and access to *pure entity objects* through entity relationship objects being possible. Based on the introduced layer, the CDMM-P's client application could not only see all objects available in the CDMM-P from the traditional class-based version of the object-oriented approach, but could also use any of the following graph data model scanning strategies:

- *pure entity classes* based strategy,
- *entity relationship classes* based strategy,
- mixed strategy adjusted to current needs.

Two first strategies are mutually symmetrical and can be used interchangeably.

8. Reflectiveness vs. static nature of data model

The construction of an application based on CDMM-P may have one of the following characters:

- static – it is assumed that the developer knows a priori the data model which is run-time loaded,
- dynamic – it is assumed that the developer does not know the data layer model.

In the first case, the application source code is simpler for implementation, but it does not allow for any change of static structure of the data model. In the second case, the developer can dynamically query the *pure entity classes* for their entity relationships. The developer can also query the entity relationship classes regarding their *pure entity classes*. The developer can then execute appropriate operations on objects of these classes. It is important from the CDMM-P perspective that there are no limitations for the choice between static and/or dynamic model of implementation of the application based on CDMM-P. Moreover, these two approaches can be mixed.

9. Standardization of CRUD operations on data layer

For the sake of the application of CDMM-P to the data layer, it is possible to limit the set of operations on the *pure entity* and *entity relationship classes* mentioned above to CRUD (Create, Read, Update and Delete) operations. Besides typical operations executed on entity classes in a traditional approach, here we may execute them not only on entities (operations on *pure entity classes*) but also on entity relationships. The proposition of a pre-defined set of

such operations is one of the goals of CDMM-P. For the purpose of the introduction of the set of predefined CRUD operations, the CDMM-P should itself give access to entity relationships visible to the client from the perspective set to the *pure entity class*. This mechanism is crucial for CDMM-P and distinguishes it from other potential solutions. It is possible to achieve this goal through the introduction of the ac*cessor notion. The accessor is responsible for putting the appropriate perspectives which were presented above. In the case of the standardization of CRUD operations described here, such an accessor should guarantee the ability of getting access to the entity relationship from the appropriate *pure entity class*. The accessor itself can be obtained through the following polymorphic operation:

```
BaseClass getAccessor(pure-entity-class, entity-relationship-class)
```

where

`BaseClass` – base class for all data model elements

`pure-entity-class` – *pure entity class*

`entity-relationship-class` – *entity relationship class*

Thus, the set of standardized operations, which can be executed on the object accessor to the *pure entity class* visible from the perspective put on *pure entity class*, may have the following form in pseudo-code:

```
void add(relationship-container, relationship-element)
T get(relationship-container)
int count(relationship-container)
List<T> getAll(relationship-container)
T get(relationship-container, index)
int count(relationship-container, relationship-element-class)
T get(relationship-container, relationship-element-class, index)
List<T> getAll(relationship-container, relationship-element-class)
```

where

`relationship-container` – *pure entity object* its *entity relationship* with other *pure entity objects* are visible through;

`relationship-element` – *pure entity object* bind to the *entity relationship* with *pure entity object* which gives access to object via the relationship obtained from entity;

`relationship-element-class` – information about the class of *pure entity object*

`index` – index of the *pure entity object* in a collection

It is worth noting that each *pure entity class* may have many *entity relationships*, which in turn may cause difficulties in CDMM-P's implementation in contemporary programming languages. Nevertheless, reaching this goal is possible.

10. Testing specificity

The two most important modifications of traditional approaches to testing are presented below. The first is related to unit testing of isolated classes and the second, to unit-like scenario tests responsible for testing class interconnections.

10.1. Unit testing

One of the consequences of weakening of the dependency and making classes independent is making unit tests of these classes also independent. As a result, each *pure entity class* and *entity relationship class* can be tested in isolation. Looking from the perspective of reusability, it must be underlined that both *pure entity* and *entity relationship classes* can migrate between different projects together with their unit tests, as long as the projects are based on CDMM-P. These kinds of tests constitute the additional layer of tests responsible for methods testing all data layer classes. This test layer is not known in a traditional object-oriented approach due to compilation dependencies between entity classes.

10.2. Semi-automatically generated scenario tests

For the sake of the dynamic run-time interconnecting of *pure entity classes* by *entity relationship classes,* the necessity for testing these classes in the context of their data model arises. It is however, worth pointing out here that scenario tests skeletons can be generated automatically from the same model as the CDMM-P classes are organized with the layer dynamically loaded. Thus, the proposed model plays the role of the parameter for both implementation and tests. The skeletons mentioned above could be implemented against unit testing frameworks. However, in order to generate these tests, the required objects of these classes must also be created on the basis of the association of the classes with their descriptions. Thus, such tests take the form of semi-automatic tests. The scenario test's source code is generated automatically from the objects' information that must be introduced by a developer. Based on this approach, the developer need not write the test code manually, but still keeps control over the test via the possibility of object initialization. Obviously, the CDMM-P does not eliminate the possibility of the implementation of manual scenario tests in any form, as well as introduction of modifications into already generated tests.

11. Conclusions

A new paradigm for software data layer design and implementation was introduced in this paper. The concept of the proposed approach was described at a general level to open new research fields leading to the implementation of the paradigm in different technologies. Such implementations will be presented in further research publications expanding the CDMM-P approach to the Java EE platform.

This paradigm can be used both for enterprise systems' data layer design and implementation and for the construction of modeling languages.

Finally, it is worth underlining that the concept of the paradigm CDMM-P proposed here is based upon the open ontology approach.

All diagrams were prepared with the help of Visual Paradigm UML modeling tool according to the Academic Partner Program agreement signed with Cracow University of Technology.

References

[1] Aßmann U., Zschaler S., Wagner G., *Ontologies, meta-models, and the model driven paradigm*, [In] C. Calero, F. Ruiz, M. Piattini (eds.), Ontologies for Software Engineering and Software Technology, Springer, 2006, 249-273.

[2] Bendera A., Poschlada A., Bozica S., Kondova I.. *A service-oriented framework for integration of domain-specific data models in scientific workflows*, [In:] J. Smith (ed.), Procedia Computer Science 18, International Conference on Computational Science, 2013, 1087-1096.

[3] Biletskiy Y., Ranganathan G., *A semantic approach to a framework for business domain software systems*, Computers in Industry, **61**, 2010, 750-759.

[4] Calero C., Ruiz F., Piattini M., *Ontologies for Software Engineering and Software Technology*, Springer, 2006.

[5] Chung L., Noguera M., Subramanian N., Garrido J., *Novel approaches in the design and implementation of system/software architectures*, The Journal of Systems and Software, **85**, 2012, 459-462.

[6] Guerra J.L. de E., Cuadrado J., *Reusable abstractions for modeling languages. Information Systems*, **38**, 2013, 1128-1149.

[7] Diaz I., Llorens J., Genova G., Fuentes J., *Generating domain representations using a relationship model. Information Systems*, **30**, 2005, 1-19.

[8] Djurić D., Devedžić V., *Magic potion: Incorporating new development paradigms through meta-programming*. IEEE Softw., **27** (5), Sep./Oct. 2010, 38-44.

[9] Djurić D., Gašević D., Devedžić V., *Ontology modeling and mda. Journal on Object Technology*, **4** (1), 2005, 109-128.

[10] Djurić D., Jovanović J., Devedžić V., Šendelj R., *Modeling ontologies as executable domain specific languages*, presented at the 3rd Indian Software Eng. Conf., 2010.

[11] *Ecore meta model in*: Eclipse Modeling Framework: www.eclipse.org/modeling/emf.

[12] Falbo R., Guizzardi G., Duarte K., *An ontological approach to domain engineering*. Procs. 14th Int. Conf. on Software Eng. and Knowledge Eng., 2002.

[13] Fung K., Low G., *Methodology evaluation framework for dynamic evolution in composition-based distributed applications*, The Journal of Systems and Software, **82**, 2009, 1950-1965.

[14] Gallardo J., Molina A., Bravo C., Redondo M., Collazos C., *An ontological conceptualization approach for awareness in domain-independent collaborative modeling systems: Application to a model-driven development method*, Expert Systems with Applications, **38**, 2011, 1099-1118.

[15] Gašević D., Djurić D., Devedžić V., *Model Driven Engineering and Ontology Development*, Springer-Verlag, 2009.

[16] Gašević D., Kaviani K., Milanovic M., *Ontologies, software engineering*, In Handbook on Ontologies, Springer-Verlag, 2009.

[17] Guizzardi G., *Ontological foundations for structural conceptual models*, Telematica Instituut Fundamental Research Series, **15**, 2005.

[18] G. Guizzardi. *On ontology, ontologies, conceptualizations, modeling languages, and (meta)models. In Frontiers in Artificial Intelligence and Applications*, Vol. 155, Amsterdam 2007, 18-39, Conference on Databases and Information Systems IV, IOS Press. Selected Papers from the Seventh International Baltic Conference DB and IS 2006.

[19] Halloway S., *Programming Clojure*, Pragmatic Bookshelf, 2009.
[20] Henderson-Sellers B., Barbier F., *What is this thing called aggregation?*, R. Mitchell, A. Wills, J.B.B. Meyer (eds.), Proceedings of TOOLS29 EUROPE99, IEEE Computer Society Press, Silver Spring, 1999, 216-230.
[21] Hickey R., *The clojure programming language*, In Proceedings of the 2008 symposium on Dynamic languages, 2008.
[22] Hickey R., *Clojure homepage*, http://www.clojure.org, 2009.
[23] Hofmeister C., Kruchten P., Nord R., Obbink H., Ran A., America P., *A general model of software architecture design derived from five industrial approaches*, The Journal of Systems and Software, **80** (1), Jan 2007, 45-50.
[24] Holanda O., Isotani S., Bittencourt I., Elias E., Tenório T., Joint: *Java ontology integrated toolkit. Expert Systems with Applications*, 4**0**, 2013, 6469-6477.
[25] Javed F., Mernik M., Gray J., Bryant B., Mars: *A meta-model recovery system using grammar inference*. Information and Software Technology, **50**, 2008, 948-968.
[26] Laarman A., Kurtev I., *Ontological meta-modelling with explicit instantiation*, [In] M. van den Brand, D. Gašević, J. Gray (eds.), SLE 2009, LNCS 5969, Springer-Verlag, Berlin 2010, 174-183.
[27] Langlois B., Jitia C., Jouenne E., *DSL classification*, In Proc. OOPSLA 7th Workshop on Domain Specific Modeling, University Park, PA, Citeseer 2007.
[28] Malhotra R., *Meta-modeling framework: A new approach to manage meta-model base and modeling knowledge*, Knowledge-Based Systems, **21**, 2008, 6-37.
[29] Merson P.. *Data model as an architectural view*, Technical Note CMU/SEI-2009-TN-024, Software Engineering Institute, Carnegie Mellon University, 2009.
[30] Mika P., *Social networks and the semantic web. Semantic web and beyond*, Springer, 2007.
[31] Molina A., Gallardo J., Redondo M., Ortega M., Giraldo W., *Metamodel-driven definition of a visual modeling language for specifying interactive groupware applications: An empirical study*, The Journal of Systems and Software, **86**, 2013, 1772-1789.
[32] Opdahl A., Henderson-Sellers B., Barbier F.. *Ontological analysis of wholepart relationships in oo models*. Information and Software Technology, **43**, 2001, 387-399.
[33] Peng X., Zhao W., Xue Y., Wu Y., *Ontology-based feature modeling and application-oriented tailoring*, In Reuse of Off-the-Shelf Components, Springer-Verlag, New York 2006, 87-100.
[34] Reinhartz-Berger I., *Utilizing domain models for application design and validation*. Information and Software Technology, **51**, 2009, 1275-1289.
[35] Reinhartz-Berger I., *Towards automatization of domain modeling*, Data and Knowledge Engineering, **69**, 2010, 491-515.
[36] Spinellis D., *Rational meta-programming*, IEEE Softw., **25** (1), 2008, 78-79.
[37] Szekely B., Betz J., Jastor: Typesafe. *Ontology driven rdf access from java*, http://jastor.sourceforge.net, 2009.
[38] Tairas R., Mernik M., Gray J., *Using ontologies in the domain analysis of domain-specific languages, In Models in Software Engineering*, Springer-Verlag, New York 2009, 332-342.

CONTENTS

MATHEMATICS

PHYSICS

COMPUTER SCIENCE

TREŚĆ

MATEMATYKA

FIZYKA

INFORMATYKA